

Picosecond non-linear infrared spectroscopy in zeolites and solution

Citation for published version (APA):

Bonn, M. (1996). *Picosecond non-linear infrared spectroscopy in zeolites and solution*. [Phd Thesis 2 (Research NOT TU/e / Graduation TU/e), Chemical Engineering and Chemistry]. Technische Universiteit Eindhoven. <https://doi.org/10.6100/IR471950>

DOI:

[10.6100/IR471950](https://doi.org/10.6100/IR471950)

Document status and date:

Published: 01/01/1996

Document Version:

Publisher's PDF, also known as Version of Record (includes final page, issue and volume numbers)

Please check the document version of this publication:

- A submitted manuscript is the version of the article upon submission and before peer-review. There can be important differences between the submitted version and the official published version of record. People interested in the research are advised to contact the author for the final version of the publication, or visit the DOI to the publisher's website.
- The final author version and the galley proof are versions of the publication after peer review.
- The final published version features the final layout of the paper including the volume, issue and page numbers.

[Link to publication](#)

General rights

Copyright and moral rights for the publications made accessible in the public portal are retained by the authors and/or other copyright owners and it is a condition of accessing publications that users recognise and abide by the legal requirements associated with these rights.

- Users may download and print one copy of any publication from the public portal for the purpose of private study or research.
- You may not further distribute the material or use it for any profit-making activity or commercial gain
- You may freely distribute the URL identifying the publication in the public portal.

If the publication is distributed under the terms of Article 25fa of the Dutch Copyright Act, indicated by the "Taverne" license above, please follow below link for the End User Agreement:

www.tue.nl/taverne

Take down policy

If you believe that this document breaches copyright please contact us at:

openaccess@tue.nl

providing details and we will investigate your claim.



ISCHA BONN

**PICOSECOND NON-LINEAR
INFRARED SPECTROSCOPY
IN ZEOLITES AND SOLUTION**

PICOSECOND NON-LINEAR INFRARED SPECTROSCOPY
IN ZEOLITES AND SOLUTION

PROEFSCHRIFT

ter verkrijging van de graad van doctor aan
de Technische Universiteit Eindhoven, op gezag
van de Rector Magnificus prof.dr. M. Rem voor
een commissie aangewezen door het College van
Dekanen in het openbaar te verdedigen op
woensdag 18 december 1996 om 16.00 uur

door

MISCHA BONN

GEBOREN TE NIJMEGEN

Dit proefschrift is goedgekeurd door de promotoren:

prof.dr. R.A. van Santen

prof.dr. A.W. Kleyn

copromotor: dr. H.J. Bakker

The work described in this thesis was performed at the FOM-Institute for Atomic and Molecular Physics (AMOLF), Kruislaan 407, 1098 SJ, Amsterdam, The Netherlands, where copies of this thesis are available. This work is part of a collaborative research program of the Stichting Fundamenteel Onderzoek der Materie (Foundation for Fundamental Research on Matter) with financial support from the Nederlandse Organisatie voor Wetenschappelijk Onderzoek (Netherlands Organization for the Advancement of Research), and the Schuit Institute of Catalysis at the Eindhoven University of Technology.

Aan Rob en Tineke

Aan Hester

This thesis is based on the following papers:

Fast energy delocalization after vibrational relaxation of a deuterated zeolite hydroxyl,
M. BONN, M.J.P. BRUGMANS, A.W. KLEYN AND R.A. VAN SANTEN,
J. Chem. Phys. **102**, 2181 (1995).

Enhancement of the vibrational relaxation rate of surface hydroxyls through hydrogen bonds with adsorbates,
M. BONN, M.J.P. BRUGMANS, A.W. KLEYN AND R.A. VAN SANTEN,
Chem. Phys. Lett. **223**, 309 (1995).

Solvent dependent vibrational relaxation pathways after resonant infrared excitation to $v=2$,
M. BONN, M.J.P. BRUGMANS, H.J. BAKKER,
Chem. Phys. Lett. **249**, 81 (1996).

Vibrational dephasing mechanisms in hydrogen-bonded systems,
M. BONN, M.J.P. BRUGMANS, A.W. KLEYN, R.A. VAN SANTEN AND H.J. BAKKER,
Phys. Rev. Lett. **76**, 2440 (1996).

Infrared picosecond transient hole-burning studies of the effect of hydrogen bonds on the vibrational lineshape,
M. BONN, M.J.P. BRUGMANS, A.W. KLEYN, R.A. VAN SANTEN AND H.J. BAKKER,
J. Chem. Phys. **105**, 3431 (1996).

The dynamics of infrared photodissociation of methanol clusters in zeolites and in solution,
M. BONN, H.J. BAKKER, A.W. KLEYN AND R.A. VAN SANTEN,
J. Phys. Chem. (Letter), **100**, 15301 (1996).

Infrared induced conversion of methanol adsorbed to acid zeolites,
M. BONN, H.J. BAKKER, J.A. LERCHER, A.W. KLEYN AND R.A. VAN SANTEN,
to be published.

Time dependence of vibrational relaxation of deuterated hydroxyls in acidic zeolites,
M. BONN, M.J.P. BRUGMANS, A.W. KLEYN, R.A. VAN SANTEN AND A. LAGENDIJK,
Stud. Surf. Sc. Cat. **84**, 493 (1994).

An investigation of vibrational dephasing mechanisms in hydrogen-bonded systems,
M. BONN, M.J.P. BRUGMANS, A.W. KLEYN, R.A. VAN SANTEN AND H.J. BAKKER,
In: "Femtochemistry. Ultrafast Chemical and Physical Processes In Molecular Systems." Ed.
M. Chergui, World Scientific Publishing Co. Singapore (1996), p. 475.

Infrared holeburning spectroscopy in acid zeolites,
M. BONN, M.J.P. BRUGMANS, H.J. BAKKER, A.W. KLEYN AND R.A. VAN SANTEN,
Stud. Surf. Sc. Cat. **97**, 567 (1996).

Other publications of the author of this thesis:

Multiphonon decay of stretch vibrations in zeolites,

M.J.P. BRUGMANS, M. BONN, H.J. BAKKER AND A. LAGENDIJK,
Chem. Phys. **201**, 215 (1995).

Generation of incoherent mid-infrared photon echoes with parametrically downconverted light,

S. WOUTERSEN, M. BONN, M.J.P. BRUGMANS, U. EMMERICHS AND H.J. BAKKER,
Opt. Lett. **21**, 1579 (1996).

Spectral Diffusion of Molecular Vibrations on a Picosecond Time-Scale,

M.J.P. BRUGMANS, H.J. BAKKER, M. BONN, A.W. KLEYN, R.A. VAN SANTEN AND A.
LAGENDIJK,

to appear in the conference proceedings of the 7th International Conference on Time-Resolved Spectroscopy.

Coherent picosecond vibron-polaritons as a probe of vibrational lifetimes

M. BONN, S. WOUTERSEN AND H.J. BAKKER,
to be published.

Contents

1	Introduction	1
1.1	General	1
1.2	Fundamental research in catalysis	2
1.2.1	Zeolites	4
1.3	Molecular vibrations	5
1.3.1	Linear absorption spectra and vibrational dynamics	6
1.3.2	Non-linear infrared spectroscopy	13
1.4	Experimental setup for non-linear infrared spectroscopy	15
1.5	Outline of this thesis	20
2	Vibrational relaxation of deuterated hydroxyls in acidic zeolites	21
2.1	Introduction	22
2.2	Experimental	22
2.3	Results	25
2.4	Discussion	28
2.5	Calculation of the transients	30
2.6	Conclusions	33
3	Enhancement of the vibrational relaxation rate of surface hydroxyls through hydrogen bonds with adsorbates	35
3.1	Introduction	36
3.2	Experimental	36
3.3	Results	37
3.4	Energy Transfer Mechanisms	39
3.5	The effect of hydrogen bonding on the relaxation rate	43
3.6	Conclusions	44
4	Fast energy delocalization upon vibrational relaxation of a zeolite surface hydroxyl	45
4.1	Introduction	46
4.2	Experimental	46
4.3	Results	47
4.4	Fast energy delocalization	50
4.5	Lattice temperature	53
4.6	Conclusions	56

5	Infrared picosecond transient hole-burning studies of the effect of hydrogen bonds on the vibrational lineshape	57
5.1	Introduction	58
5.2	General lineshape theory	59
5.3	Theoretical models for dephasing in hydrogen-bonded systems	60
5.4	Experimental	63
5.5	Differences between a solid and a gas-phase hydrogen bond	64
5.6	Coupling mechanism for hydrogen-bond induced dephasing	75
5.7	Conclusions	84
6	The dynamics of infrared photodissociation of methanol in zeolites and in solution	85
6.1	Introduction	86
6.2	Infrared dynamics of methanol clusters in solution and adsorbed to NaY	86
6.3	Conclusion	99
7	Infrared induced conversion of methanol in acid zeolites	101
7.1	Introduction	102
7.2	Methanol adsorption structure and linear infrared spectra	102
7.3	The infrared conversion of methanol in acidic Y zeolite	105
7.4	The dynamics of methanol conversion in acidic Y zeolite	107
7.5	Conclusions	112
8	Solvent-dependent vibrational relaxation pathways after successive resonant IR excitation to $v = 2$	113
8.1	Introduction	114
8.2	Results and Discussion	116
8.3	The effect of solvent on the relaxation pathway	122
8.4	Conclusions	123
	Bibliography	125
	Summary	131
	Nawoord	133
	Curriculum Vitae	135

Chapter 1

Introduction

1.1 General

A simplified picture of a chemical bond between two atoms is that of a miniature spring. In contrast to a classical spring, the energy contents of this molecular spring is quantized: The amounts of energy that can be transferred to the vibration of the spring are discrete, giving rise to distinct vibrational transitions. The energy spacing between the separate levels is, to a first approximation, Planck's constant times the frequency of the vibration. The frequency is determined by the strength of the chemical bond and the reduced mass of the vibration. Strong bonds as well as the involvement of light atoms result in high frequencies. If the vibration leads to an oscillatory dipole moment, it can be driven by an electromagnetic field resonant with the vibration: A transition between the energy levels can occur if the frequency of the light is equal to the frequency of the vibration. The frequency range of light that can be absorbed by vibrational transitions lies in the mid- and far-infrared region of the electromagnetic spectrum. With infrared spectroscopy the vibrational absorption spectrum can be investigated, *viz.* the frequencies at which light is absorbed, the width of these resonances and the absorption intensities. In theory, infrared spectroscopy allows for the determination of the force constants of chemical bonds, and, for sufficiently simple systems, the symmetry of the (molecular) system.[1] Hence, infrared spectroscopy is a widespread analytic tool in chemistry in general and catalysis in particular[2].

Each vibration in a molecular system involves, in principle, a displacement of all atoms in the system. For some modes, especially high-frequency vibrations, the displacement is limited largely to two or three specific atoms. These modes are commonly

referred to by the atoms involved in the vibration. This is the type of vibration under investigation in this thesis: the O–H (O–D) stretch vibration of (deuterated) surface hydroxyls in zeolites, the C–H stretch vibration of iodoform (CHI_3) and the O–H stretch vibration of methanol (CH_3OH).

This thesis deals with time-resolved (picosecond) infrared spectroscopy on these vibrations. From these experiments information on the time evolution of vibrational excitations is obtained. This information can generally not be obtained with conventional –frequency domain– infrared spectroscopy. The essence of the technique is that the molecular spring is excited and that the relaxation of the spring is monitored in real-time. Relaxation rates as well as information on relaxation pathways ('where does the energy flow?') can be obtained, providing insights into important chemical and physical properties of the systems under study. For instance, the redistribution of vibrational energy is an important factor in chemical reaction kinetics. The rate of vibrational (energy) relaxation relative to the rate for coupling into the reaction coordinate may dictate reaction rates and pathways.

In the following section the research described in this thesis is put in a broader perspective, and zeolites are introduced. In section 1.3 it is shown how the vibrational dynamics are connected to the infrared absorption lineshape. Different mechanisms giving rise to infrared absorption line broadening are discussed and a mathematical model describing these mechanisms is introduced. In the same section it is shown how non-linear spectroscopic techniques can be used to obtain information on the vibrational dynamics, and why this type of information can usually not be obtained with conventional linear spectroscopy. In section 1.4 the experimental setup is introduced, along with a description of the different experiments it allows for. In the last section of this Chapter the outline of this thesis is presented.

1.2 Fundamental research in catalysis

The past decades have seen a tremendous increase in the development and application of catalysts in industrial processes, ranging from small-scale applications in e.g. medicine production to large-scale hydrocarbon cracking in the petrochemical industry.[3] Due to the complexity of the catalysts themselves and the catalyzed reaction, the exact mechanism behind the catalytic activity and the reaction pathways are not always clear. As a consequence, the development of new catalysts, their optimization and the determination of their optimum working conditions have been achieved mostly through trial and error. Conversely, it is evident that knowledge of the microscopic characteristics of the catalyst along with the relevant mechanisms and dynamics at a molecular

level, would in principle allow for the *a priori* knowledge of catalytic behaviour and –ideally– the design of specifically active catalysts. Generally, attempts to obtain this type of information on the dynamics of the catalyzed reaction on a molecular scale, are made from *indirect* studies of overall chemical kinetics and thermodynamics, often with the help of various classical spectroscopic techniques. Direct access to the dynamics requires the use of more complicated experimental techniques, e.g. by means of (ultra-fast) time-resolved experiments [4] or by studying model catalysts under very well-defined conditions in ultra high vacuum (UHV) [5]. One drawback of this type of research is that the equipment used is usually very specific. The experimental techniques can therefore only be applied to a limited number of systems. Furthermore, the experimental circumstances under which systems can be investigated are generally not very realistic; thermodynamic variables such as temperature and pressure have to be well-defined and kept within a limited range to allow for a straightforward interpretation of the experimental data. Inevitably, this leads to experimental circumstances different from those encountered in industrial catalysis. It is only when *all* the details of the reaction mechanism, kinetics and thermodynamics are revealed, that the findings can be extrapolated to predict the catalytic behaviour under different (more realistic) conditions. Despite these disadvantages, it is evident that by means of these fundamental techniques new insights into reaction mechanisms can be obtained and new concepts can be introduced.

Another justification of this type of experiment lies in the verification of a different approach to a fundamental understanding of catalysis: that of (e.g. *ab initio*) modeling of catalysts.[6] In this rapidly growing field, the results of the modeling inherently provide insights into microscopic mechanisms and, possibly, the relevant dynamics. However, if possible, the results of these molecular modeling techniques should be verified experimentally to establish the validity of the computational procedure and its results.

In this thesis, we investigate the vibrational dynamic behavior of the catalytically active sites in acid zeolites, the effect of interaction with simple molecules, and the vibrational dynamics of these simple molecules themselves, when interacting with the zeolite. Insight into the dynamics of the interaction between the hydroxyl group and the zeolite lattice, as well as an understanding of the dynamics of the interaction between the hydroxyl and adsorbates, are essential for a fundamental understanding of the catalytic properties of the hydroxyl groups.

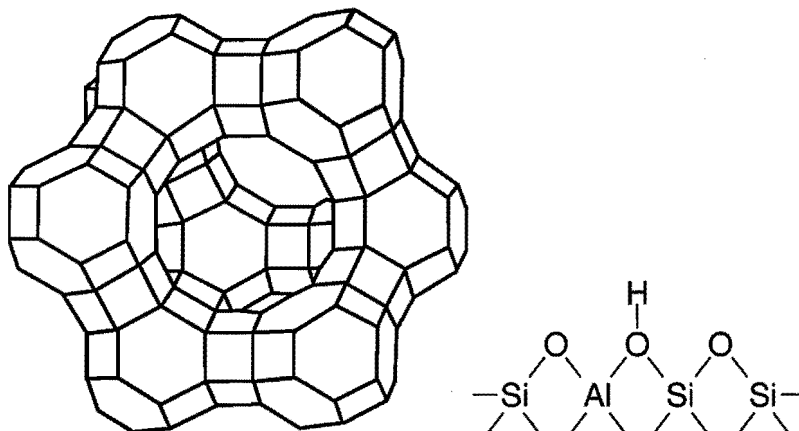


Figure 1.1: *The Faujasite structure of Y zeolite. A line stands for an oxygen atom connecting a silicon atom to another silicon atom or to an aluminum atom. The close-up shows a bridging hydroxyl group, responsible for the acidic properties of proton-exchanged zeolites.*

1.2.1 Zeolites

Zeolites, also known as molecular sieves, are crystalline aluminosilicates with large internal surfaces due to the presence of microscopic channels and pores. A large variety of zeolite structures exists.[7, 8] The structure of Y zeolite is depicted in Fig. 1.1. The three-dimensional structure is formed by the interconnecting SiO_2 and $\text{AlO}_2^{(-)}$ units; the silicon and aluminum atoms are all tetrahedrally coordinated by oxygen atoms. At the sites where an aluminum atom is incorporated in the zeolite lattice, positive charge compensation is required. This can be achieved by, for example, sodium cations (Na^+). Zeolites have cation exchange capacity, and when H^+ -exchanged they are solid acids.[9] The proton binds covalently to one of the oxygen atoms next to the aluminum, giving rise to catalytically active bridging hydroxyl ($\text{Si}-\text{O}^{\text{H}}-\text{Al}$) groups, pointing into the zeolite cavity. A microscopic picture of such a hydroxyl group is depicted in Fig. 1.1. These catalytic sites are frequently referred to as Brønsted sites. Acidic zeolites are widely applied in hydrocarbon conversion reactions in the petrochemical industry.[9] For example, acid zeolites are used as catalysts in hydrocarbon cracking processes, in which long-chain carbon molecules (distillates from crude oil) are converted into more valuable fuel fractions (gasoline and diesel) of smaller molecular size. The cleavage of a C-C bond involves the protonation of one of the carbon atoms, and is therefore an acid-catalyzed reaction; the proton is 'lent' by the acid catalyst. Utilizing the zeolite

type of solid acid instead of liquid acid as a catalyst has numerous advantages. Apart from the fact that it is much easier to separate reaction products from catalysts in solid-acid catalyzed processes, solid acids also diminish environmentally hazardous emission and safety problems. Acid zeolites can be stored and handled easily, because they hold their acidity internally. Furthermore, metal clusters can be incorporated into zeolites to combine acidic activity with metal catalysis, and, also of great importance, the structure of zeolites allows for shape-selective catalysis.

Conventional infrared spectroscopy is a frequently employed tool in the investigation of the zeolite acidic hydroxyl groups, very often in combination with probe molecules (for a review, see e.g. Ref. [10]). In most of these studies, the shift of the zeolite O–H stretching band, or the change in vibrational spectrum of the adsorbate upon adsorption is investigated. In the following section molecular vibrations, conventional (linear) infrared absorption spectroscopy and time-resolved non-linear spectroscopy will be briefly discussed.

1.3 Molecular vibrations

Let us consider a bond between two atoms. The Born-Oppenheimer approximation states that electrons adapt infinitely fast to changes in nuclear position. We can therefore choose a certain internuclear separation, and solve the Schrödinger equation for the electrons alone. Then we can repeat the procedure for a different separation, and thus obtain the energy of the system as a function of internuclear separation. A schematic example for the O–D bond of a deuterated zeolite hydroxyl is depicted in Fig. 1.2. The electronic ground state potential is approximated by a Morse potential, a simple anharmonic potential.[11] The shape of the potential (the anharmonicity) can be determined from the first vibrational transition and the dissociation energy. The minimum of the potential determines the equilibrium position between the two nuclei [6], and the depth of the potential is equal to the dissociation energy plus the zero-point vibrational energy. At room temperature, practically all the population will be in the $v=0$ ground state (see left inset in Fig. 1.2), since the thermal energy ($k_b T=207 \text{ cm}^{-1}$ at room temperature) is very small compared to the vibrational energy. For an infrared active vibration, the $v=0$ to $v=1$ transition will give rise to an infrared absorption band centered around 2650 cm^{-1} . In the following, the interaction of light with the two-level system ($v=0$ and $v=1$) will be described, with particular emphasis on the processes that give rise to the width of an absorption line. It will be demonstrated how the dynamics of the vibration are related to the absorption linewidth, and how they can be investigated in detail by means of non-linear spectroscopy.

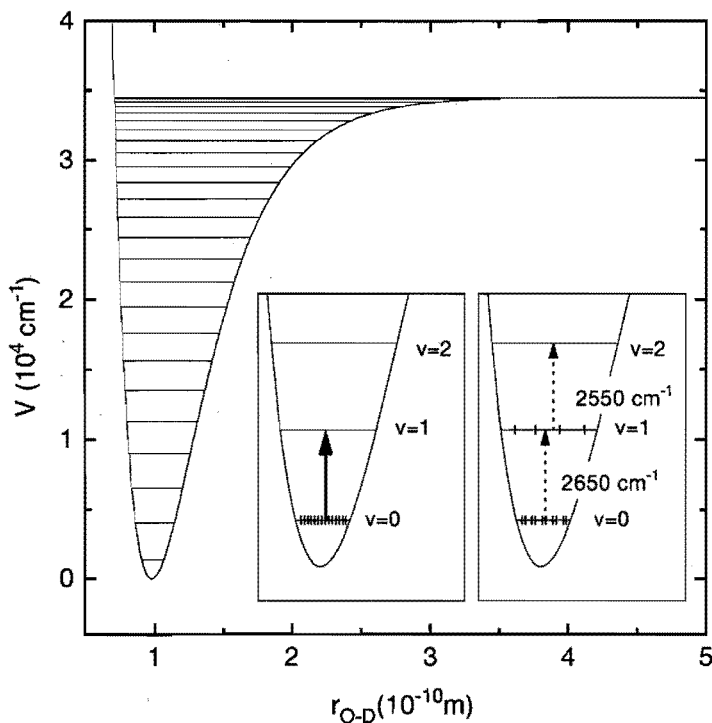


Figure 1.2: The vibrational potential for the O–D stretch bond of a deuterated zeolite hydroxyl, approximated by a Morse potential. Due to the anharmonicity, the level spacing decreases with increasing vibrational quantum number and the number of bound levels is finite. Insets show the bottom of the potential well relevant to our experiments.

1.3.1 Linear absorption spectra and vibrational dynamics

An electromagnetic field (light) of frequency ω close to the resonance frequency ω_0 of a vibrational transition of a two-level system will induce a dipole moment $\vec{\mu}(t)$ in that oscillator (provided, of course, that the transition dipole moment between $v=0$ and $v=1$ is non-zero).[12] For an ensemble of N oscillators, this will result in a macroscopic linear polarization $\mathbf{P}(t)$:

$$\mathbf{P}(t) = \sum_{i=1}^N \vec{\mu}_i(t) \quad (1.1)$$

The absorption spectrum $I(\omega)$ associated with such a transition is determined by the Fourier transform of the macroscopic dipole moment correlation function[13]:

$$I(\omega) = \frac{1}{2\pi} \int_{-\infty}^{\infty} dt \langle \mathbf{P}(0) \cdot \mathbf{P}(t) \rangle e^{i\omega t} \quad (1.2)$$

This means that the width of an absorption line is determined by the decay of the macroscopic polarization correlation function $\langle \mathbf{P}(0) \cdot \mathbf{P}(t) \rangle$. The faster the decay of the polarization correlation function, the broader the absorption band. Decay of the macroscopic polarization can be caused by (i) amplitude decay of each oscillator individually or (ii) the fact that the oscillating microscopic dipole moments of different oscillators will run out of phase and no longer interfere constructively after a certain period of time: The macroscopic dipole moment is said to *dephase*.

For a (sub-)ensemble of two-level systems with the same transition frequency (i.e. the same energy level spacing), the polarization created by the field, and its subsequent decay caused by dephasing can be described by the optical Bloch equations, which make use of the density operator formalism. The wavefunction Ψ describing a two-level system can, at all times, be expressed as a linear combination of the two eigenfunctions φ_1 and φ_2 :

$$\Psi(\mathbf{r}, t) = C_1(t)\varphi_1(\mathbf{r}) + C_2(t)\varphi_2(\mathbf{r}) \quad (1.3)$$

Because the *products* of the coefficients C_i determine expectation values of observables (rather than the bare coefficients themselves), it is practical to work with the four elements of the density matrix ρ_{ij} , defined as:

$$\rho_{ij} \equiv \langle C_i C_j^* \rangle, \quad (1.4)$$

where the brackets denote the ensemble average. For a two-level system, the density matrix is a 2×2 matrix, of which the diagonal elements are real and represent the normalized population of the ground (ρ_{11}) and excited (ρ_{22}) states, so that $\rho_{11} + \rho_{22} = 1$. The off-diagonal elements (ρ_{12} and ρ_{21}) are usually complex and describe the coherent polarization set up by the light field:

$$\mathbf{P} = N(\vec{\mu}_{21}\rho_{12} + \vec{\mu}_{12}\rho_{21}), \quad (1.5)$$

with $\vec{\mu}_{ij}$ the matrix elements of transition dipole moment operator. The phenomenological Bloch equations state that the matrix elements of the density matrix decay exponentially in time after the field is turned off, with time constants T_1 and T_2 for the diagonal and off-diagonal elements, respectively. This results in an exponential decay of the macroscopic polarization with time-constant T_2 , so that

$$\langle \mathbf{P}(0) \cdot \mathbf{P}(t) \rangle \propto e^{(-t/T_2)} \quad (1.6)$$

The resulting absorption line will exhibit a Lorentzian lineshape of width Γ_{hom} :

$$2\pi\Gamma_{\text{hom}} = \frac{2}{T_2} \quad (1.7)$$

The homogeneous dephasing time T_2 then simply reflects the dephasing of an ensemble of oscillators with the same center frequency. This time-constant can be partitioned into contributions from elastic and inelastic dynamic interactions of the two-level systems with their environment (called 'the heat bath'), with two associated time constants. The inelastic interactions result in a finite population lifetime of the excitation; population in the excited state will decay back to the ground state. The time constant associated with population decay (decay of ρ_{22}) is defined as T_1 . Vibrational population (or energy-, T_1 -) relaxation is mostly non-radiative and entails the redistribution of the vibrational energy into a set of modes with lower energy which are anharmonically coupled to the mode represented by the two-level system.[14-16] These modes are called 'accepting modes'; together these receive the excess energy upon de-excitation of the oscillator. The elastic processes give rise to *pure* dephasing, leading to the loss of mutual coherence between oscillators with the same center frequency. Pure dephasing can be interpreted as very fast, small frequency jumps around the central frequency. In contrast to the population (energy) decay process, pure dephasing is usually interpreted as an elastic process¹ – no energy is transferred between the mode and the bath.[17] The time-constant associated with pure dephasing is called the pure dephasing time T_2^* . It can be shown that the two processes contribute to the line-broadening as:

$$2\pi\Gamma_{\text{hom}} = \frac{2}{T_2} = \frac{1}{T_1} + \frac{2}{T_2^*} \quad (1.8)$$

This is the generally employed expression for the linewidth of a homogeneously broadened transition, applicable to an ensemble of oscillators with the same transition frequency.

However, dephasing can also be caused by a simple *static* difference in transition frequencies between the different oscillators. The phase difference after time t as a result of a frequency difference $\Delta\omega = \omega_1 - \omega_2$ between two oscillators is: $\Delta\phi(t) = \Delta\omega t / 2\pi$. It is clear that after a certain time the oscillators with different frequencies will no longer interfere constructively, causing the macroscopic dipole moment to decay. In the Bloch equations, these *static* contributions to the dephasing (and line-broadening) were not considered. In condensed phases at room temperature, population/energy lifetime

¹Strictly speaking, this is not true. The pure dephasing process itself results from continuous two-way energy exchange (albeit small amounts) between the high-frequency mode and the bath. However, this leads only to an adiabatic modulation of the transition frequency, not to a net energy transfer between the two.

(T_1 -) contributions to linewidths of high-frequency modes are generally much smaller than pure dephasing effects. In this case, pure dephasing (rapid changes in transition frequencies) and static contributions (static differences in transition frequencies) are the two causes for dephasing: Differences and/or fluctuations in frequency are responsible for the dephasing process. For a complete and general description of the line-broadening (dephasing) processes (containing both dynamic and static contributions), we will therefore consider an oscillator with a time-dependent, stochastically modulated frequency $\omega(t)$ [18]:

$$\omega(t) = \omega_0 + \delta\omega(t) \quad (1.9)$$

The resulting absorption spectrum can be calculated exactly if two assumptions are made with respect to the noise term $\delta\omega(t)$, in the so-called Gauss-Markov description.[18] The first is that $\delta\omega(t)$ is to have a Gaussian distribution with a zero mean value.² Let D be the width of this frequency distribution available to the oscillator, i.e. the root mean square amplitude of the frequency excursions, so that the time-correlation function of the frequency modulation reads:

$$\langle \delta\omega(0)\delta\omega(t) \rangle = D^2 f(t) \quad (1.10)$$

The function $f(t)$ describes the decay of this correlation function and contains the information on the typical time-scale(s) of the frequency modulation process. The second assumption is that the time evolution of $\delta\omega(t)$ can be described by a Markovian process:[18] This implies that $f(t)$ decays exponentially in time with time constant τ_c :

$$f(t) = e^{-t/\tau_c} \quad (1.11)$$

Physically, the assumption of exponential decay requires that the relaxation of the bath be very rapid compared to relaxation of the two-level system.³ Thus, τ_c is a measure of the time during which the oscillator retains the same frequency within the spectral distribution of width D . This allows for the calculation of the absorption lineshape $I(\omega)$ for an ensemble of oscillators whose transition frequencies are determined by the two

²This is not an unreasonable assumption, since if the frequency modulation is caused by many, relatively weak, random, independent contributions, the central limit theorem states that the statistics for the frequency modulation process will be Gaussian indeed.

³For a quantity that can be described by a Markovian process (i.e. exponential time decay of the correlation function), the magnitude at time $t_0 + \Delta t$ is solely determined by its magnitude at t_0 , independent of the system state at $t_0 - \Delta t$, i.e. the system has no memory. This approximation does not hold for systems with feedback, in which e.g. decay of the polarization affects the exact transition frequency.

parameters D and τ_c . The macroscopic polarization correlation function $\langle \mathbf{P}(0) \cdot \mathbf{P}(t) \rangle$ can be written in terms of the two parameters[19]:

$$\langle \mathbf{P}(0) \cdot \mathbf{P}(t) \rangle \propto \exp(-D^2 \tau_c^2 [e^{(-t/\tau_c)} + t/\tau_c - 1]) \quad (1.12)$$

The situation in which the static contributions can be neglected, (i.e. the limit which is described by the Bloch equations) the dephasing and the concurrent line-broadening are caused by small, rapid frequency excursions of the oscillators due to *dynamic* interactions with the heat bath. This means that the frequency modulation is very rapid; the system is in the so-called fast modulation limit ($D\tau_c \ll 1$). In this limit, it is impossible to discern between the different oscillators spectroscopically, since –on average– they will all have the same center frequency ω_0 : The absorption line is homogeneously broadened. By the term 'indiscernible spectroscopically', it is meant that it is impossible to selectively excite different oscillators in a homogeneous absorption band, since, for $D\tau_c \ll 1$, a light pulse of duration shorter than τ_c (which would be necessary to 'beat' the modulation process) will spectrally be much broader than D , due to the finite product of pulse duration and spectral bandwidth.[20] In case of a homogeneous line, the width of the absorption line is determined by both D and τ_c . The expression between the square brackets in the rhs of Eq. (1.12) can be approximated by its second term t/τ_c , and so the polarization time correlation function will decay exponentially in time:

$$\langle \mathbf{P}(0) \cdot \mathbf{P}(t) \rangle \propto \exp(-D^2 \tau_c t) \quad (1.13)$$

so that $D^2 \tau_c$ can be identified as the inverse of the dephasing time T_2 in Eq. (1.6) of the Bloch picture (since we are neglecting lifetime (T_1 -) contributions, $T_2 = T_2^*$). This results in a homogeneously broadened line with a Lorentzian shape, the width of which will be proportional to $D^2 \tau_c$:

$$I(\omega) \propto \frac{1}{(\omega - \omega_0)^2 + (D^2 \tau_c)^2} \quad (1.14)$$

Note that a *faster* frequency modulation, i.e. smaller τ_c , results in a *slower* decay of $\langle \mathbf{P}(0) \cdot \mathbf{P}(t) \rangle$, and hence a *narrower* absorption line. This seemingly counter-intuitive result (a "faster perturbation" leading to a "better defined" frequency) can be understood as follows: If the modulation of the transition frequency is sufficiently rapid, the net phase evolution of the oscillators resembles that of the central frequency of the distribution and, as a consequence, the average phase difference between oscillators develops relatively slowly. As a result, the macroscopic polarization decays slowly, resulting in a sharp absorption band. This phenomenon is well-known in magnetic resonance spectroscopy as motional narrowing.[21]

The situation where dephasing is caused by differences in frequencies between the oscillators, i.e. where the broadening of the absorption line is caused by a (static) frequency difference between the oscillators, is described in this formalism by a *slow* frequency modulation: The time-scale of the frequency fluctuation is long compared to the width of the frequency distribution. This is called the slow modulation limit, for which $D\tau_c \gg 1$. Due to the slow modulation of the transition frequencies, the frequencies of the different oscillators are different and can be regarded as effectively fixed. This results in an inhomogeneously broadened absorption line: The width of the absorption line is determined only by the static distribution of transition frequencies. Mathematically, this implies that the exponential term e^{-t/τ_c} in the expression of $\langle \mathbf{P}(0) \cdot \mathbf{P}(t) \rangle$ in Eq. (1.12) can be approximated as the first three terms in its Taylor expansion, resulting in:

$$\langle \mathbf{P}(0) \cdot \mathbf{P}(t) \rangle \propto \exp(-D^2 t^2) \quad (1.15)$$

and, with help of Eq. (1.2):

$$I(\omega) \propto e^{-(\omega - \omega_0)^2 / D^2}, \quad (1.16)$$

resulting in a Gaussian lineshape of width $\sim D$. As one would expect, the resultant inhomogeneously broadened lineshape in this limit is determined *only* by D , the width of the spectral distribution, i.e. the range of possible transition frequencies.

It is clear that in the homogeneous limit changes in the transition frequency occur 'infinitely' fast, and in the inhomogeneous limit 'infinitely' slow. The beauty of this formalism lies in the fact that it also allows for the description of systems which are neither totally homogeneous, nor totally inhomogeneous. In this intermediate regime ($D\tau_c \approx 1$), a larger linewidth can be caused by either a slower modulation (larger τ_c) or a larger spectral distribution D . The shape of the corresponding absorption band is neither Gaussian nor Lorentzian, but exhibits a lineshape in between the two shapes. This intermediate regime is sometimes referred to as 'non-Markovian', since the decay of the macroscopic polarization of the ensemble of oscillators can no longer be described as a Markovian decay of single oscillators.

In real-life systems the different limits of fast, slow and, possibly, intermediate modulation usually apply simultaneously: There are *two* or more modulation processes at work, some very fast and some very slow, with a well-defined separation of time-scales. The slow processes, characterized by D and τ_c , so that $D\tau_c \gg 1$, result in inhomogeneous broadening. Fast frequency modulation processes (characterized by D' and τ'_c with $D'\tau'_c \ll 1$), account for the broadening of the homogeneous lines hidden under the inhomogeneously broadened overall absorption band. In solids, the static component leading to the inhomogeneous broadening can be caused by slightly different environments of the oscillators due to e.g. crystal defects, whereas the dynamic component

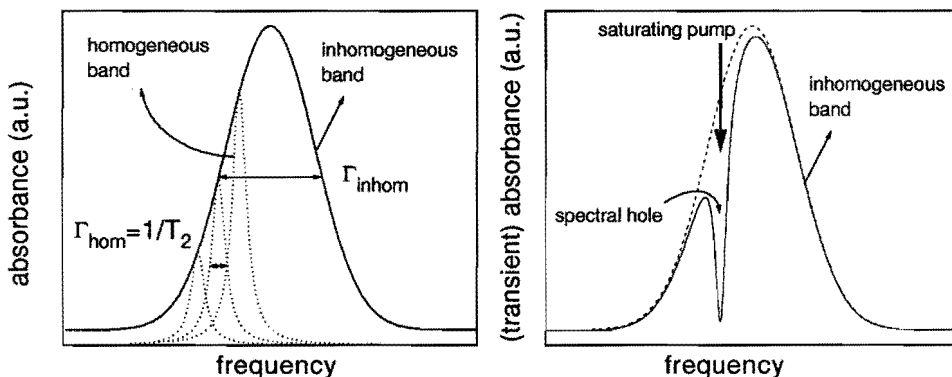


Figure 1.3: Left panel: *Inhomogeneous and homogeneous broadening of an absorption band. An inhomogeneously broadened absorption band (solid line) is composed of several homogeneous absorption bands (dotted lines). Right panel: The technique of spectral hole-burning reveals inhomogeneous broadening and allows for the determination of the homogeneous linewidth. An intense, narrow-banded light source selectively excites a sub-set of resonant homogeneous lines. The width of the hole is determined by the homogeneous linewidth and the laser bandwidth.*

(leading to the broadening of the homogeneous lines) can be caused by the rapidly fluctuating occupation number of a low-frequency (phonon) mode anharmonically coupled to the oscillator. Similarly, in gases the slow process can be caused by a distribution of translational degrees of freedom (Doppler broadening), whereas fast intermolecular collisions lead to homogeneous line-broadening. Intermediate situations ($D\tau_c \approx 1$) can occur when the transition frequency changes on a time-scale comparable to the inverse of the frequency distribution, for example, when the exact transition frequency of a molecule is determined by relatively slow changes in its surroundings (e.g. solvent molecule reorientation). Another example of spectral diffusion is the diffusion of an excitation through the inhomogeneous absorption band, from one homogeneous line to another, caused by e.g. dipole-dipole coupling.[22]

In summary, we see that slow bath processes lead to inhomogeneous broadening of the absorption line: in this case the absorption band is made up of many homogeneous lines. The width of the overall absorption line contains information on the *static* frequency distribution. This situation is schematically depicted in the left panel of Fig. 1.3. For a sub-ensemble for which the bath states associated with the slow modulation process are identical (i.e. a sub-ensemble of oscillators with the same center

frequency constituting one homogeneous line), and the fast process is sufficiently fast, the line-broadening processes can be described by the optical Bloch equations. The homogeneous linewidth is determined by the dynamics of the vibration, the population and pure dephasing lifetimes. In Figure 1.3, the homogeneous lines are hidden under an inhomogeneous distribution. It is also possible that inhomogeneous broadening is absent. With conventional, linear spectroscopy, it cannot be determined whether the broadening of an absorption band is due to homogeneous or inhomogeneous effects. This distinction can be made with non-linear spectroscopy. Moreover, the appropriate non-linear technique allows for the determination of the homogeneous linewidth, even in case of strong inhomogeneous broadening, and the determination of both the vibrational population lifetime T_1 and the pure dephasing time T_2^* .

1.3.2 Non-linear infrared spectroscopy

In the expression for the absorption line $I(\omega)$ derived in the previous section, the *linear* polarization was considered. From a macroscopic point of view, for sufficiently small fields, the polarization $\mathbf{P}(t)$ induced by the field $\mathbf{E}(t)$ is proportional to the applied field [23]:

$$\mathbf{P}(t) = \int_{-\infty}^{\infty} \chi^{(1)}(t-t') \cdot \mathbf{E}(t') dt', \quad (1.17)$$

with $\chi^{(1)}$ the linear susceptibility. The susceptibility $\chi^{(1)}$ is complex, and the real and imaginary parts of its Fourier transform $\chi^{(1)}(\omega)$ are related to the refractive index and the extinction (absorption) coefficient.[24] Naturally, it is connected to the microscopic properties of the sample. When recording an absorption spectrum, the requirement that the field strengths are sufficiently small for Eq. (1.17) to remain valid, is amply met. The conventional absorption spectrum is therefore referred to as linear.

If, due to the presence of light fields of high intensities the optical properties of the sample are modified, the response of the sample to the applied field is non-linear: Eq. (1.17) breaks down because terms of higher order are required to describe the interaction between light and matter[23]:

$$\begin{aligned} \mathbf{P}(t) = & \int_{-\infty}^{\infty} \chi^{(1)}(t-t_1) \cdot \mathbf{E}(t_1) dt_1 \\ & + \int_{-\infty}^{\infty} \int_{-\infty}^{\infty} \chi^{(2)}(t-t_1; t-t_2) : \mathbf{E}(t_1)\mathbf{E}(t_2) dt_1 dt_2 \\ & + \int_{-\infty}^{\infty} \int_{-\infty}^{\infty} \int_{-\infty}^{\infty} \chi^{(3)}(t-t_1; t-t_2; t-t_3) : \mathbf{E}(t_1)\mathbf{E}(t_2)\mathbf{E}(t_3) dt_1 dt_2 dt_3 \\ & + \dots \end{aligned} \quad (1.18)$$

in which $\chi^{(2)}$ and $\chi^{(3)}$ are the second and third order susceptibility.

Due to the necessity of intense light fields, non-linear optical phenomena have been studied extensively with the use of lasers. Examples of second order ($\chi^{(2)}$ -) non-linear processes are sum- and difference frequency generation, second harmonic generation, and, the process which we use to generate the infrared pulses, parametric generation.[25] Examples of third order ($\chi^{(3)}$ -) processes are third harmonic generation and self-focusing.[25]

The non-linear character of the time-resolved infrared spectroscopy described here, manifests itself by a breakdown of the Lambert-Beer law: The absorbed radiation power depends non-linearly on the incident power. This is a consequence of the fact that a significant amount of vibrations is excited, and these excited oscillators can no longer absorb the light. Accordingly, this technique is often referred to as saturation spectroscopy, since the transition is saturated.

In the experiments, a powerful infrared laser pulse is used to resonantly excite a significant fraction of a (sub-)ensemble of oscillators to their first excited vibrational state (right inset of Fig. 1.2). This will lead to an increased transmission around the $v=0 \rightarrow v=1$ transition frequency, since less ground state groups are available to absorb the light. Simultaneously, an induced absorption will be detectable at slightly lower frequencies due to excited state ($v=1 \rightarrow v=2$) absorption. These changes and their time-evolution are monitored by a second pulse, which is sufficiently weak to ensure that the measured changes are linear in probe intensities. Obviously, the return of the transmission to equilibrium reflects the decay of the population back to the ground state. Thus, the vibrational population lifetime T_1 can be obtained. Secondly, the strong infrared pulses can also be used to investigate whether an absorption line is homogeneously or inhomogeneously broadened. In this experiment, we make use of the fact that we can generate a pair of independently tunable laser pulses. The first, powerful (pump) pulse is tuned to the top of the absorption band, promptly followed by the second (at small time delay) which is scanned in frequency. After the passage of the pump pulse through the sample, the absorption band will decrease in amplitude (excited groups can no longer absorb light). In case of inhomogeneous broadening, the pump pulses will only excite those groups that are resonant, and only the center of the absorption band will decrease in amplitude: A spectral hole is burnt in the absorption band.[20] This is illustrated in the right panel of Fig. 1.3. Hence it is clear that this technique allows for the separation of inhomogeneous and homogeneous contributions to the overall absorption line. The width of the spectral hole is determined by the homogeneous linewidth, which in turn is determined by the energy (T_1) and pure dephasing (T_2^*) lifetimes. (Eq. (1.8)) Since we can independently

determine T_1 (from the transmission decay experiment), we can calculate T_2^* , thus obtaining both vibrational lifetimes.

Other techniques capable of measuring (one of) these lifetimes, such as coherent[26] or incoherent[27] infrared photon-echo spectroscopy, and time-resolved Raman spectroscopic techniques (e.g. CARS, SCRS[28][29]), all seem very impractical on zeolite samples due to the large degree of scattering by the zeolite samples. The zeolite samples are not transparent for visible light, and scatter the infrared light quite strongly.

1.4 Experimental setup for non-linear infrared spectroscopy

As described above, infrared saturation spectroscopy is based on exciting a significant fraction of vibrational groups. Due to the small cross sections of vibrational transitions, high infrared light intensities are required. A second prerequisite is that the time duration of the pulses be short compared to the relaxation times, typically tens of picoseconds. Thirdly, the light source must be tunable, allowing for resonant excitation of the vibration under investigation, so that only one specific vibrational degree of freedom is excited. These demands can be met by parametric generation and amplification of infrared laser pulses using a picosecond Nd:YAG laser.[29] In this non-linear optical process the 1064 nm light from the Nd:YAG laser (ω_3) is converted into *two* new fields (signal and idler, ω_1 and ω_2), under the condition that $\omega_1 + \omega_2 = \omega_3$. This process takes place in a birefringent LiNbO₃ crystal, so that the frequencies of the two generated fields can be tuned by changing the angle between the polarization of the incoming Nd:YAG pulse and the optical axis of the LiNbO₃ crystal. The long-wavelength idler (ω_2), tunable from 2500 to 4500 cm⁻¹, is used in the experiments.

The setup for the generation of picosecond infrared pulses is depicted in Fig. 1.4. This setup initially consisted of *one* infrared branch, as constructed by Bakker[30] and Planken[31]. We extended the setup with a second branch to perform two-colour spectroscopy.[32] The 35 ps pulses from an actively and passively mode-locked Nd:YAG laser (repetition rate 10 Hz) are used to pump two identical parametric branches, each consisting of three 5 (or 3) cm long LiNbO₃ crystals (optical axis cut at 47.1°). The infrared generated in the first crystal is amplified in the two other crystals, resulting in $\sim 150 \mu\text{J}$ idler energy per pulse. The wavelength and spectral contents of the infrared pulses are monitored by frequency doubling the signal pulses in a BBO crystal and registering the spectrum of this light by means of an Optical Multichannel Analyser (OMA). Conservation of energy dictates that the bandwidth of the generated signal pulse is identical to that of the idler pulse, so that the idler bandwidth can be deduced

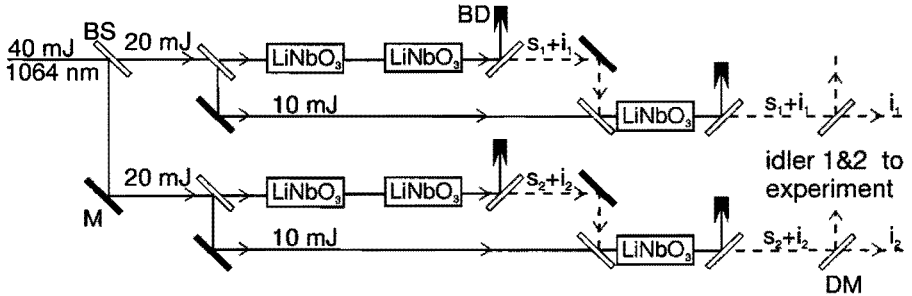


Figure 1.4: Setup for the generation of short, intense tunable infrared pulses. A single 40 mJ pulse from the Nd:YAG laser is split into four equal parts (solid lines) (BS = beamsplitter, M = mirror), which are used to generate and amplify infrared signal (s) and idler (i) pulses (dashed lines). Residual (non-converted) 1064 nm light is collected in beam dumps (BD) after the second and third crystal, and dichroic mirrors (DM) deflect the signal beams (s_1 and s_2) out of the infrared beam. Delays that ensure temporal overlap of infrared ($s+i$) and YAG pulses in the third crystal are not shown.

from the bandwidth of the doubled signal. An example of a spectrum is shown the left panel of Fig. 1.5. The spectral full width at half maximum (FWHM) of the pulses depends on the frequency of the generated light, and is typically 6 cm^{-1} at 2600 cm^{-1} and 30 cm^{-1} at 3600 cm^{-1} .

In the right panel of Fig. 1.5 an autocorrelate of an idler pulse is shown. This correlate is obtained by deflecting $\sim 50\%$ of the idler beam onto a variable delay, and joining the two parts of the pulse in a LiNbO₃ crystal. If the process is properly phase-matched (i.e. the crystal is positioned under the right angle) the second harmonic of the idler can be generated from the two pulses. This can only occur when the two pulses overlap in time. Hence the pulse duration can be obtained by recording the doubled idler intensity as a function of delay between the two pulses. The duration of the infrared pulses is typically 20 ps. Combining this value with the 6 cm^{-1} bandwidth of the pulses, a time-bandwidth product of 3.5 is found. For bandwidth-limited Gaussian pulses, this product is 0.44 [20], demonstrating that the pulses are highly incoherent.

The experimental configuration for the time-resolved pump-probe experiments is depicted in Fig. 1.6. A small fraction of light from the first branch, which will be used as probe, is deflected onto a variable delay (a retro-reflector on a motorized translation stage). An increase in pathlength of 1 mm corresponds to a delay of 3.33

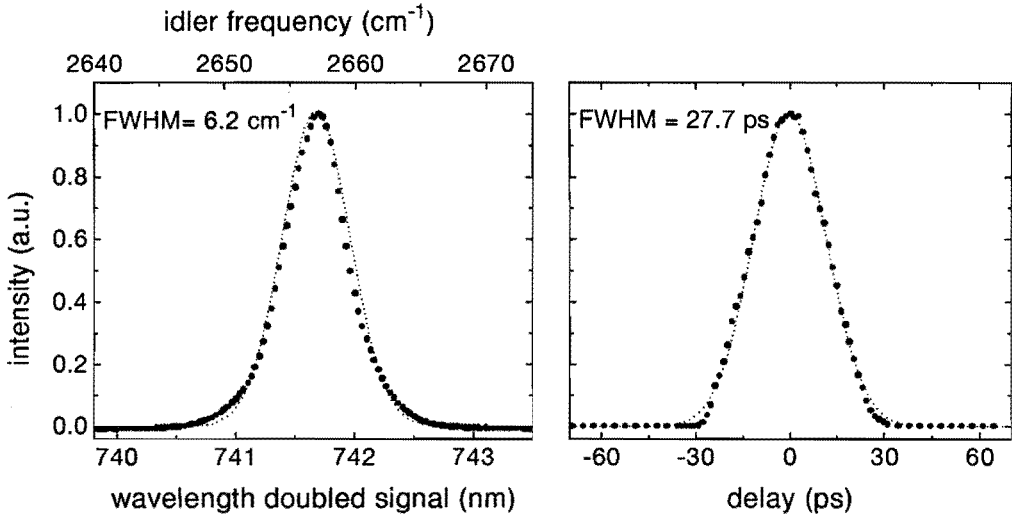


Figure 1.5: Infrared laser characteristics. Left panel: Spectrum of the doubled signal. The corresponding idler frequencies are denoted in the upper abscissa. Dots are data, the dotted line is a Gaussian fit. The idler pulses have a spectral width of a few wavenumbers in this frequency region. Right panel: Autocorrelation trace of the idler pulse. Dots are data, the dotted line is a Gaussian fit. The full width at half maximum (FWHM) of the fitted Gaussian corresponds to a pulse duration of $27.7/\sqrt{2}=19.6$ ps, where the original pulse is assumed to have a Gaussian temporal profile.

ps. The remaining part of the energy can be used as a pump pulse. One or two pump pulses and the probe pulse are focused onto the same spot on the sample with a CaF_2 lens. The focus size is typically 0.3 mm (full width at half maximum) assuming a Gaussian beam waist.

The set-up allows for three kinds of experiments. The first type of experiment is a (one-color) pump-probe delay scan experiment. In this experiment the pump pulse is tuned to the relevant absorption frequency. As a result, a considerable fraction ($\sim 10\%$) of the oscillators is excited from their $v=0$ to $v=1$ vibrational state. Due to the vibrational (self-)anharmonicity the excited state $v=1 \rightarrow v=2$ absorption is red-shifted (typically by ~ 100 cm^{-1}) from the $v=0 \rightarrow v=1$ absorption (see Fig 1.2). The excitation induced by the pump pulse therefore results in a bleaching of the $v=0 \rightarrow 1$ absorption on a picosecond time scale, i.e. a temporary increase of transmission of light

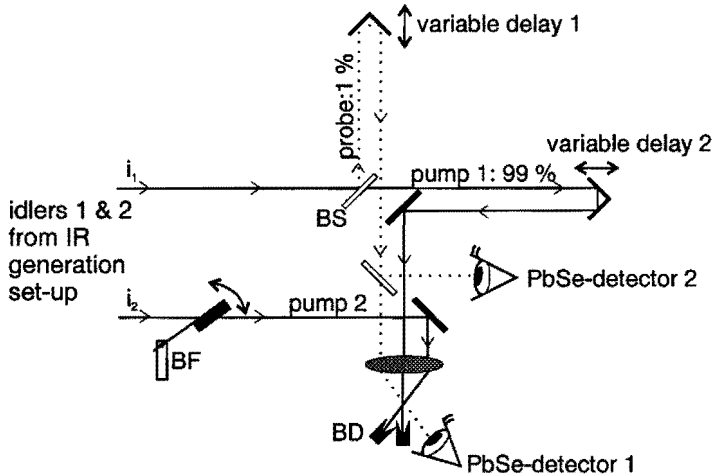


Figure 1.6: Pump-probe configuration for non-linear infrared spectroscopy. Pump and probe beams are focused onto the sample with a 10 cm CaF_2 lens. In reality, the PbSe photoconductive cells monitor the IR light after it is diffusely reflected. The abbreviation BF stands for beam flag, that regulates the pump repetition rate.

at this wavelength through the sample. The subsequent equilibration of the population-distribution can therefore be monitored by measuring the transmission of a weak probe pulse (of the same color) whose time delay with respect to the pump-pulse can be varied. In general, excited population decays exponentially with time, and, since the transmission is proportional to the exponent of the population (Lambert-Beer), the expression for the relaxation of the pump-induced transmission changes reads[30]:

$$\ln[T(t)/T_0] \sim \exp(-t/T_1), \quad (1.19)$$

where $T(t)$ is the transmission at time t , T_0 is the transmission in absence of the pump pulse and T_1 is the energy lifetime of the vibration. Thus the vibrational lifetime of the first excited state can be obtained. It should be mentioned that monitoring the population difference between the ground and first excited state does not necessarily render the lifetime in the first excited state. Intermediate levels may play a role in the decay process. In that case the time evolution of the population difference between $v=0$ and $v=1$ is determined by *two* (or more) decay constants. With a two-colour pump-probe delay scan, it can be determined whether or not decay from $v=1$ occurs

directly to $v=0$. In these experiments, the decay of the $v=1\rightarrow 2$ transient, excited-state absorption band, called the hot band, can be measured. If the decay of this pump-induced absorption is synchronous with the decay of the pump-induced transmission at the fundamental ($0\rightarrow 1$) frequency, it is evident that the decay is effectively direct.

The second type of experiment is a two-color frequency-scan experiment. In this experiment transient absorption spectra are recorded. The pump pulse is tuned to the peak of the $0\rightarrow 1$ absorption band, the delay between the pump and probe pulse is fixed, and the wavelength of the probe is scanned. A spectrum $\ln[T(t_d)/T_0]$, at fixed time delay t_d , is recorded, which reflects the pump-induced spectral changes. This is called a transient spectrum. As stated above, the spectral effect of the pump pulse is twofold: After the pump pulse has excited the oscillators to their first excited state, the $0\rightarrow 1$ transition is bleached, resulting in an increased transmission at this frequency, but simultaneously absorption from $v=1$ to $v=2$ becomes possible. From the width of the spectral hole that is burnt in the $0\rightarrow 1$ absorption band we can deduce the homogeneous linewidth for the $0\rightarrow 1$ transition. Analogously, the width of the $1\rightarrow 2$ transition (hot band) contains information on the vibrational dynamics of the $1\rightarrow 2$ transition.

In the third type of experiment, a two-color, 3-pulse, pump-pump-probe experiment, the first pump pulse is tuned to the $0\rightarrow 1$ transition, followed promptly by a second pump pulse tuned to the $1\rightarrow 2$ transition (slightly to the red). With this scheme approximately 5% of the oscillators can be excited to the second excited state $v=2$. With the probe pulse the population difference between the ground and first excited state, or between the first and the second excited state can be monitored as a function of delay between the pump pair and the probe. With this experiment, the lifetime of the *second* excited state can be obtained, as well as information on the decay route from $v=2$ down to $v=0$ (directly, or *via* $v=1$).

A reference detector is always used to account for shot-to-shot intensity fluctuations (detector 2 in Fig. 1.6). Every other pump shot was blocked with a beam flag (BF in Fig. 1.6) so that both $T(t)$ and T_0 in Eq. (1.19), i.e. the effect of the pump pulse, could be measured in one experimental run, and to suppress steady-state heating of the sample due to the relatively large amounts of energy absorbed in the sample.

The three times smaller bandwidth (allowing for better spectral resolution) and a reduced scattering of the infrared pump light at O–D stretch frequencies compared to O–H frequencies are the reasons why most of the experiments in this thesis are on deuterated zeolite samples. From the experiments that were performed on the non-deuterated O–H groups, we deduce that the results in this thesis for the O–D groups hold for the O–H groups as well.

1.5 Outline of this thesis

The outline of this thesis is as follows: In Chapters 2, 3 and 4 the results of one-colour pump-probe experiments are presented. In Chapter 2 the vibrational relaxation of zeolite hydroxyls in vacuum is investigated. In Chapter 3 we examine the effect of weakly bound adsorbates on the vibrational relaxation rate of the hydroxyls, and Chapter 4 investigates what happens to the excess energy *after* vibrational relaxation.

Two-colour infrared (hole-burn) and two-colour pump-pump-probe experiments are presented in Chapter 5, where we investigate the homogeneous linewidth of the zeolite hydroxyl in vacuum and hydrogen-bonded to adsorbates. Throughout this thesis, the results of the time-resolved experiments on zeolites will be compared to results in liquids, where a multitude of experiments has provided appreciable understanding of vibrational relaxation processes. These insights can be used for a better interpretation and understanding of the relaxation experiments in zeolites. In Chapter 6 the two-colour technique is applied to study the vibrational dynamics of methanol in solution and adsorbed to a sodium zeolite, and in Chapter 7 of methanol adsorbed to the acid form of the same zeolite. Dessert is served in Chapter 8, which reports an investigation of vibrational relaxation of small organic molecules in solution, in particular the effect of intermolecular solute-solvent interactions on vibrational relaxation rates and pathways. The results of this study are used to understand part of the results in Chapter 5.

Chapter 2

Vibrational relaxation of deuterated hydroxyls in acidic zeolites

In this picosecond time-resolved study of the vibrational dynamics of deuterated zeolite hydroxyls, we conclude from the lifetime of the O–D stretch vibration that the protons in Y zeolite as well as in Mordenite are hydrogen-bonded to zeolite framework oxygen atoms. In contrast, for the deuterated zeolite ZSM-5 no evidence for hydrogen bonding is found.

2.1 Introduction

Acidic zeolites are widely applied in hydrocarbon conversion reactions in the petrochemical industry. Their acidity is due to Brønsted active hydroxyl groups, the catalytically active sites. The hydroxyl group is located between a silicon and an aluminum atom. The relation between the infrared absorption frequency of the O–H stretch vibration, the local environment of the zeolite hydroxyl and its acidity has been the subject of ongoing research.[6, 33–39] We apply non-linear picosecond infrared spectroscopy to investigate the dynamics of the O–D stretch vibration of deuterated hydroxyls in zeolites. From these one-colour pump-probe experiments we obtain the vibrational population lifetime T_1 of this vibration, which cannot be obtained by conventional infrared spectroscopy, due to the fact that the width of the absorption bands is determined by inhomogeneous broadening (see Chapter 1): The population lifetimes are in the order of 100 ps [40–46], corresponding to a bandwidth of 0.05 cm^{-1} (see Eq. (1.8)), whereas the absorption linewidths are in the order of 30 cm^{-1} . With the investigation of *deuterated* zeolite hydroxyls (O–D instead of O–H) novel information on the vibrational dynamics of these groups in several zeolites is obtained, due to the better signal-to-noise and enhanced spectral resolution.

2.2 Experimental

Three different zeolites were investigated in the experiments: Y-zeolite, Mordenite and ZSM-5. The properties of these zeolites and their infrared O–D absorption bands can be found in Table 2.1. Our zeolite samples consist of pressed self-supporting discs of 3.5 to 6 mg/cm^2 . Recently, especially the acidity of the zeolite Mordenite has been the subject of much research.[34–39] Proton loaded zeolites were obtained by heating *in vacuo* (for Y and ZSM-5 at least 1 h at 723 K, for Mordenite 1 h at 823 K) zeolites in which Na^+ cations were exchanged by NH_4^+ cations. Deuteration was achieved by adding 500 mbar of D_2 -gas (Messer Griesheim, 99.7%) at 723 K and allowing exchange for 1 hour, resulting in approximately 70% H→D exchange.

An extensive description of the experimental setup can be found in Chapter 1. In short, for these one-colour pump-probe experiments, a generated IR pulse is split into a pump pulse (99%) and a weak probe pulse (1%). A considerable fraction ($\sim 10\%$) of the hydroxyl groups is excited from their $v=0$ to $v=1$ vibrational state by the pump pulse tuned to the hydroxyl absorption frequency. Due to a large anharmonicity (the O–D $v=1\rightarrow v=2$ absorption is shifted by about 100 cm^{-1} from the $0\rightarrow 1$ fundamental absorption[43, 47]) the excited O–D ($v=1$) cannot absorb the pump light. The equili-

Table 2.1: Overview of some experimental parameters and results of the experiments: Zeolite chemical composition [$D/(Si+Al)=0.7 \times H/(Si+Al)$], properties of the absorption bands (center frequency $\tilde{\nu}_{\max}$ and full width at half maximum $\Delta\tilde{\nu}$), and observed lifetimes.

Zeolite	Si/Al	D/(Si+Al)	band	$\tilde{\nu}_{\max}$ (cm^{-1})	$\Delta\tilde{\nu}$	T_1 (ps)
Y	2.8	0.19	LF	2620	42	20 – 60
			HF	2684	20	100 – 130
Mordenite	6.7	0.09	LF	2649	40	30 –
			HF	2664	22	– 95
ZSM-5	16	0.04		2665	23	50

bration of the excited population can then be monitored by measuring the transmission the probe pulse whose time delay with respect to the pump-pulse can be varied: The decay of the pump-induced transparency reflects decay of excited state population. The values for the vibrational lifetimes can therefore be obtained by fitting an exponential to the signal for large delay (see Eq. 1.19). For lifetimes comparable to, or shorter than the pulse duration of 20 ps, the whole signal can be used to extract the vibrational lifetime. The transient can then be fitted by numerically solving the set of coupled spatio-temporal rate equations for a two-level system describing the passage of the pump pulse through the sample:

$$\frac{\partial \Delta N(z, t_p)}{\partial t_p} = -\frac{\sigma_{01}}{h\tilde{\nu}} I_{\text{pump}}(z, t_p) \Delta N(z, t_p) + (1/T_1)[1 - \Delta N(z, t_p)] \quad (2.1)$$

$$\frac{\partial I_{\text{pump}}(z, t_p)}{\partial z} = -\frac{\sigma_{01}}{V} \Delta N(z, t_p) I_{\text{pump}}(z, t_p), \quad (2.2)$$

in which $\Delta N(z, t_p)$ denotes the the space- and time-dependent normalized population difference between the ground ($v=0$) and excited state ($v=1$), $\Delta N = N_0 - N_1$, t_p the time coordinate in a moving frame ($t_p = \hat{t} - (\hat{z}/c)$)[20], z denotes the coordinate along which the light propagates ($z = \hat{z}$), σ_{01} the absorption cross section for the $0 \rightarrow 1$ transition, $h\tilde{\nu}$ the IR photon energy, $I_{\text{pump}}(z, t_p)$ the pump intensity and V the irradiated volume. After integrating these equations over sample length z , they reduce to one differential

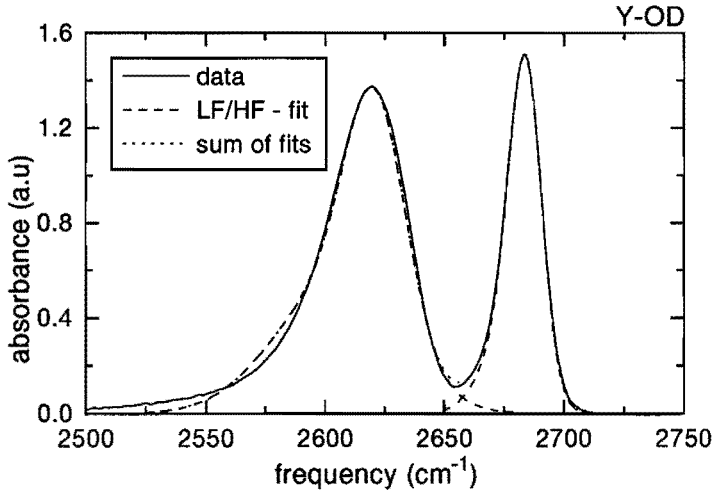


Figure 2.1: Absorption spectrum for O–D absorption bands for deuterated zeolite Y. The LF-peak at 2620 cm^{-1} is caused by hydroxyls situated in the small sodalite cages, the HF-peak by hydroxyls sticking into the super cage. Fits are double-Gaussian fits to both LF- and HF-peak.

equation for the spatially integrated population difference $\int_{z=0}^{z=L} \Delta N(z, t_p) dz$. This differential equation is solved numerically by means of a Runge-Kutta scheme[48], after which the transmission of the probe is evaluated. The amount of transmitted probe is determined by the population difference between the two levels associated with the appropriate transition:

$$T_{\text{probe}}(t + t_p) = T_{\text{probe}}^{\text{in}} \exp\left[-\frac{\sigma_{01}}{V} \int_{z=0}^{z=L} \Delta N(z, t + t_p) dz\right] \quad (2.3)$$

These calculations require as input laser pulse parameters (duration, energy and frequency) and sample parameters (cross-sections, density, sample length and relaxation times). Apart from the relaxation times all these parameters can be determined independently.

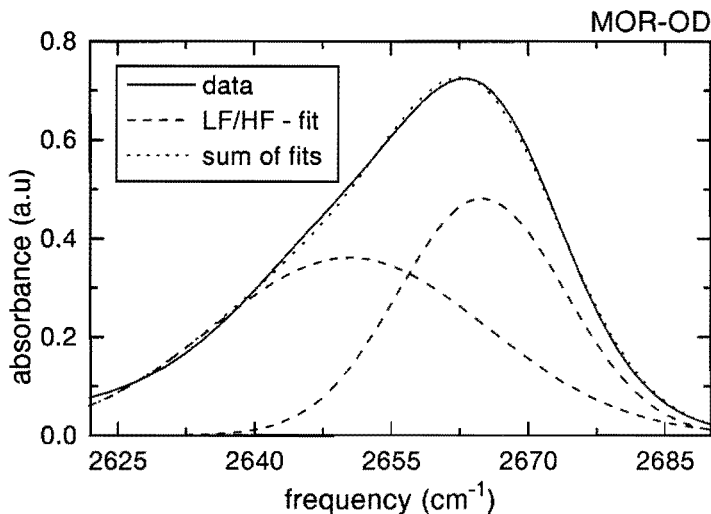


Figure 2.2: Absorption spectrum for D-Mordenite in the O–D stretching region. Dashed lines are Gaussian deconvolutions corresponding to O–D oscillators situated in 8-ring cavities (LF) and 12-ring cavities (HF).

2.3 Results

In Figures 2.1 and 2.2 the conventional infrared absorption spectra for zeolite D-Y and D-Mordenite are depicted. It is well known that in zeolite Y the LF-peak is caused by hydroxyls located in the small cages, whereas the HF-peak is caused by hydroxyls in the larger cavities.[49] In a recent paper [38] it was demonstrated that —similar to Y-zeolite— the absorption band of Mordenite consists of two contributions as well: LF- and HF- subpeaks, resulting from hydroxyls in the small 8-ring cages ($2.6 \times 5.7 \text{ \AA}$) and in the larger 12-ring cages ($6.5 \times 7.0 \text{ \AA}$), respectively. The deconvolution was carried out for our O–D absorption spectra and the results obtained (see Fig. 2.2) were similar to those for the O–H groups found in ref [38].

Three typical results of pump-probe experiments for deuterated Y zeolite are shown in Figure 2.3. If the laser-frequency is tuned to the red side of the LF absorption band (at 2611 cm^{-1}), a T_1 of 32 ps is found. At the blue side of this absorption band (at 2639 cm^{-1}) a much larger T_1 of 60 ps is observed. With the laser tuned to the HF absorption band a lifetime of $T_1=124 \text{ ps}$ is observed.

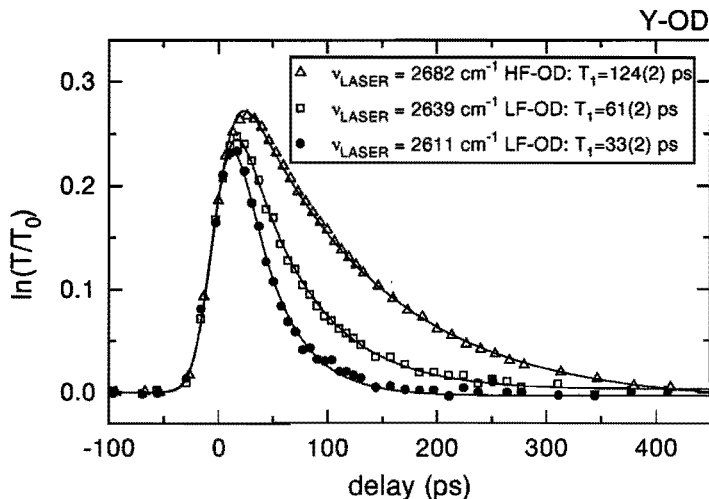


Figure 2.3: Relative transmission of an infrared probe pulse $\ln(T/T_0)$ (T_0 is the transmitted probe energy in absence of the pump pulse) as function of the delay between pump and probe pulses for zeolite Y-O-D at three laser frequencies. The vibrational relaxation times, strongly dependent on frequency, are denoted in the graph. To allow for a better comparison, the 2682 cm^{-1} $\ln(T/T_0)$ values were divided by 2. The lines are solutions to Equations (2.1)-(2.3), with relaxation times (and errors) denoted in the graph.

In principle, only a two-colour experiment directly yields the population lifetime of the excited vibrational mode. In these experiments, relaxation of the $v=1 \rightarrow 2$ transient absorption is monitored after excitation of the $v=0 \rightarrow 1$ fundamental. It could be possible that decay from $v=1$ is not direct to $v=0$, but intermediate levels play a role in the relaxation process. If that were so, then the decay of the pump-induced transmission at $v=0 \rightarrow 1$ would be different from the decay of the pump-induced absorption at $v=1 \rightarrow 2$. A result of a two-color experiment on the LF-OD groups in Y zeolite is shown in Fig. 2.4. It is clear that the decay of the induced transmission at 2639 cm^{-1} is identical to the decay of the induced absorption ($v=1$ to $v=2$) at 2528 cm^{-1} . Hence it is clear that $v=1$ excited state population decays directly to the $v=0$ ground state. Furthermore, it has been demonstrated that, in contrast to the undeuterated O-H groups, for the O-D experiments spectral diffusion is negligible[22] (due to lower concentrations of oscillators and smaller transition dipole moments compared to the O-H vibrations).

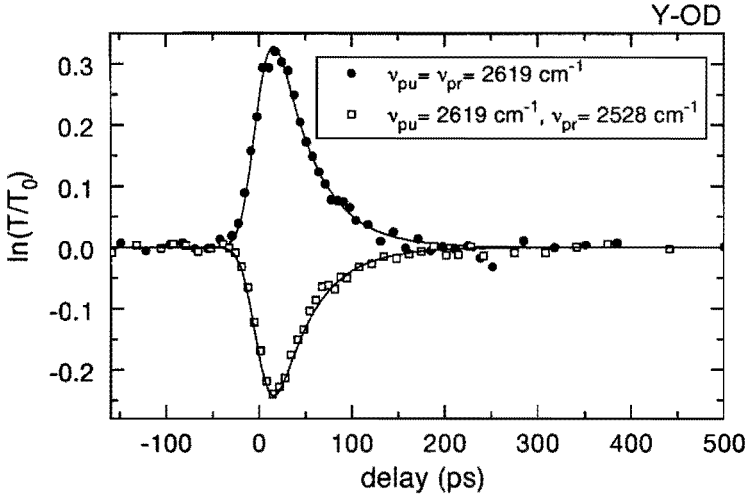


Figure 2.4: Transmission changes due to an infrared pump pulse at 2619 cm^{-1} probed at the fundamental (\bullet : $v=0$ to $v=1$, 2619 cm^{-1}) and the hot-band transition (\square : $v=1$ to $v=2$, 2528 cm^{-1}), as a function of delay between pump and probe. The two measurements can be described by one calculation (mirrored around $y=0$), demonstrating that from the one-colour experiments the lifetime of the $v=1$ first excited state can be extracted.

Also, effects caused by the finite laser bandwidth (spectral averaging), which are known to mystify the interpretation of decay times as vibrational lifetimes (the 'Brugmans-effect'[22]) are of little consequence for O-D experiments. Therefore, the decay of the pump-induced transmission changes can be straightforwardly interpreted in terms of vibrational population decay.

In Fig. 2.5 T_1 is plotted as a function of laser-frequency scanned through the two absorption bands for Y-zeolite. In the zeolite Mordenite, a similar behaviour of T_1 with frequency is observed (Fig. 2.6). For deuterated ZSM-5 the absorption spectrum and the lifetime T_1 as a function of frequency $\tilde{\nu}$ can be found in Fig. 2.7. Within experimental accuracy, the vibrational relaxation time T_1 seems to be independent of frequency for this zeolite. It should be noted that due to the low density of O-D groups in this zeolite (high Si/Al-ratio), the transient $\ln(T/T_0)$ -signals are small resulting in relatively large uncertainties in the measured lifetime.

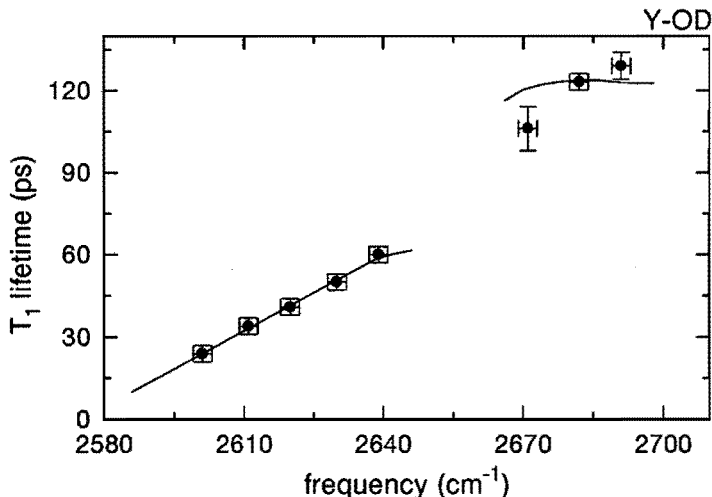


Figure 2.5: T_1 as a function of laser frequency for D-Y. Closed circles are data points, error bars denote $\pm 2\sigma$. The lines are simulations with T_1^{HF} fixed at 123 ps. It is evident the simulations cannot adequately describe data.

2.4 Discussion

Vibrational relaxation entails the redistribution of the vibrational energy into a number of low-frequency vibrations, under the condition that the sum of energies of these accepting modes equals that of the relaxing mode (energy match condition).[14–16] Possible accepting modes are Si/Al–O stretching and bending modes (frequencies typically $\sim 400\text{--}1100\text{ cm}^{-1}$)[50], and O–D in-plane and out-of-plane bending modes (frequencies ~ 900 and $\sim 300\text{ cm}^{-1}$, respectively)[51, 52]. It is remarkable that upon an increase in the oscillator energy of 1% (going from 2611 to 2639 cm^{-1}), the relaxation rate increases by almost a factor of two (from 34 to 61 ps, See Fig. 2.3). It is highly unlikely that this drastic effect is caused by a better energy match between the O–D stretch energy and the sum of energies of the accepting modes at lower frequencies, since the density of states of the low-frequency modes is very broad.[50–53]

This type of frequency dependence has been observed previously for the population lifetime of the vibrations of (i) surface hydroxyls on colloidal silica[54], (ii) hydroxyls in fused silica [55, 56] (iii) O–H groups in natural micas[57], (iv) S–H groups in vitreous

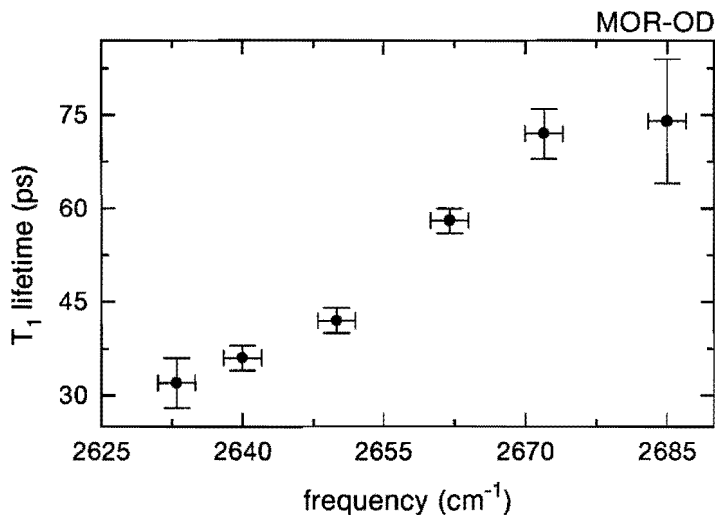


Figure 2.6: T_1 as a function of laser frequency for Mordenite O-D. Again, T_1 is found to increase with frequency. Error bars denote $\pm 2\sigma$.

As_2S_3 [58] and (v) of undeuterated hydroxyls in zeolites H-Y and H-Mordenite[44]. In these studies, it was shown that an increase of T_1 with frequency is caused by different degrees of hydrogen bonding. In case of the zeolite, the hydroxyls are hydrogen-bonded to lattice oxygen atoms[44]: hydroxyls with a stronger H-bond will have a weakened O-H bond and consequently exhibit a decreased absorption frequency. Simultaneously the H-bond enhances the coupling to accepting modes, which results in a faster decay.[44] The effect of the hydrogen bond on the anharmonic coupling, responsible for the faster decay, is discussed in more detail in the following Chapter. Hydrogen bonding thus accounts for the decrease in T_1 at lower frequencies. In a previous time-resolved vibrational study on undeuterated HY-zeolites, the lifetime for the hydroxyls situated in the large cages responsible for the HF-band was found to be independent of frequency[44], contrary to our findings for the O-D groups. A problem with the experiments on the undeuterated zeolites was the fact that the laser bandwidth exceeded the HF-OH absorption linewidth: Measured T_1 times are essentially spectral averages of actual T_1 's within the laser bandwidth. The effects of this spectral averaging are minimized by investigating O-D vibrational relaxation instead of O-H, since the laser bandwidth is over a factor of three smaller at O-D absorption frequencies compared

to O-H frequencies (11 and 34 cm^{-1} , respectively). This broadening is inherent in the generation of our infrared pulses.[59] By contrast, on deuteration the absorption linewidths are only 30% narrower.

For the LF-OD groups of Y zeolite, it is clear that the observed frequency dependence can be attributed to hydrogen-bonding of the deuterated hydroxyl groups. However, the frequency dependence of T_1 in Mordenite might be due to two *frequency independent* contributions — an HF-contribution with T_1^{HF} and an LF-contribution with T_1^{LF} — spectrally averaged by the effects described above. The second possibility is that there is a real frequency dependence in one or both of the sub-peaks. As for the observed frequency dependence of T_1 of the HF-peak in Y-OD, this can also be caused by either overlap with the LF-peak and spectral averaging effects due to the $\sim 11 \text{ cm}^{-1}$ laser bandwidth, or a real frequency dependence. To check whether or not our data can be explained by this type of averaging effects effects, we calculated the transient transmission changes.

2.5 Calculation of the transients

In general the expression for the time-dependent transmission for a homogeneously broadened absorption peak after a pump pulse reads:

$$T(t) = \int_0^\infty d\tilde{\nu} L(\tilde{\nu}) \exp[-A(\tilde{\nu})(1 - 2f_0 \exp(-t/T_1))] \quad (2.4)$$

where $T(t)$ is the transmitted energy of the probe pulse at delay t , $L(\tilde{\nu})$ the laser band, $A(\tilde{\nu})$ the absorption band, and f_0 the excited fraction of oscillators at $t=0$. In Eq. (2.4) the fraction of excited oscillators does not depend on frequency, as would be the case for inhomogeneous broadening; for inhomogeneously broadened bands the expression is somewhat more complicated. This simplification does not affect the results of our calculations, however. If the total absorption band can be split into two subbands, i.e. having a high-frequency (HF) and low-frequency (LF) component, the total absorption band can be written as: $A(\tilde{\nu}) = A^{\text{LF}}(\tilde{\nu}) + A^{\text{HF}}(\tilde{\nu})$, and the time-dependent transmission reads:

$$T(t) = \int_0^\infty d\tilde{\nu} L(\tilde{\nu}) \exp[-A^{\text{HF}}(\tilde{\nu})(1 - 2f_0 \exp(-t/T_1^{\text{HF}})) - A^{\text{LF}}(\tilde{\nu})(1 - 2f_0 \exp(-t/T_1^{\text{LF}}))] \quad (2.5)$$

Thus, the effect of the two contributions with different T_1 times can be calculated. This procedure enables us to calculate $T(t)$, the transmission of the probe pulse, by solving

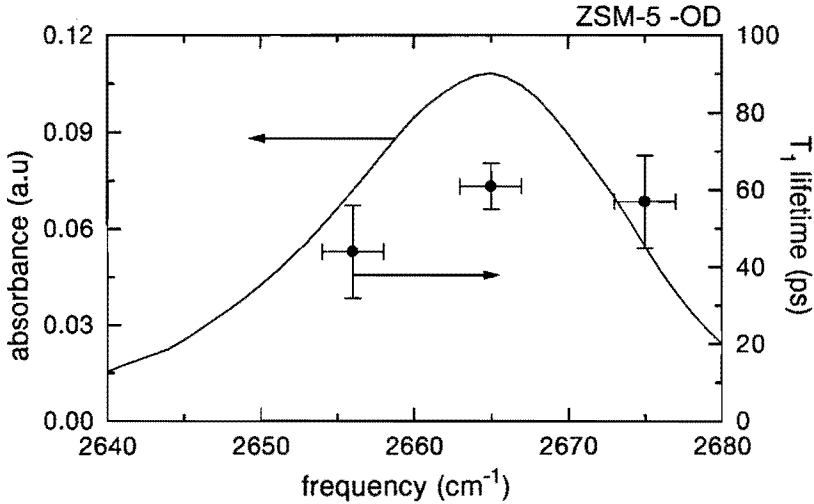


Figure 2.7: Absorption spectrum and vibrational relaxation times for D-ZSM-5. Right axis corresponds to absorption spectrum (dotted line), left axis to T_1 -times (black circles).

Eq. (2.5) numerically. Subsequently, the calculated $\ln[T(t)/T_0]$ is treated in the same way as the data to extract a lifetime T_1^{calc} . We can perform this calculation at different frequencies and in this fashion we obtain $T_1^{\text{calc}}(\tilde{\nu})$, and compare it to the experimentally observed frequency dependence of the lifetime $T_1(\tilde{\nu})$. Input variables are $A^{\text{LF}}(\tilde{\nu})$ and $A^{\text{HF}}(\tilde{\nu})$ with corresponding T_1^{LF} and T_1^{HF} , optionally frequency dependent.

For zeolite D-Y we calculated what the outcome of our experiments would be for T_1^{LF} increasing linearly with frequency as observed, and T_1^{HF} independent of frequency with a value of 123 ps. The results of this calculation for are presented in Fig. 2.5 together with the data. A comparison between the observed and calculated dependence of T_1 on frequency indicates that the observed dependence at HF-OD frequencies cannot be due to overlap of different (LF and HF) absorption bands in the spectrum with the laser band; the data cannot be reproduced by the calculations with frequency independent T_1^{HF} . This is conclusive evidence for a frequency dependent T_1^{HF} , contrary to what was previously found for the O-H groups.[44] The frequency dependence of the T_1^{HF} points to a very weak hydrogen bond for these hydroxyls, since the lifetimes are much larger than for the LF-OD groups.

An effort to reproduce the dependence of T_1 on frequency for Mordenite with T_1^{LF}

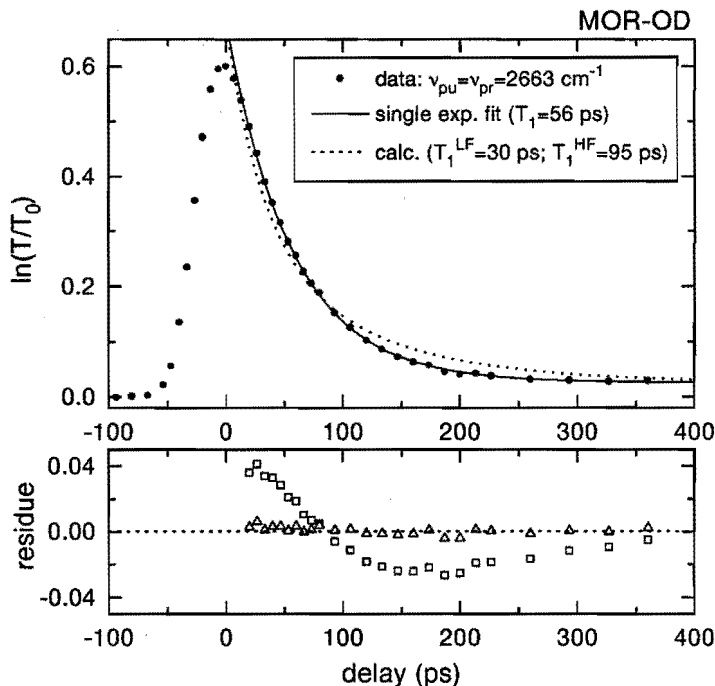


Figure 2.8: Upper panel: Results of a pump-probe experiment at the top of the Mordenite O–D peak. Data (full circles), single exponential fit (solid line) and simulation (dotted line). The result of the simulations has a distinct non-exponential decay, contrary to the data. Lower panel: Residues from subtracting the two fits from the data indicate the aptness of the simple exponential fit (Δ), in contrast to the double exponential decay (\square).

and T_1^{HF} both independent of frequency, resulted in values of 30 and 95 ps. While these values describe the frequency dependence of the $T_1(\bar{\nu})$ -data very well, two fixed lifetimes imply that the decay of $\ln[T(t)/T_0]$ at intermediate effective decay times (e.g. 56 ps) is doubly exponential, since the calculated decay curves are a mixture of T_1^{LF} - and T_1^{HF} -decay. This is conflicting with experimental data. Experimentally we only observe clear single exponential decays; in Fig. 2.8 the experimental data and the result of the simulation are plotted. Despite the good description of the $T_1(\bar{\nu})$ -data, the clear single exponential decay of $\ln[T(t)/T_0]$ defies the existence of two fixed lifetimes. We can thus conclude that one or both of the two subpeaks must exhibit frequency dependent

behaviour with respect to T_1 , indicative of hydrogen bonding.

For D-ZSM-5 (spectrum and $T_1(\tilde{\nu})$ in Fig. 2.7.) no significant dependence of the lifetime on the frequency could be found. It should be noted that the frequency range over which the experiments were performed is small (20 cm^{-1}) compared to the experiments on Y and Mordenite. The protons in ZSM-5 are all situated in the 10-ring channel and it was shown recently that these protons are energetically very similar.[60,61] Apparently the differences are sufficiently small so that no difference in hydrogen bond strength between the different protons can be detected, accounting for the absence of a significant frequency dependence.

2.6 Conclusions

Frequency-dependent T_1^{OD} vibrational lifetimes are observed in zeolite Y, both for the HF- and LF-peak, confirming the previously observed hydrogen bonding of the LF-hydroxyls in the small sodalite cages. The frequency dependence of the HF-hydroxyls is tentatively attributed to weak hydrogen bonding of these hydroxyls.

For Mordenite this frequency dependence of T_1 is found as well. It is asserted with the help of a simple model that this dependence must be due to an intrinsic dependence of T_1 on $\tilde{\nu}$ in one or both of the two hydroxyl species causing the absorption peak in Mordenite. The most likely candidate are the hydroxyls in the smaller 8-ring cages, causing the downshifted and broadened LF- absorption peak, by analogy with Y-zeolite.

For ZSM-5, within experimental accuracy, no frequency dependence of the lifetime is observed, indicative of the absence of a distribution of hydrogen bond strengths in this zeolite, in accordance with the observation that the hydroxyls in ZSM-5, although crystallographically different, are energetically very similar.

Chapter 3

Enhancement of the vibrational relaxation rate of surface hydroxyls through hydrogen bonds with adsorbates

With time-resolved (picosecond) infrared saturation spectroscopy the interaction of zeolite surface hydroxyls with small adsorbed molecules is investigated. It is found that the presence of the adsorbate, which is weakly hydrogen bonded to the zeolite hydroxyl causes the vibrational lifetime of the zeolite hydroxyl to decrease significantly. Remarkably, this enhancement of the de-excitation is not due to energy transfer to internal degrees of freedom of the adsorbed species, nor is the energy used for a one-photon desorption process. Rather, it is due to the fact that the hydrogen bond act as an additional accepting mode, allowing for faster energy flow out of the excited hydroxyl.

3.1 Introduction

The catalytically active site in acid zeolite catalysts is the Brønsted hydroxyl (O–H) group, located between a silicon and an aluminum atom, pointing into the zeolite cavity.[9] Knowledge of the interaction between the Brønsted catalytic sites and adsorbed species is essential for a fundamental understanding of zeolite catalysis. Time-resolved (picosecond) infrared spectroscopy has been proven to be a powerful tool in the investigation of the vibrational dynamics of the condensed phase in general [29] and the zeolite hydroxyl in particular [22, 40, 42–44, 53, 62, 63]. In this Chapter, we employ this technique to investigate the effect of small molecules adsorbed to the zeolite hydroxyls on the lifetime of the hydroxyl stretching mode.

3.2 Experimental

We investigated the vibrational lifetimes of hydroxyls in two zeolites: Y and Mordenite. The zeolite samples consist of pressed self-supporting crystalline zeolite discs of 5 mg/cm². Acid forms of zeolites were obtained by *in vacuo* heating (1 h at 743 K) of Mordenite in which Na⁺ cations were exchanged by NH₄⁺ cations. The Mordenite under investigation was specified by Si/Al- and H/(Si+Al) atomic ratios of 6.7 and 0.13 respectively. For the partially exchanged zeolite Y, Si/Al= 2.8 and H/(Si+Al)= 0.07. In some of the experiments the zeolite hydroxyls were deuterated by exposing the zeolite disc to 500 mbar of D₂-gas (Messer Griesheim, 99.7%) at 693 K and allowing exchange for 1 hour, resulting in approximately 70% exchange as observed from the absorption spectra. Adsorption of argon, oxygen, nitrogen and methane was performed at 100 K at pressures ranging from 200 mbar to 2 bar, constant during the experiments.

The experimental setup and the one-colour pump-probe technique have been described in Chapter 1. In short, the pump pulse excites a considerable fraction ($\approx 10 - 20\%$) of the O–D oscillators from their $v=0$ to $v=1$ vibrational state. Due to the ~ 100 cm⁻¹ anharmonicity of the vibration [43, 47], the absorption is bleached on picosecond time scales, so that the equilibration of the population-distribution can be monitored by measuring the transmission of the probe pulse. The decay of the pump-induced transmission with time is related to the vibrational lifetime of the excitation T_1 , as: $\ln[T(t)/T_0] \sim \exp(-t/T_1)$, where $T(t)$ is the transmitted energy of the probe pulse at delay t and T_0 is the transmitted probe energy in absence of the pump pulse.

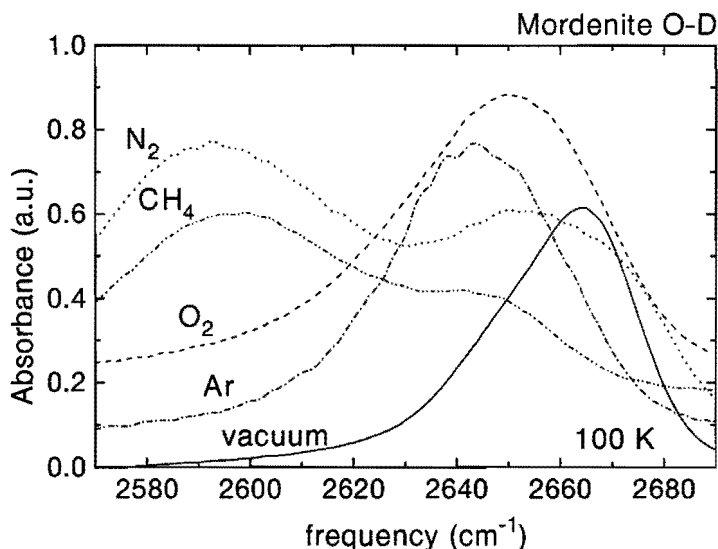


Figure 3.1: Absorption spectra in the O–D stretch region of Mordenite O–D in vacuum and with several molecules adsorbed. All spectra were recorded at 100 K. Note the shift to lower frequencies upon adsorption.

3.3 Results

A downshift of the O–D absorption frequency occurs upon adsorption of argon, nitrogen, oxygen and methane on D-Mordenite at 100 K (Fig. 3.1). This is caused by a weakening of the original O–D-bond due to the presence of the hydrogen bond between the hydroxyl deuteron and the adsorbed species.[64] Note that upon adsorption of N₂ and CH₄ two distinctive peaks appear: a low-frequency peak due to the perturbed species, i.e. hydroxyls at which adsorption is occurring, and the residue of the non-perturbed species, on which no adsorption takes place, at higher frequencies.

Two typical results of pump-probe experiments for the case of nitrogen adsorption are depicted in Fig. 3.2. The absorption spectrum for this sample is shown as the dotted line in Fig. 3.1. For the unperturbed O–D groups ($\tilde{\nu} = 2667 \text{ cm}^{-1}$), T_1 -times are equal to those found for the O–D sample in vacuum at this frequency ($T_1 = 60(\pm 4)$ ps). The hydrogen bonded species ($\tilde{\nu} = 2592 \text{ cm}^{-1}$), are found to relax faster ($T_1 = 10(\pm 6)$ ps), and an *increased* transmission after vibrational relaxation is observed.

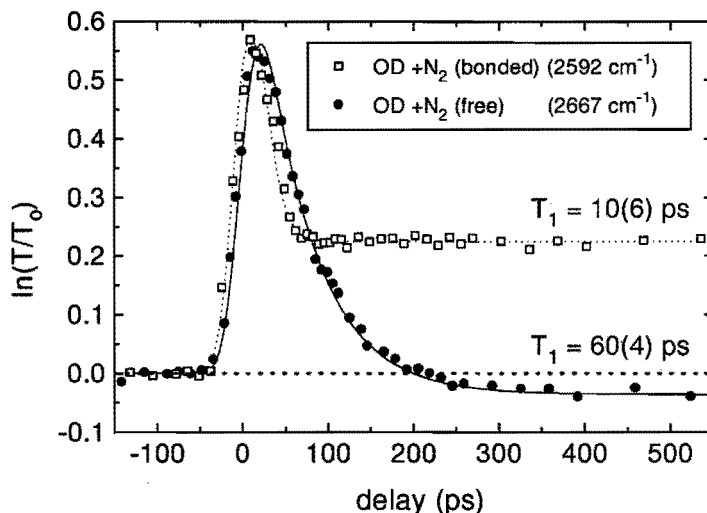


Figure 3.2: Results of pump-probe experiments at two different laser frequencies of a Mordenite sample with N_2 adsorbed (absorption spectrum depicted as dotted line of Fig. 3.1). Relative transmission of an infrared probe pulse $\ln[T(t)/T_0]$ (T_0 is the transmitted probe energy in absence of the pump pulse) as a function of the delay between pump and probe pulses. The values for the fitted energy decay times T_1 (and the corresponding standard deviations) were obtained by numerically solving the appropriate differential rate equations (2.1)-(2.3), the result of which are shown as lines in the figure. The vibrational relaxation time is found to drop dramatically upon hydrogen-bonding and for the hydrogen-bonded species an increased transmission is observed after relaxation.

In Fig. 3.3 the results of the pump-probe experiments are summarized: the vibrational lifetime decreases continuously with decreasing frequency, and the lifetime is hardly dependent on the species adsorbed. The lifetimes were obtained by numerically solving the appropriate differential equations given in the previous Chapter [Eq. (2.1)-(2.3)], that simultaneously account for population excitation and relaxation (multiple absorption steps are allowed). To describe the transmission offsets after relaxation, a third level was incorporated. In this model, relaxation from $v=1$ takes place to $v=0^*$, from which absorption to $v=1^*$ can occur with a slightly different cross-section. For lifetimes shorter than the pulse duration, an accurate estimate of the lifetime can be obtained from the width and magnitude of the signal.

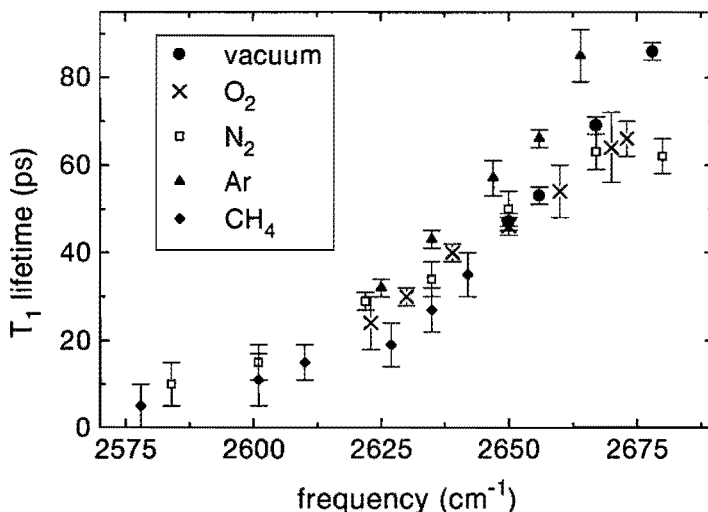


Figure 3.3: The vibrational lifetime T_1 as a function of laser frequency for Mordenite O-D with and without adsorption. T_1 is found to increase with frequency. The laser bandwidth with Gaussian shape has a full width at half maximum of 10 cm^{-1} . Error bars denote $\pm 2\sigma$.

Also, we adsorbed N_2 on the so-called HF (high-frequency) hydroxyls in zeolite Na/HY. In zeolite Y there are two types of hydroxyls, with distinctly separated absorption bands (Fig. 3.4). The low-frequency (LF) hydroxyls are situated in the small cages, whereas the HF sites are situated in the large super cages.[65] In the partially exchanged sample used here, mostly HF oscillators are present (Fig. 3.4). Coincidentally, adsorption of N_2 on the HF hydroxyls shifts the HF oscillator frequency to that of the LF hydroxyls.[63] The absorption spectra and results of time-resolved measurements for the vacuum sample and the sample with N_2 adsorbed are shown in Fig. 3.4, respectively. Upon adsorption of N_2 , the lifetimes of the HF hydroxyls decrease by over a factor of three and perfectly coincide with the lifetime of the vacuum LF hydroxyls.

3.4 Energy Transfer Mechanisms

From picosecond transmission measurements on ethanol dissolved in CCl_4 , it was found that the breaking of hydrogen bonds is an effective relaxation channel for the vibrationally excited hydrogen-bonded ethanol hydroxyl.[66] Whereas the monomeric

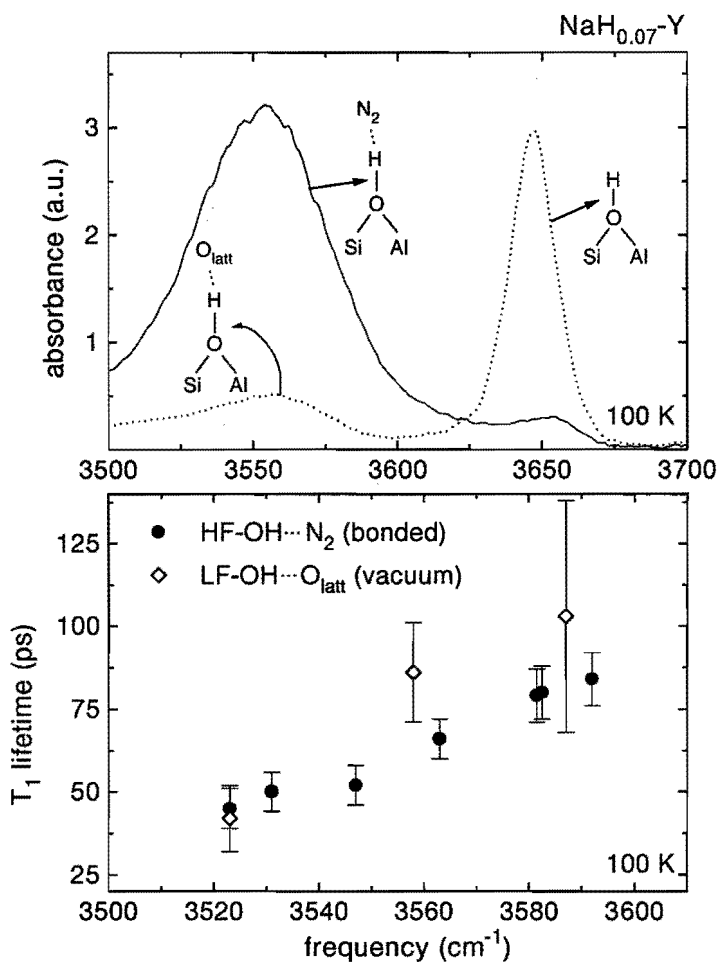


Figure 3.4: Upper panel: Absorption spectrum for the O–H region of zeolite NaH_{0.07}Y (dotted line). Due to the low level of exchange, mainly HF-hydroxyls are present. Upon adsorption of N₂ the absorption band shifts to lower frequencies, coinciding with the LF absorption band (solid line). Lower panel: Vibrational lifetimes for the vacuum LF species and the hydrogen-bonded HF species, both absorbing at the same frequency. The lifetimes and the dependence thereof on frequency are very similar. Note the different ordinate scales for the two figures.

O–H stretching mode exhibited a T_1 lifetime of 70 ps[67], the hydrogen-bonded ethanol showed a lifetime of 5 ps. Also, a fast re-association of the hydrogen bond was observed with a time constant of 20 ps. In our experiments, an increased transmission after complete vibrational relaxation as shown in Fig. 3.2, was observed for all hydroxyls to which a molecule was adsorbed. The increased transmission was found to persist over 2 ns. In principle, this could be due to desorption of the adsorbed species upon vibrational relaxation of the hydroxyl, i.e. a breaking of the hydrogen bond as observed for ethanol (for nitrogen, the heat of adsorption on the zeolite hydroxyl is $1000 \text{ cm}^{-1}/\text{bond}$, i.e. about one third of the vibrational quantum[68]). If desorption were to take place upon vibrational relaxation, the oscillator frequency would shift back to its unperturbed value. Hence, the hydroxyl would no longer absorb light at the laser frequency, since the oscillator frequency would be shifted out of the laser band. This could account for the observed increase in transmission after relaxation (Fig. 3.2), but would require that the hydrogen bond re-association time is much larger ($\gg 2 \text{ ns}$) for the zeolite-adsorbate system than for ethanol in solution (20 ps). Indeed, one would expect re-association to take place faster in liquid ethanol due to the higher density of molecules.

On the other hand, it will be shown in the next Chapter that, upon vibrational relaxation of zeolite hydroxyls, the excess O–D stretch energy becomes delocalized very rapidly (within 10 ps), culminating in an effective heating of the zeolite lattice.[69] As hydrogen bonds are very sensitive to temperature changes, this could also be the cause of the increased transmission after vibrational relaxation. To check whether the transmission offset is due to a *direct* one-photon desorption process or *indirect* desorption due to ultrafast heating, we performed the experiment with decreasing pump-energy.

With decreasing pump-energy, and consequently less heating of the zeolite, relaxation of the transmission to the original equilibrium transmission occurs as shown in Fig. 3.5. This rules out the possibility of one-photon desorption: the magnitude of the signal is proportional to the number of excited oscillators and the offset proportional to the number of shifted oscillators. In case of one-photon desorption one would expect the ratio of the two to be independent of pump-energy. The desorption we observe must then be thermal and indirect, due to rapid delocalization of the excess energy[69]. Thus we conclude that, in contrast to liquid ethanol, *direct* dissociation of the hydrogen bond as a one-photon desorption process, does not occur upon relaxation of the vibrationally excited oscillator.

In principle the internal low-frequency modes of the adsorbed molecule could act as accepting modes, allowing for part of the excess vibrational energy to be transferred to an adsorbate vibrational mode. In this case, one would expect the relaxation rate to

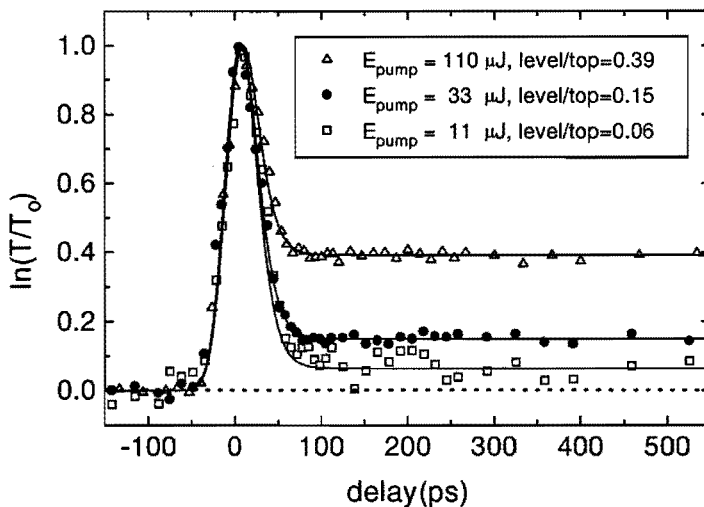


Figure 3.5: Three pump-probe experiments for N_2 -perturbed oscillators in *D*-Mordenite with different pump energies. The signals are scaled to 1. With decreasing pump energy, relaxation to original transmission occurs. The level/top-ratios (ratio of long-time and maximum signal) are also denoted in the graph.

depend critically on the exact internal low-frequency mode distribution of the adsorbed species. We observe, however, that the lifetime is hardly dependent on the adsorbed species (Fig. 3.3, only for Ar the lifetimes seem somewhat larger). This leads us to conclude that there is no direct energy flow from the excited hydroxyl into internal degrees of freedom of the adsorbed molecule: If specific modes of the adsorbed molecules would act as accepting modes, one would expect different lifetimes for different adsorbates, contrary to what is observed. It is only the *magnitude* of the perturbation of the oscillator by the hydrogen bond, *viz.* the hydrogen bond strength, that determines the relaxation rate and not the specific characteristics of the adsorbed species. This is corroborated by the finding that the N_2 -perturbed HF oscillators in the Y zeolite show the same lifetimes as the vacuum LF species absorbing at the same frequency: In Ref. [44] it was shown that in vacuum the LF hydroxyls are already hydrogen bonded to oxygen lattice atoms. Also here, the vibrational relaxation rate is determined by the magnitude of the perturbation, independent whether the perturbation is due to zeolite lattice oxygen or molecular nitrogen.

3.5 The effect of hydrogen bonding on the relaxation rate

From the above, it is clear that, as far as internal degrees of freedom of the adsorbates is concerned, the presence of the adsorbate does not create any new major pathway for the vibrational energy to flow into. It is apparent, however, that despite the fact that the hydrogen bond remains intact upon vibrational relaxation, its presence greatly enhances the relaxation rate.

The rate of vibrational relaxation k_{vr} of the excited vibration is generally described by Fermi's golden rule[14, 15, 70, 71]:

$$k_{vr} = \frac{2\pi}{\hbar} \sum_{a,a'} |\langle r', a' | V | r, a \rangle|^2 \rho(E) \delta(E(r', a') - E(r, a)) \quad (3.1)$$

In Eq. (3.1), r and r' designate the initial and final state of the initially excited vibration (the O–D stretching mode, in our case), while a and a' refer to the accepting modes. The ket $|r, a\rangle$ denotes the system with excited O–D stretching mode, and thermally populated accepting modes. The bra $\langle r', a'|$ denotes the final state, after relaxation. The density of states is $\rho(E)$ for the accepting modes in the relaxation process and the delta-function $\delta(E(r', a') - E(r, a))$ ensures conservation of energy. The summation shows that the true relaxation rate is a sum of contributions from all possible pathways. The increase in relaxation rate by the hydrogen bond can therefore be caused by an increase in overlap between the final $\langle r', a'|$ and initial $|r, a\rangle$ wavefunctions. This effect, in turn, can be partitioned into effects on the r -coordinates and on the a -coordinates. By increasing the (self-)anharmonicity of the O–D stretching mode (r -coordinate), the overlap will evidently increase[44]. On the other hand, the accepting modes (a -coordinates) will also be affected by the hydrogen bond, resulting in a larger overlap. In this case, the enhanced relaxation rate is due to an energy mismatch compensation by the hydrogen bond. This type of mechanism was used to explain and model the solvent-dependent vibrational relaxation rate of the C–H stretching mode of small organic molecules.[72] A second possibility is that, upon hydrogen bonding, the anharmonic coupling term V contains contributions of the form $R_{\text{OD}}^p \cdot R_{\text{H-bond}}^q$ (with $p, q > 0$), so that energy from the excited O–D stretching mode (designated by coordinate R_{OD}) can flow into the hydrogen bond (designated by coordinate $R_{\text{H-bond}}$). In this case, the hydrogen bond acts as an additional accepting mode, thus accelerating the relaxation process. This interpretation was demonstrated to be consistent with temperature-dependent relaxation measurements of zeolite O–H and O–D groups[53]. This indicates that the hydrogen bond with the adsorbate enhances the relaxation by

acting as an additional accepting mode into which part of the excess vibrational energy can flow. The experiments described here corroborate the findings of the previous Chapter, where we attributed the decrease in lifetime with decreasing frequency to hydrogen bonding.

In summary, we attribute the large increase in the vibrational relaxation rate upon adsorption to an energy flow from the excited O–D group into the hydrogen bond, upon relaxation. The hydrogen bond remains intact, however, and no energy is transferred to the adsorbate itself.

3.6 Conclusions

We have measured the lifetimes of surface hydroxyls in zeolites perturbed by small adsorbates. The decay is more rapid for the hydrogen-bonded hydroxyls, but independent of adsorbate. We find no evidence for energy transfer processes between the zeolite hydroxyl and the adsorbate, and observe that the hydrogen bond between the hydroxyl and the adsorbate remains intact. We conclude that the enhancement of the vibrational relaxation rate is due to an increase in the coupling between the hydroxyl and the zeolite lattice, presumably caused by a minor energy flow into the hydrogen bond, which acts as an additional accepting mode.

Chapter 4

Fast energy delocalization upon vibrational relaxation of a zeolite surface hydroxyl

In this time-resolved study of vibrational dynamics of deuterated surface hydroxyls at acid sites in the zeolite Mordenite, we investigate vibrational relaxation and observe transient bandshifts of the O–D stretch vibration after relaxation. It is shown that after infrared excitation of the stretching mode of the surface hydroxyls, the excess energy is rapidly distributed over delocalized low-energy lattice modes upon de-excitation. This is asserted from the observation that non-excited hydroxyls at different frequencies are perturbed by the relaxation of their excited counterparts effectively immediately after this relaxation. An upper limit of 10 ps for the energy delocalization time is found. This assignment allows for accurate estimates of local lattice temperatures after relaxation of the vibration.

4.1 Introduction

Vibrational energy transfer processes have been studied extensively during the past decades. In the gas phase, substantial information has been obtained on the (re)distribution of vibrational energy and energy decay routes.[73] In the condensed phase however, a lot of questions still remain unresolved due to the short timescales involved and the fact that this information in general cannot be obtained from measurements in the frequency domain. Time-resolved (picosecond) infrared spectroscopy has thus been proven a powerful tool in the investigation of the vibrational dynamics.[29] Here we present the results of a time-resolved vibrational study on the deuterated version of the acid form of zeolite Mordenite. In order to gain better insight into the dynamics of vibrational relaxation of zeolite surface hydroxyls, and the coupling between the hydroxyl and the zeolite lattice, we performed a time-resolved vibrational study of deuterated hydroxyls.

4.2 Experimental

The zeolite samples consist of pressed self-supporting crystalline zeolite discs of 5 mg/cm². Acid forms of Mordenite were obtained by *in vacuo* heating (1 h at 743 K) of Mordenite in which Na⁺ cations were exchanged by NH₄⁺ cations. The Mordenite under investigation was specified by Si/Al- and H/(Si+Al)-ratios of 6.7 and 0.13 respectively. Deuteration was achieved by exposing the zeolite disc to 500 mbar of D₂-gas (Messer Griesheim, 99.7%) at 693 K and allowing exchange for 1 hour, resulting in approximately 70% exchange as observed from the absorption spectra.

The experimental setup and the one-colour pump-probe technique have been described in Chapter 1. In short, the pump pulse excites a considerable fraction (~10%) of the O-D oscillators from their $v=0$ to $v=1$ vibrational state. Due to the anharmonicity of the vibration[43,47], the absorption is bleached on picosecond time scales, so that the equilibration of the population-distribution can be monitored by measuring the transmission of the probe pulse. The decay of the pump-induced transmission with time is related to the vibrational lifetime of the excitation T_1 , as[30]: $\ln[T(t)/T_0] \sim \exp(-t/T_1)$, where $T(t)$ is the transmitted energy of the probe pulse at delay t and T_0 is the transmitted probe energy in absence of the pump pulse. For the experiments in this Chapter, it is important to recall that the pump repetition rate can be regulated from 1 to 10 shots per second by a mechanical shutter (BF in Fig. 1.6).

4.3 Results

In Figure 2.2 of Chapter 2 the conventional infrared absorption spectrum for deuterated Mordenite is depicted in the O–D stretch region. Three typical results of room temperature one-colour pump-probe experiments for deuterated Mordenite are shown in Fig. 4.1. With the laser tuned to the top of the absorption band (2662 cm^{-1}) the transmission is found to return to its equilibrium value T_0 with a time constant of 55 ps (upper panel of Fig. 4.1). If the laser-frequency is tuned to the low-frequency side of the absorption band (at 2640 cm^{-1}), two striking changes occur in the measured decay: a decay with smaller time constant of 36 ps is found and the relative transmission $\ln[T(t)/T_0]$ is found to relax to a negative value (middle panel of Fig. 4.1); after decay of the excited oscillators, the absorbance has increased. Contrary effects are observed on the high frequency side of the absorption peak (at 2672 cm^{-1}); a larger lifetime T_1 is observed and after relaxation an increase in transmission is detected (lower panel of Fig. 4.1). So the experiments present us with the vibrational lifetime T_1 as well as an offset (level) of the transmission after vibrational relaxation.

The data can theoretically be reproduced by numerically solving the appropriate set of coupled spatio-temporal rate equations (See Eq. (2.1)-(2.3) in Chapter 2). The calculations need as input the pulse parameters of both pump and probe (pulse shape, duration and intensity) and sample parameters (absorption cross section, oscillator density and sample length). As in Chapter 3, a third level was incorporated to describe the transmission offsets after relaxation. In this model, relaxation from $v=1$ takes place to $v=0^*$, from which absorption to $v=1^*$ can occur with a slightly different cross-section. Fit parameters are the time constant T_1 and the absorption cross section after vibrational relaxation. The results of the calculations are shown as solid lines in Figure 4.1. Clearly, our experiments can very well be described by a simple model with (i) a single time constant accounting for population decay and (ii) the change in cross section of the relaxed oscillators. The frequency dependence of the lifetime is discussed in Chapter 2.

The level to which the transmission was found to relax —normalized to the magnitude of the signal (top)— is plotted versus wavenumber in Fig. 4.2. Exciting on the low-frequency side of the absorption band, the absorption is enhanced after relaxation of the excited oscillators. On the high-frequency side, there is a decrease in absorption after relaxation. This points to a red-shift of the absorption peak caused by the vibrational relaxation; the absorption band is shifted towards the laser band (into resonance), with the laser at low frequencies, and shifts away from the laser at high frequencies. The observed relaxation of the transmission to non-equilibrium (Fig. 4.1), a second change in transmission upon vibrational relaxation, is not caused by 'thermal

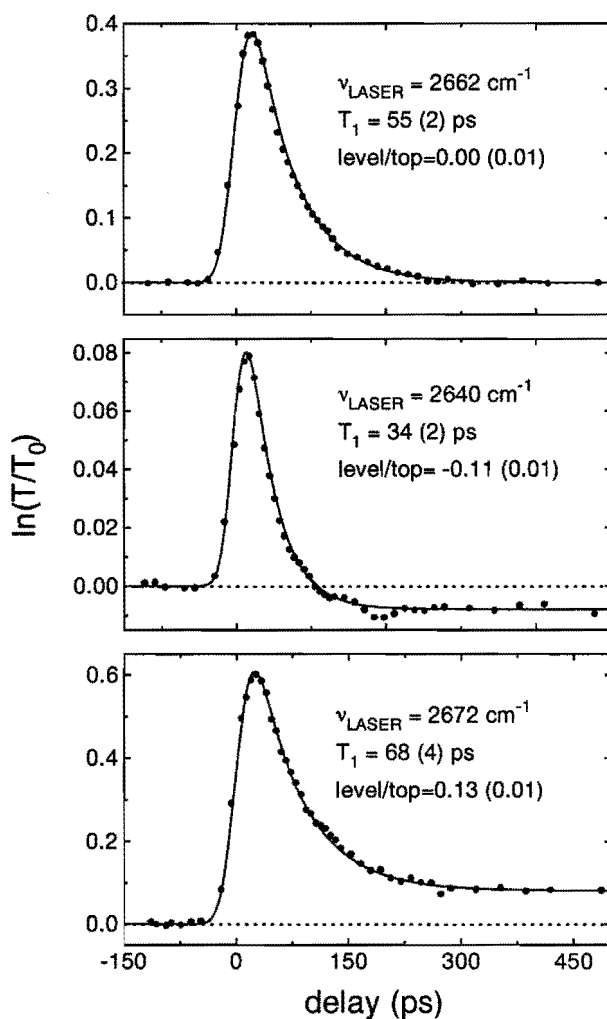


Figure 4.1: Typical results of pump-probe experiments: Relative transmission of an infrared probe pulse $\ln[T(t)/T_0]$ as function of the delay between pump and probe pulses at three laser frequencies; at the top of the absorption peak (2662 cm^{-1}), on the low frequency side of the absorption peak (2640 cm^{-1}) and at 2672 cm^{-1} . Fitted lifetimes (and errors) are denoted in the graph. The corresponding absorption spectrum can be found in Figure 2.2 of Chapter 2.

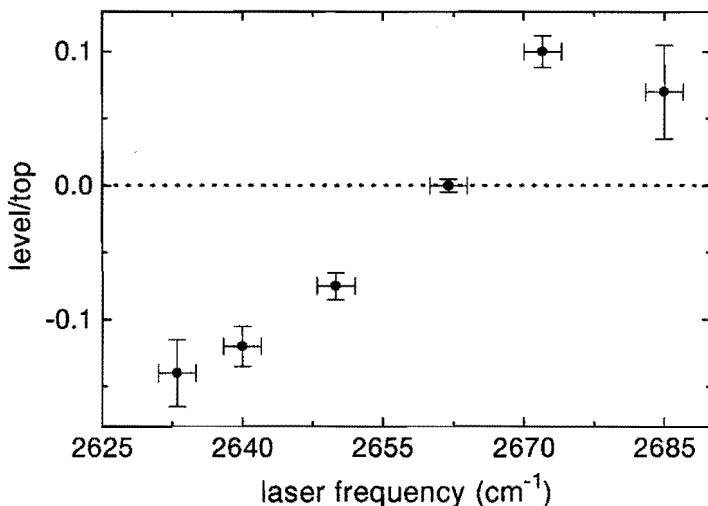


Figure 4.2: The observed level to which the logarithm of the normalized transmission ($\ln[T(t)/T_0]$) was found to relax, normalized to the magnitude of the signal, as a function of laser frequency. After relaxation, on the red side of the absorption peak a decrease in transmission is observed, on the blue side an increase.

lensing', which has been shown negligible in this kind of experiment.[74]

At this point it is important to note that there are *three* relevant timescales for the transmission changes in the experiment: (i) the vibrational lifetime T_1 , (ii) the onset time of the level, i.e. the time between vibrational relaxation and the change in transmission hereby caused (considered instantaneous in our calculations, but not necessarily so [see below]), and (iii) the slow relaxation time of this last effect (the observed offset of the transmission is constant for 2 ns after vibrational relaxation, but has faded when the next probe pulse travels through the sample (after 100 ms). Double relaxation effects have also been observed before for a number of different fluids[59, 75–79], but not in vibrational relaxation experiments on surface hydroxyls.

4.4 Fast energy delocalization

To understand the three relaxation times mentioned above, it is helpful to consider possible relaxation processes subsequent to excitation. The first process to occur after vibrational excitation is the (down-)conversion of the O–D vibrational energy into excitations of accepting modes[14–16]. The time-scale of this process is, of course, the vibrational lifetime T_1 . Coupling of these low-frequency modes to the bath, in turn, will result in a *local* thermalization of the excess energy (within the laser focus), with a speed determined by the decay rate of the accepting modes. Thirdly, the 'local bath' will equilibrate with its environment by heat diffusion out of the laser focus, into the rest of the sample. Experimentally, the system is found to relax to a non-equilibrium state which is stationary for at least 2 ns after the vibrational relaxation. This is manifested in a transmission after vibrational relaxation different from the transmission before; somehow the absorption frequencies of the oscillators are affected by the vibrational relaxation. Although we expect the last relaxation process (heat diffusion) to be slow on experimental time scales, slow decay of the accepting modes cannot *a priori* be excluded as the cause of our observations. Indeed, slow decay of accepting modes has been observed previously: In a time resolved study of the C–H-stretch vibration in CHBr_3 it was found that after excitation of the C–H vibration there are *two* consecutive relaxation processes.[59] First the energy is transferred to other vibrations within the molecule, the accepting modes. Due to anharmonic coupling between the accepting modes and the C–H vibration, excitation of the accepting modes affect the C–H-stretch frequency, resulting in a transient bandshift, thus changing the transmission at the original frequency. The accepting modes were shown to have lifetimes up to nanoseconds. This effect causes the transmission to relax with two time constants: first the pump-induced transmission decays with the vibrational lifetime constant T_1 whereafter a second relaxation process is observed, with a much larger time constant, reflecting relaxation of the accepting modes.

It is therefore clear that there are *two* possible explanations for the effects we observe: The 'long-lived accepting mode' hypothesis and the 'short-lived accepting mode' hypothesis. The long-lived accepting mode hypothesis can be visualized as follows, in complete analogy to the relaxation of the C–H-stretch vibration in CHBr_3 : Decay of the excited O–D oscillator entails the redistribution of the energy into accepting modes, for which the sum of energies is in resonance with the O–D vibrational energy.[14–16] If the excitation of one of the accepting modes, brought about by de-excitation of the O–D stretching mode, causes the O–D stretch frequency to change, and the lifetime of this accepting mode excitation is sufficiently large, this would account for the observed offset of transmission after vibrational relaxation. In this case the onset time of the

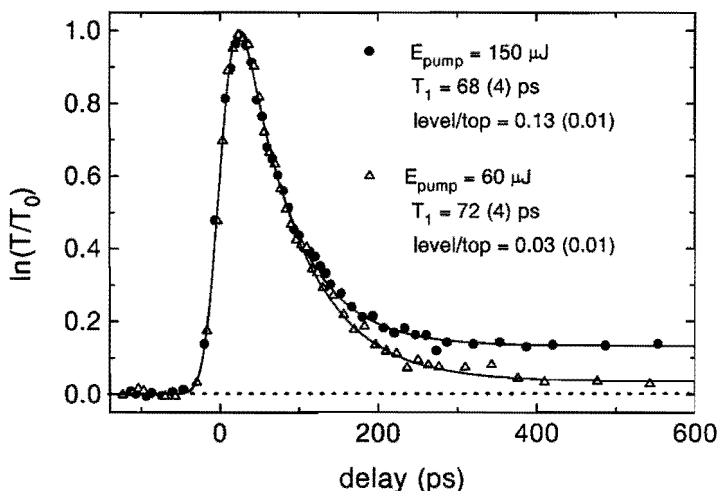


Figure 4.3: Observed transmission changes at 2672 cm^{-1} for two different pump energies. The amplitude of the signals are scaled to 1 (multiplied by factors 1.8 and 4.2, respectively). Clearly, for lower pump energies relaxation close to equilibrium transmission T_0 occurs.

transmission after relaxation is zero, in agreement with the data.

Diametrically opposed to this is the 'short-lived accepting mode' possibility which requires the accepting modes to decay extremely *fast*. In this scenario the energy in the O–D vibrational quantum is rapidly redistributed over the zeolite lattice, causing *all* the oscillators to shift in frequency. Although it would inevitably take some time to 'delocalize' the excess energy, the data indicate that this delocalization time would have to be very short, since all data sets are well accounted for with a zero onset time. The long- and short-lived hypotheses have previously been denoted as 'medium induced vibrational relaxation' and 'direct vibrational energy dissipation', respectively.[80]

There are two indications as to whether the effect is due to a long- or short-lived accepting mode, both in favor of the short-lived hypothesis: Firstly we found a dependence of the offset of the transmission after relaxation on pump pulse energy. Experiments with gradually decreasing pump energy, reveal the level/top-ratio to continually decrease, and go to zero for sufficiently small pump energies (see Fig. 4.3). From the short-lived point of view, this dependence can easily be explained: there will be a smaller perturbation of the oscillators and hence a smaller shift of the absorp-

tion band when less energy is deposited onto the lattice due to the excitation of less O–D oscillators. In the short-lived picture, the energy is used to shift the absorption frequency of *all* the oscillators, not just the ones that were excited. In the long-lived hypothesis a conflict arises: The maximum $\ln[T/T_0]$ -signal (top) is proportional to the O–D excitation density. In analogy, it is the accepting mode excitation density that determines the long-time signal (level). One would expect a 1:1 correlation between the accepting mode excitation density and the O–D excitation density and also a linear correlation between the shift of the high-frequency mode and the accepting mode excitation density and hence a level/top-ratio *independent* of the actual degree of excitation, contrary to what is observed.

A second point in favor of the short-lived hypothesis is that a similar dependence of the transmission-offset after vibrational relaxation was found on O–D concentration: for lower O–D concentrations (achieved by allowing less exchange with D_2) the offset after relaxation decreased. The preceding argument holds here as well; for lower oscillator densities, less oscillators will be excited and less energy will be dumped onto the zeolite lattice.

It is thus concluded that the observed effect is caused by short-lived accepting modes; we experimentally observe a very rapid redistribution of the energy of the excited oscillator into delocalized modes. The absorption band of all the oscillators is almost instantaneously redshifted due to the vibrational relaxation of excited oscillators. From our calculations it is concluded that the time between the relaxation and the resulting bandshift, i.e. the onset time of the transmission offset, must be smaller than 10 ps.

Indeed, one would expect the accepting modes to decay rapidly compared to the O–D stretching mode. Previous studies of O–H and O–D relaxation in zeolites[53], on silica surfaces[81] and inside fused silica[55] show that the initial relaxation process for an O–H quantum decays into four or five accepting modes, three for O–D. Possible accepting modes for the O–D vibration relaxation process, e.g. O–D bending modes or Si/Al–O stretching modes, all have frequencies ranging from 400 to 1000 cm^{-1} [50, 52, 82, 83]. From considerations of the energy gap law[84], one would expect that the accepting modes excited on de-excitation of the O–D oscillator would decay fast relative to the O–D oscillator itself, rather than slow. The energy gap law states that the vibrational relaxation rate should exhibit a (super-)exponential dependence on the number of accepting modes involved in the relaxation process: If the number of accepting modes decreases by one, the vibrational relaxation time should decrease by at least an order of magnitude. Although it was demonstrated recently that the energy gap law is a crude approximation[53] (not only the number of accepting modes

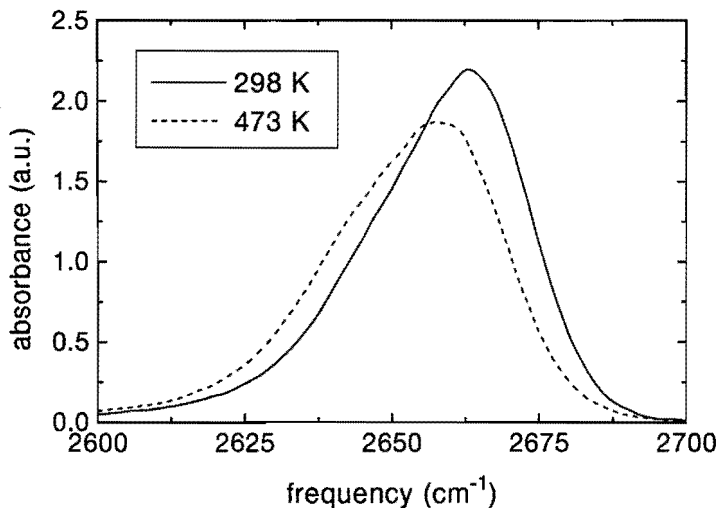


Figure 4.4: Absorption spectrum in the O–D stretch region for deuterated Mordenite at two different temperatures. On increasing the temperature, the absorption band is seen to shift to lower wavenumbers and decrease in intensity.

determines the relaxation rate, but also the number of possible relaxation channels[53]), one would still expect a relatively fast relaxation of accepting modes due to the fact that the energy gap between the O–D accepting modes and *their* subsequent accepting modes is a lot smaller than the energy gap between the O–D oscillator and its accepting modes. Hence, it is most unlikely that the accepting mode-excitations have lifetimes exceeding nanoseconds.

4.5 Lattice temperature

The observation of very rapid dispersion of the excess energy after de-excitation of the oscillators, indicates that the offset of the transmission is due to an elevated lattice temperature immediately after vibrational relaxation. Indeed, the O–D stretch absorption band was found to shift to lower wavenumbers on raising the temperature as can be observed in Figure 4.4. Vibrational relaxation causes an almost immediate increase of lattice temperature, which, in turn, causes the absorption band to shift. The result is an increased absorption at the low-frequency side of the peak and decreased absorp-

tion at the high-frequency side after relaxation of the excitation as was observed in the experiments (Fig. 4.3).

The dependence of the absorption band on temperature can qualitatively be understood as follows: an increase in the temperature promotes population of low-frequency vibrations or phonons. This increase in population of these low-frequency modes affects the O–D stretch frequency directly or through modes that are coupled to this stretching mode. Hence an increase in temperature causes a shift (and broadening) of the absorption band (see e.g. ref [85]).

Since we know the change in transmission induced by the vibrational relaxation (Fig. 4.3), we can make an estimate of the increase in lattice temperature causing this change in transmission by considering the temperature dependence of the absorption spectrum. The expression for the transmission T as a function of temperature Θ of a laser probe pulse with intensity $L(\tilde{\nu})$ through a sample with temperature dependent absorption band $A(\tilde{\nu}, \Theta)$ reads:

$$T(\Theta) = \int_0^{\infty} d\tilde{\nu} L(\tilde{\nu}) \exp[-A(\tilde{\nu}, \Theta)] \quad (4.1)$$

From the experiments we obtain the transmission of the probe pulse after vibrational relaxation relative to room temperature transmission. By measuring the absorption spectrum $A(\tilde{\nu})$ as a function of temperature Θ we can subsequently determine the magnitude of the temperature increase corresponding to the observed offset of the transmission. The momentary increase in temperature causing the offset in transmission was found to vary from 10 K pumping the flanks of the absorption peak to 30 K at absorption maximum and could be determined accurately. The lattice temperature increases as calculated from the offset in transmission after relaxation, are shown in Fig. 4.5.

From the calculations it was found that at the top of the absorption peak about 100 of the 150 μJ pump energy is absorbed. If this energy is evenly distributed over the laser focus (0.2 mm beam waist), this would result in a temperature increase of approximately 15 K, in good agreement with the values deduced from the experiments. Previous ultrafast heating experiments with infrared laser pulses in liquids with a molecular thermometer, showed similar temperature increases with somewhat lower pump energies.[86]

A potential pitfall in the experiments is the steady-state heating of the sample due to the relatively large amounts of energy absorbed in the sample. Vibrational lifetimes are intrinsically dependent on temperature; at higher temperatures decay is more rapid.[84] We checked for steady-state heating effects by measuring T_1 as a function of pump repetition rate; no effect of heating on the lifetime could be detected

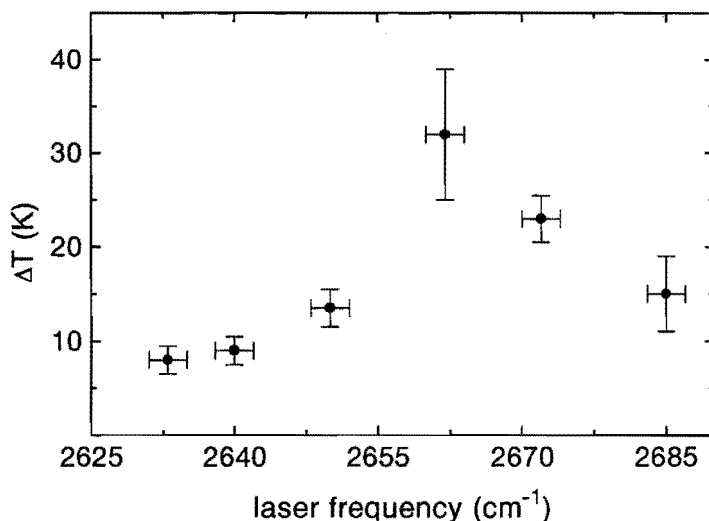


Figure 4.5: Transient temperature changes as a function of laser frequency, determined from the signal offset (level/top-ratio). Note that, as would be expected, the largest temperature increases are observed at the absorption maximum.

for repetition rates of 5 Hz and lower. All aforementioned experiments were performed at this repetition rate. For pump repetition rates larger than 5 Hz steady-state heating occurs due to the cumulative temperature effect of the pump pulses; the time between pump pulses does not allow for thermal equilibration of the sample. Experimentally, for repetition rates higher than 5 Hz not only a smaller T_1 is observed, but also a change in the offset of the transmission after vibrational relaxation compared to the offset at lower repetition rates (in absence of steady-state heating). This can be understood by noting that, at different initial steady-state temperatures the effect of the same temperature increase (due to a single pulse) on transmission will be different. Since we know the single pulse temperature increase at room temperature (Fig. 4.5), we can now make an estimate of the steady-state temperature increase for repetition rates exceeding 5 Hz, from the change in transmission-offset. At pump repetition rates of 10 shots per second, a steady-state temperature increase of 100 ± 10 K could be detected with the laser tuned to the top of the absorption band.

It is important to note that the conclusions drawn in this study also hold for the non-deuterated zeolite surface hydroxyls as well as for (deuterated) surface hydroxyls

on colloidal silica. The long-time signal offsets can also be observed for these systems, albeit less clear. The reported temperature effects are even more important for O-H-experiments owing to the larger possible pump-energies and absorption cross sections[44].

4.6 Conclusions

We studied the vibrational dynamics of deuterated surface hydroxyls in the zeolite Mordenite. After infrared excitation of surface hydroxyls we observe relaxation of the transmission (reflecting the population relaxation) to non-equilibrium. A satisfactory explanation is presented in terms of a fast redistribution of the energy in the excited oscillators after vibrational relaxation, which affects the absorption frequency of all hydroxyls in the zeolite; it is found that upon relaxation of the O-D oscillator, energy is not stored in local modes (e.g. O-D bending), but is dispersed over the zeolite lattice within 10 ps. The induced change in lattice temperature is manifested as relaxation of the transmission to elevated and decreased levels, depending on the exact excitation frequency. This allows for accurate determination of the lattice temperature in the laser focus immediately after vibrational relaxation as well as steady-state temperature increases.

Chapter 5

Infrared picosecond transient hole-burning studies of the effect of hydrogen bonds on the vibrational lineshape

With infrared transient hole-burning spectroscopy we have investigated the influence of OD \cdots X hydrogen bonds on the vibrational lineshape of O–D stretch vibrations in acid zeolites. The effect of hydrogen bonding on the lineshape depends critically on the type of hydrogen bond. For hydrogen bonding in a rigid structure, the hydrogen bond is responsible for the *inhomogeneous* broadening, but the *homogeneous* linewidth is determined by coupling to a $\sim 200\text{ cm}^{-1}$ lattice mode as concluded from the temperature dependence of the homogeneous linewidth. When the hydrogen bond is formed with an adsorbing molecule, the coupling between the high-frequency O–D stretch vibration and the low-frequency OD \cdots X hydrogen-bond stretching mode does determine the homogeneous linewidth. The difference between the two systems can be explained by the different hydrogen-bond potentials. Variation of the adsorbate provides a means of obtaining conclusive information on the coupling mechanism between the high-frequency O–D stretching mode and the low-frequency OD \cdots X hydrogen-bond stretching mode.

5.1 Introduction

Infrared absorption lineshapes have received considerable attention in the past decades, since it is clear that the center frequency and the width of an absorption line contain information on the interaction of a molecule or oscillator with its surroundings.[17, 87] The effect of hydrogen bonds on the vibrational lineshape is particularly interesting, since the absorption linewidth of a hydrogen-bonded complex is typically an order of magnitude larger than that of the free molecule. Although this problem has received considerable attention in both theoretical[13, 88–94] and experimental[95–102] studies, there is substantial ambiguity as to the exact cause of this broadening and its appropriate theoretical description.

In this Chapter we investigate the effect of hydrogen bonding on the vibrational lineshape of O–D stretch vibrations of deuterated hydroxyls in zeolites. Weak hydrogen bonds are formed by hydrogen bonding of the deuterated hydrogen atom of the hydroxyl group with zeolite lattice oxygen atoms, or by adsorption of simple molecules to available O–D sites in the zeolite. We have investigated the resulting absorption line with both conventional and time-resolved saturation IR spectroscopy. The latter technique allows us to separate homogeneous from inhomogeneous contributions to the lineshape. It is found that the effect of the hydrogen bond on the homogeneous vibrational lineshape depends strongly on the nature of the hydrogen bond; absorption lines which are indistinguishable with conventional IR spectroscopy can hide very different homogeneous vibrational dynamics. The zeolite system allows us to 'tune' the relevant physical parameters determining the absorption line, by choosing adsorbates with different masses and hydrogen bond strengths. Thus we are able to obtain conclusive information on the coupling between the O–D stretch vibration and the OD...Adsorbate hydrogen bond stretching mode.

The O–D groups under investigation are the acid sites in the microporous aluminosilicate zeolites. These acid zeolites are used in solid acid catalyzed processes (e.g. hydrocarbon cracking in the petrochemical industry).[9] Insight in the dynamics of the microscopic interaction between the catalytic site and adsorbates is of essential interest for a fundamental understanding of zeolite catalysis and the theoretical description of these processes.

5.2 General lineshape theory

In the stochastic model described in Chapter 1, the infrared transition is considered to be an oscillator with a time dependent transition frequency. The transition frequency is modulated by interactions of the oscillator with the heat bath. The loss in phase relation caused by this modulation process causes a decay of the vibrational coherence, resulting in a line-broadening. Following the description in Chapter one, we assume that the frequency modulation is a Gauss-Markov process: The distribution of frequencies is Gaussian and the time-evolution of the fluctuating part of the transition frequency $\delta\omega(t)$ can be described by a Markovian process (the decay of the time-correlation function of $\delta\omega(t)$ is exponential):

$$\langle \delta\omega(0)\delta\omega(t) \rangle = D^2 e^{-t/\tau_c} \quad (5.1)$$

D is the width of the Gaussian frequency distribution and τ_c the correlation time of the fluctuations, representing the typical time-scale for the frequency modulation process. The expression for the absorption line in terms of D and τ_c is:

$$I(\omega) = \frac{1}{2\pi} \int_{-\infty}^{\infty} dt \exp(-D^2 \tau_c^2 [e^{(-t/\tau_c)} + t/\tau_c - 1]) \times \exp(i\omega t) \quad (5.2)$$

In the static, inhomogeneous limit ($D\tau_c \gg 1$) the macroscopic polarization will exhibit Gaussian decay, resulting in a Gaussian, inhomogeneously broadened absorption line, while in the limit of rapid modulation ($D\tau_c \ll 1$) the macroscopic polarization will decay exponentially, culminating in a Lorentzian absorption line. For shorter τ_c the line will become narrower. This phenomenon is well-known in magnetic resonance spectroscopy as motional narrowing.[21] The stochastic model can interpolate between these two limits, allowing for the calculation of the linewidth for arbitrary D and τ_c .

In general, there exist two or more modulation processes, some slow ($D\tau_c \gg 1$) giving rise to inhomogeneous broadening, and some fast ($D'\tau'_c \ll 1$) responsible for the broadening of homogeneous lines under the inhomogeneous distribution. Inhomogeneous broadening is due to *static* structural properties of the sample, occurring when different oscillators have slightly different transition frequencies due to the different environments they experience. Homogeneous broadening ($D'\tau'_c \ll 1$) is connected to the two-fold *dynamics* of the vibration: For an ensemble of oscillators with the same center frequency, line broadening will occur due to the loss of coherence, the dephasing of the excitation. Anharmonic coupling to phonons, for example, will lead to a loss in phase memory of an oscillator. These are called pure dephasing (T_2^* -) processes. Dephasing and the accompanying line-broadening will also occur due to the finite lifetime (T_1) of the excitation, resulting in a homogeneous linewidth $2\pi\Gamma_{\text{hom}} = T_1^{-1} + 2T_2^{*-1}$.

Recent developments in time-resolved spectroscopy have allowed for the separation of static and dynamic contributions to the vibrational linewidth. (Quasi-)homogeneous¹ vibrational lineshapes can be measured with IR transient hole-burning techniques [103, 104] and recently the time-resolved observation of homogeneous vibrational dephasing by means of an infrared photon-echo experiment was reported.[26, 27].

Transient infrared hole-burning spectroscopy allows for the investigation of absorption lines by selectively exciting a sub-ensemble of oscillators within the overall absorption line. The presence of inhomogeneous broadening can be revealed, and the (quasi-)homogeneous linewidth, determined by the vibrational dynamics can be obtained, providing us with the complete vibrational dynamics of the system.

In the following section we will present a short overview of theoretical models describing vibrational (homogeneous) dephasing in hydrogen-bonded systems. In particular, we are interested in how the different theories link D and τ_c , which determine the linewidth, to physical quantities of the system.

5.3 Theoretical models for dephasing in hydrogen-bonded systems

A great number of sophisticated theoretical models have been developed to describe vibrational lineshapes[13, 88–94, 105, 106], some specifically addressing the effect of hydrogen bonds[13, 92–94, 105, 106]. Here, we will give a brief review of the relevant theories, the concomitant predictions and previous applications of these theories to explain the experimental observations.

In most of these theories the dephasing of the high-frequency $\overleftarrow{X}-\overrightarrow{H} \cdots \overleftarrow{Y}$ ν_s stretching mode (corresponding to the $\sim 2600 \text{ cm}^{-1}$ O–D stretching mode for our system) in the hydrogen-bonded $X-H \cdots Y$ system is due to anharmonic coupling of this mode to the low-frequency ($\sim 100 \text{ cm}^{-1}$) $\overleftarrow{X}-H \cdots \overrightarrow{Y}$ ν_σ stretching mode. We will refer to the normal coordinates of the high-frequency ν_s and the low-frequency ν_σ stretching modes as r_s and r_σ , respectively. The two modes are expected to be strongly coupled since they lie along the same spatial coordinate and it has therefore been surmised that there is a strong correlation between the ν_s^{XH} frequency and the $X \cdots Y$ hydrogen bond distance r_σ . The importance of the coupling of the two stretching motions for the infrared spectrum of the high-frequency ν_s mode was first pointed out by Marechal and Witkowsky[92]. The key point of this theory was the recognition that the coordinate

¹In time-resolved experiments, the absorption band may seem homogeneous for $D'\tau_c' \approx 1$ (different from the homogeneous $D'\tau_c' \ll 1$), if the spectral diffusion process is faster than the time-resolution in the experiments. This explains the use of the term '(quasi-)homogeneous'.

of the $\nu_\sigma(\text{XH}\cdots\text{Y})$ mode r_σ determines the frequency of the $\nu_s(\text{X-H})$ mode. In this theory the relatively fast motion of coordinates r_s is separated from the slow motion in coordinates r_σ , in a vibrational Born-Oppenheimer approximation.[92] The result of this adiabatic description is a stick spectrum (absorption lines are delta-functions) associated with the $\nu_{\text{X-H}}=0$ to $\nu_{\text{X-H}}=1$ transition, made up of a vibrational progression in the ν_σ mode. The width of the overall absorption line is determined by how much the ν_σ mode can change its energy in going from $\nu_{\text{X-H}}=0$ to $\nu_{\text{X-H}}=1$. The theory was successfully employed to calculate infrared spectra for a single hydrogen-bonded complex; also, the agreement with experimental data for a gas-phase dimer and a hydrogen-bonded crystal was excellent.[92]

Bratos showed that in case of a hydrogen-bonded liquid it is not sufficient to consider a single hydrogen bonded complex.[13] In this model the description of the broad, featureless absorption spectrum presupposes a static distribution of hydrogen bond strengths, and a corresponding static distribution of transition frequencies. This means that this model describes broadening in the inhomogeneous limit of slow modulation ($D\tau_c \gg 1$).

In an extension of these static models by Robertson and Yarwood[93,94] the dynamics of the coupling were incorporated by introducing a stochastic modulation of the r_σ coordinate super-imposed on the $\nu_\sigma(\text{XH}\cdots\text{Y})$ vibration. This causes a frequency modulation of the high-frequency $\nu_s(\text{X-H})$ mode through the time evolution of r_σ , which is described classically by means of a Langevin equation. The anharmonic coupling term V_{anh} describing the effect of the coupling of the ν_σ mode and the ν_s mode on the ν_s motion is *linear* in the coordinate $r_\sigma(t)$ of the $\nu_\sigma(\text{XH}\cdots\text{Y})$ mode in the spirit of Witkowski and Bratos: $V_{\text{anh}} = K_{12}r_s^2r_\sigma(t)$, with K_{12} the coupling constant. The result of this description is that, in case the ν_σ mode is overdamped (i.e. in the absence of combination bands between the ν_s and the ν_σ modes in the absorption spectrum), the width of the spectral distribution D is given by the coupling strength of the two modes and the root-mean-square amplitude of r_σ , $D = K_{12}\langle r_\sigma^2 \rangle^{1/2}$, and the correlation time τ_c is determined by a damping parameter γ for the ν_σ mode and the ν_σ frequency: $\tau_c = \gamma/\nu_\sigma^2$. The damping parameter γ reflects the damping of the hydrogen-bond mode ν_σ due to coupling of this mode to the bath.

This description is in sharp contrast with the theory of dephasing in condensed phases by Shelby and Harris[90,91], in which the coupling depends linearly on the *occupation* of the low-frequency mode ν_σ , and hence the predominant coupling term depends on the coordinate r_σ to *second* order[90,91], $V_{\text{anh}} \propto r_\sigma^2(t)$. In this model, successfully applied to describe, amongst others, the homogeneous linewidth of a hydrogen-bonded polymer[103], the modulation of the $\nu_s(\text{X-H})$ transition frequency occurs through an-

harmonic coupling to the ν_σ low-frequency mode which undergoes energy exchange with the bath. Energy exchange between the low-frequency mode and the bath results in continuous excitation and de-excitation of the low-frequency mode. Since this mode is anharmonically coupled to the high-frequency mode, the transition frequency of the high-frequency mode is sensitive to whether or not the low-frequency mode is excited. Therefore energy exchange between the bath and the low-frequency mode will result in a modulation of the transition frequency of the high-frequency mode; the spectral distribution D is determined by the coupling strength and τ_c by the lifetime of the low-frequency mode, determined amongst others by the degree of thermal excitation of this mode. The key prediction of this theory is that, at low temperatures, the width of the absorption line will display an apparent activation energy with increasing temperature, equal to the energy of the low-frequency mode, due to the increased rate of thermal occupation of the low-frequency mode.[90,91]

Both the Robertson-Yarwood model and the Shelby-Harris model have been more or less successfully applied to describe lineshapes in hydrogen-bonded systems.[102,103] However, from these and other experiments, it is clear that temperature variation[99, 103], change in hydrogen-bond strength by different hydrogen-bond acceptor/donor[100], change of solvent[101] and isotopic substitution[102] lead to severe complications in the interpretation of the data, since too many parameters will change, affecting both D and τ_c that determine the lineshape. Furthermore, considerable problems were encountered in background subtraction for the interpretation of the linear absorption spectra[102], which has to be performed very accurately in order to obtain the true shape of the absorption band.

For strong hydrogen bonds in polar solvents, a direct dephasing mechanism has been proposed[105–107], in which the $\nu_s(X-H)$ mode is coupled directly to the solvent, due to the dipolar interaction of the hydrogen-bonded group with the local solvent field. Although this description has successfully been applied to interpret experimental data (see e.g. Ref. [107]), we will not pursue this approach since in our systems with weak hydrogen bonds in rigid structures the hydrogen bond mode does play an important role in the dephasing process, as will be shown below. In this Chapter, we will compare the Shelby-Harris and the Robertson-Yarwood models in their ability to explain our experimental results.

5.4 Experimental

The zeolite samples consist of pressed self-supporting crystalline zeolite discs of ~ 5 mg/cm². Acid forms of Y-zeolite and Mordenite were obtained by *in vacuo* heating (1 h at 743 K) of the zeolite in which (part of the) Na⁺ cations were exchanged by NH₄⁺ cations. The two types of Y zeolite are specified by Si/Al-ratios of 2.8 and H/(Si+Al)-ratios of 0.27 and 0.07, respectively. For the Mordenite the Si/Al- and H/(Si+Al)-ratios are 6.7 and 0.13 respectively. Deuteration is achieved by exposing the zeolite disc to 500 mbar of D₂-gas (Messer Griesheim, 99.7%) at 693 K and allowing exchange for 1 hour, resulting in approximately 70% exchange as observed from the absorption spectra. Adsorption of nitrogen (N₂, Messer Griesheim, 5.0), xenon (Xe, Messer Griesheim, 4.0), methane (CH₄, L'Air Liquide, 3.5) and carbonmonoxide (CO, Linde, 3.7) was performed at pressures ranging from 50 to 200 mbar, at temperatures from 100 K to 170 K.

The infrared pump energies were kept sufficiently low to justify the neglect of contributions from thermal desorption for the experiments on O-D groups with adsorbates. The laser pulse has a bandwidth of 6 cm⁻¹ (FWHM, Gaussian lineshape) at O-D absorption frequencies, which is four times smaller than the bandwidth at O-H frequencies. This better frequency resolution, and a reduced scattering of the laser pump light at O-D frequency as opposed to the O-H frequency, are the reasons for investigating the deuterated sample.

As described in Chapter 1, the set-up allows for three kinds of experiments. The first is a one-color pump-probe delay scan experiment, from which the vibrational lifetime T_1 can be obtained.

The second type of experiment is a two-color frequency-scan experiment. In this experiment transient absorption spectra are recorded. From the width of the spectral hole that is burnt in the 0→1 absorption band we can deduce the homogeneous linewidth for the 0→1 transition. Analogously, the width of the 1→2 transition (hot band) contains information on the vibrational dynamics of the 1→2 transition.

In the third type of experiment, a two-color, 3-pulse, pump-pump-probe experiment, the first pump pulse is tuned to the 0→1 transition, followed promptly by a second pump pulse tuned to the 1→2 transition (slightly to the red). With this scheme approximately 5% of the oscillators can be excited to the second excited state $v=2$. With the probe pulse the population difference between the ground and first excited state, or between the first and the second excited state can be monitored as a function of delay between the pump pair and the probe. With this experiment, the lifetime of the *second* excited state can be obtained, as well as information on the decay route from $v=2$ down to $v=0$ (directly, or *via* $v=1$).

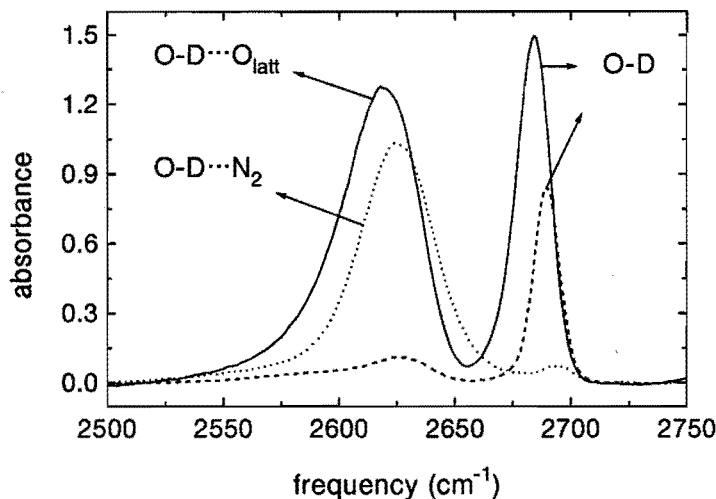


Figure 5.1: Conventional absorption spectra for two of the deuterated zeolites under investigation, $D_{0.19}Y$ (solid) and $NaD_{0.05}Y$ (dashed), and the spectrum for the latter with adsorbed nitrogen (dotted) in the O–D stretching region. Note the similarity between the vacuum LF O–D absorption band for $D_{0.19}Y$ (hydrogen-bonded to the zeolite lattice) and the HF O–D··· N_2 (hydrogen-bonded to nitrogen) of the $NaD_{0.05}Y$ zeolite.

5.5 Differences between a solid and a gas-phase hydrogen bond

In Fig. 5.1 three absorption spectra in the O–D stretching region are shown. For $D_{0.19}Y$ zeolite (36 O–D groups per $Al_{52}Si_{140}O_{384}$ unit cell), two absorption peaks appear, one around 2680 cm^{-1} , associated with high-frequency (HF) O–D groups situated in the so-called supercages, and one around 2620 cm^{-1} originating from the low-frequency (LF) sites in the smaller cages.[49] The redshift of the LF O–D peak is due to a hydrogen bond between the deuterons from the LF O–D groups to zeolite lattice oxygen atoms.[44] These O–D groups will be further referred to as $OD\cdots O_{latt}$ groups. For the same zeolite with a lower concentration of O–D groups, $NaD_{0.05}Y$ (10 O–D groups per unit cell), mainly HF O–D groups in the large cages are present. Upon addition of 50 mbar of nitrogen at 100 K, the nitrogen adsorbs to these O–D sites, resulting in a redshift of the peak due to the weak hydrogen bond to the adsorbate.[68] The resulting

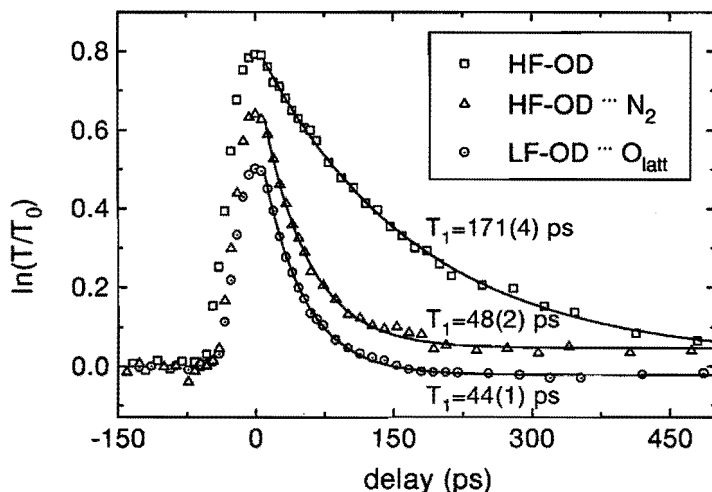


Figure 5.2: Relative transmission of an infrared probe pulse $\ln[T(t)/T_0]$ (T_0 is the transmitted probe energy in absence of the pump pulse) as function of the delay between pump and probe pulses for three different hydroxyls: The 'free' HF hydroxyls of $\text{NaD}_{0.05}\text{Y}$ in vacuum (\square), the same hydroxyls with nitrogen adsorbed (\triangle), $\text{OD}\cdots\text{N}_2$, and the LF hydroxyls of $\text{D}_{0.19}\text{Y}$ (\odot), $\text{OD}\cdots\text{O}_{\text{latt}}$, hydrogen-bonded to the zeolite lattice. Note that the population lifetimes for the latter two are practically equal. The values for the fitted population lifetimes T_1 (and the corresponding standard deviations) are denoted in the graph.

O–D groups will be further referred to as $\text{OD}\cdots\text{N}_2$ groups. Note the similarity between the LF O–D peak of $\text{D}_{0.19}\text{Y}$ due to the $\text{OD}\cdots\text{O}_{\text{latt}}$ groups and that of the HF O–D of $\text{NaD}_{0.05}\text{Y}$ with adsorbed nitrogen, due to the $\text{OD}\cdots\text{N}_2$ groups.

In Fig. 5.2 the results of one-color pump-probe experiments are shown, from which the vibrational population lifetime can be obtained. It has been demonstrated that for these O–D vibrations the decay time of the pump-induced transmission increase can be interpreted straightforwardly as the vibrational lifetime T_1 . (see e.g. Chapter 2 and [22]) Upon adsorption of nitrogen the vibrational lifetime of the O–D groups drops from 171 to 48 ps, and this lifetime coincides remarkably well with the 44 ps lifetime of the $\text{OD}\cdots\text{O}_{\text{latt}}$ groups. It was demonstrated in Chapter 3[108] that this enhancement of the vibrational relaxation rate is neither due to desorption of the nitrogen (breaking of the weak hydrogen bond could be an efficient way for the O–D group to lose a considerable

amount ($\approx 1000 \text{ cm}^{-1}$) of its excess vibrational energy), nor due to energy transfer into internal degrees of freedom of the adsorbate. The enhancement was attributed to an increased coupling of the O–D group to the lattice caused by the hydrogen bond, allowing for a more rapid energy dissipation (For details, see Chapter 3).

From Fig. 5.3 it is observed that, although the overall absorption line and the vibrational population lifetimes are similar for the two differently hydrogen-bonded O–D groups, the homogeneous linewidths are very different. Recording a transient spectrum at a delay between pump and probe of 20 ps, it is found that for the OD \cdots O_{latt} groups, the pump pulse burns a hole in the absorption spectrum (see also Ref. [22]), whereas, remarkably, for the OD \cdots N₂ groups the whole absorption band decreases in amplitude (both transient spectra were recorded at 100 K). The fact that a hole is burnt in the LF O–D absorption spectrum implies that this line is predominantly inhomogeneously broadened [20]; there is a distribution of vibrational frequencies for the O–D groups, and only those O–D groups can be excited that are resonant with the frequencies within the laser pump pulse.

In order to obtain the homogeneous linewidth, we have calculated the transient spectra.[22] In these calculations the absorption band is deconvoluted into a sum of Lorentzians of full width at half maximum $\Gamma_{\text{hom}}^{0\rightarrow 1}$:

$$A(\tilde{\nu}) = \sum_i \mathcal{L}_i(\tilde{\nu}) \quad , \quad \mathcal{L}_i(\tilde{\nu}) = a_i \frac{\Gamma_{\text{hom}}^{0\rightarrow 1}/\pi}{4(\tilde{\nu} - \tilde{\nu}_i)^2 + (\Gamma_{\text{hom}}^{0\rightarrow 1})^2} \quad (5.3)$$

where $\tilde{\nu}_i$ is the center frequency of the i^{th} homogeneous Lorentzian line of amplitude a_i . The pump pulse excites a fraction f_i^0 of each Lorentzian, determined by the spectral overlap of the i^{th} Lorentzian with the laser pump pulse as well as saturation effects (power broadening).[22] The excited spectrum then reads:

$$A_{\text{exc}}(\tilde{\nu}, t) = \sum_i [1 - 2f_i^0 e^{(-t/T_1)}] \mathcal{L}_i(\tilde{\nu}), \quad (5.4)$$

where the initially excited fraction of excited oscillators, f_i^0 , is assumed to decay exponentially with time-constant T_1 . This spectrum (for $t=20$ ps) has to be convoluted with the laser probe spectrum to obtain the experimental excited spectrum. The results of this calculation are shown as dashed lines in Fig. 5.3. The corresponding FWHM homogeneous linewidth is $0.75 \pm 0.4 \text{ cm}^{-1}$ for the OD \cdots O_{latt} groups and $13 \pm 1 \text{ cm}^{-1}$ for the OD \cdots N₂ system at 100 K. The insets of Fig. 5.3 show the absorption spectrum with and without pump pulse, along with an illustrative homogeneous Lorentzian of which the overall absorption line is built up. From the homogeneous linewidths and the independently measured T_1 , we obtain pure dephasing times $T_2^* = 20 \pm 10$ ps for the OD \cdots O_{latt} groups and 0.82 ± 0.1 ps for the OD \cdots N₂ system at 100 K.

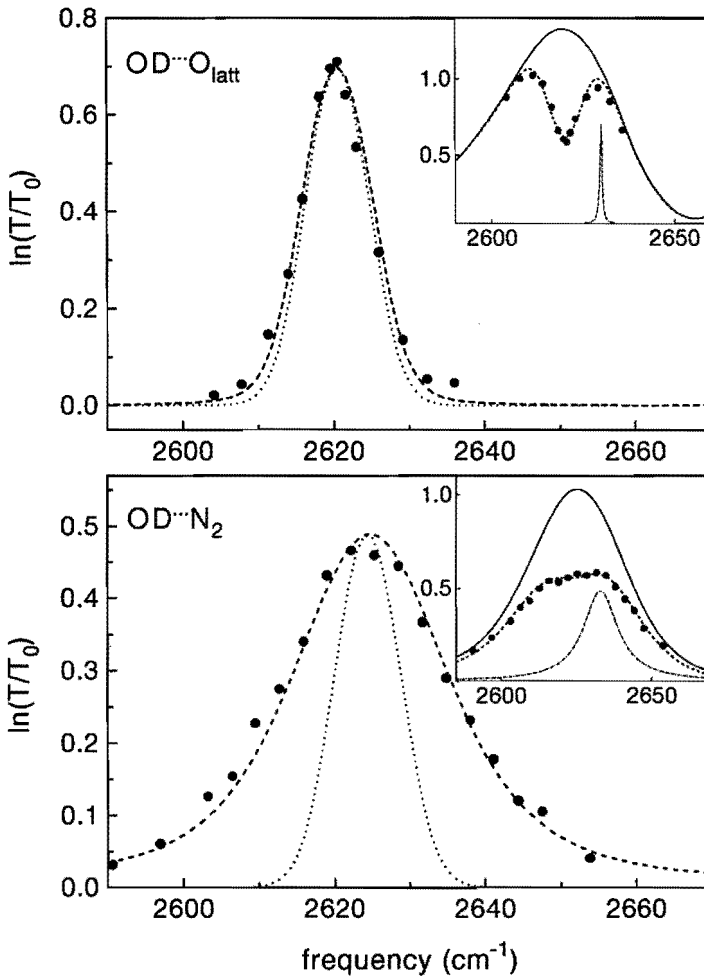


Figure 5.3: Relative transmission changes due to the pump pulse tuned to the peak of the absorption band as a function of probe frequency, at 20 ps delay between pump and probe. Full circles are data, the dotted line is the instrumental function (convolution of the 6 cm^{-1} laser pump and probe pulses, viz. the observed signal for $\Gamma_{\text{hom}} \rightarrow 0$). Upper panel: The $\text{OD}\cdots\text{O}_{\text{latt}}$ hydroxyls of $\text{D}_{0.19}\text{Y}$ at 100 K. The width of the burnt hole is almost completely determined by the 6 cm^{-1} width of the laser pulses. Lower panel: The $\text{OD}\cdots\text{N}_2$ of $\text{NaD}_{0.05}\text{Y}$ at 100 K. Virtually the whole absorption band is bleached. Dashed lines are the result of calculations described in the text. Insets show the absorption spectra from Fig. 5.1 with (dashed curve) and without (solid curve) the presence of the pump pulse, and the homogeneous Lorentzian lines constituting the absorption band (dash-dotted lines).

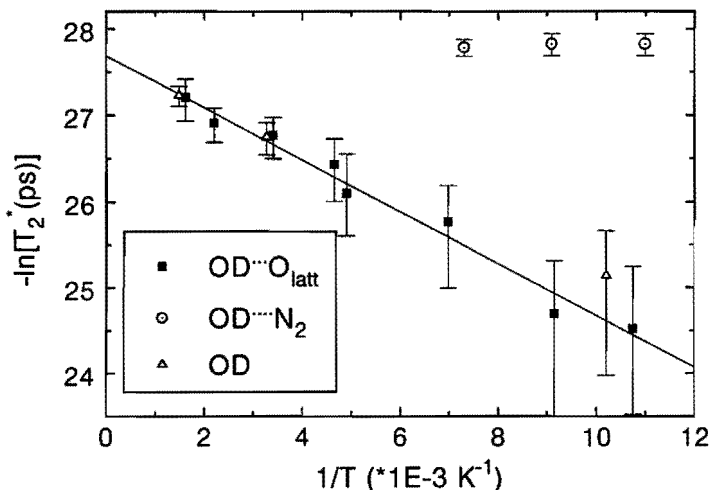


Figure 5.4: Arrhenius plot of the pure dephasing time T_2^* vs. temperature for the $\text{OD}\cdots\text{O}_{\text{latt}}$ and the $\text{OD}\cdots\text{N}_2$ hydroxyls. For both the LF OD $\text{OD}\cdots\text{O}_{\text{latt}}$ and the HF 'free' OD groups, a least squares fit gives an activation energy of $200\pm 70 \text{ cm}^{-1}$. For the OD groups bonded to nitrogen, no temperature dependence is found.

The large difference in dephasing times T_2^* indicates the presence of different dephasing mechanisms for the two systems. This is confirmed by the difference in temperature dependence of the dephasing times T_2^* for the two systems shown as an Arrhenius plot in Fig. 5.4. For the $\text{OD}\cdots\text{O}_{\text{latt}}$ groups an apparent activation energy of $200\pm 70 \text{ cm}^{-1}$ is observed. No temperature dependence is found for the $\text{OD}\cdots\text{N}_2$ groups. The temperature dependence of the pure dephasing time of the HF O-D groups, situated in the large cages in the zeolite structure (not or only very weakly H-bonded to the zeolite lattice) is also shown in Fig. 5.4. These data points coincide perfectly with those of the $\text{OD}\cdots\text{O}_{\text{latt}}$ groups, indicating that the same dephasing mechanism is operative for both the 'free' HF O-D groups and the hydrogen-bonded LF $\text{OD}\cdots\text{O}_{\text{latt}}$ groups. This implies that, although it greatly affects the vibrational population lifetime, the hydrogen bond does not play an important role in the dephasing of the O-D stretch vibration for the $\text{OD}\cdots\text{O}_{\text{latt}}$ groups. However, the hydrogen bond does affect the overall absorption band: For the $\text{OD}\cdots\text{O}_{\text{latt}}$ groups, the broadening of the whole absorption line is due to a static distribution of hydrogen-bond strengths. This

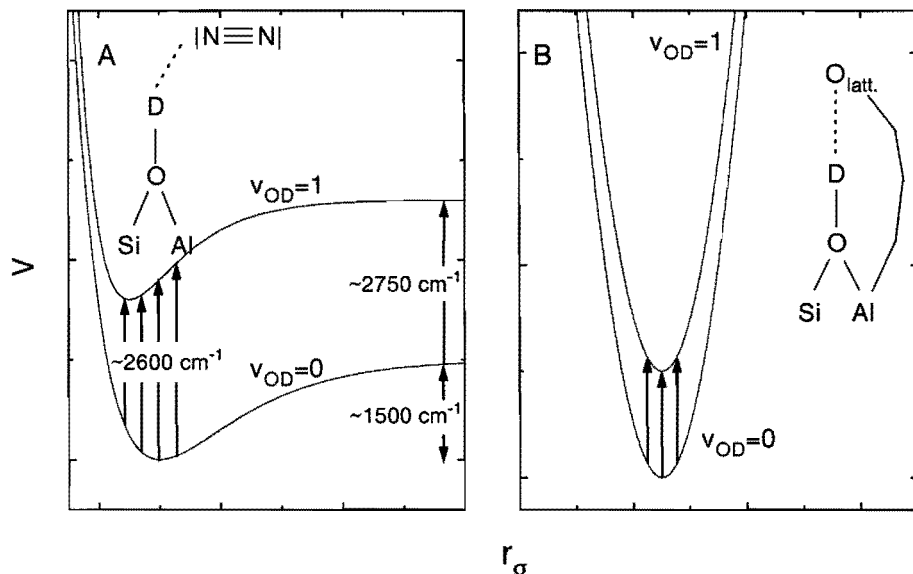


Figure 5.5: Schematic r_{OD} potentials for the two differently hydrogen bonded systems: The lower curve is for the $\nu_s(O-D)$ in the ground state, upper curve in the first excited state. A) For a hydrogen bond to an adsorbate, strongly anharmonic and dissociative. The H-bond dissociation energy is $\sim 1500 \text{ cm}^{-1}$, the transition frequency $\sim 2600 \text{ cm}^{-1}$ and $\sim 2750 \text{ cm}^{-1}$ with and without the H-bond, respectively. After Ref. [110]. B) For a hydrogen bond to fixed lattice oxygen atoms.

distribution of hydrogen-bond strengths is presumably due to the inhomogeneous distribution of Si and Al atoms throughout the zeolite lattice. It has been surmised [109] that the frequency of the O-H stretching vibration is sensitive to even the second Si/Al coordination shell. The conclusion that the inhomogeneous distribution is due to a distribution of different hydrogen bond strengths is substantiated by results of previous experiments which showed that the vibrational lifetime T_1 increases with increasing frequency within the absorption band (see Chapter 2), due to decreasing hydrogen-bond strength[44].

The large difference in the homogeneous linewidths for the $OD \cdots O_{latt}$ groups and the $OD \cdots N_2$ groups can be understood by considering the hydrogen-bond potentials for $v_{OD}=0$ and $v_{OD}=1$ for the two systems, which are schematically depicted in Fig. 5.5.

By noting that the timescales associated with the high-frequency the ν_s mode and the low-frequency ν_σ mode differ by over an order of magnitude, a vibrational Born-Oppenheimer approximation (also referred to as adiabatic approximation[92]) can be made. Thus, the slow motion of the r_σ coordinates is separated from the fast motion in the r_s coordinates. In this fashion the energies and wavefunctions of the system depend parametrically on the r_σ coordinate: The wavefunctions and eigenvalues can be calculated for a given value of r_σ , and by repeating this procedure for different r_σ , the variation of the energy of the system with this coordinate can be calculated. Thus the schematic potentials in Fig. 5.5 are obtained. In the presence of adsorbates, the potential is strongly anharmonic and dissociative. Furthermore, it is well known that the potentials for the ground and excited state are different[110]; the hydrogen bond is stronger for $v=1$ than for $v=0$, and hence the potential energy minimum is situated at smaller r_σ (O \cdots X distance) for $v=1$. [110] Since the width of the spectral distribution D is determined by the *difference* between the $v=0$ and $v=1$ potentials, i.e. by a change in the hydrogen bond upon excitation of the O-D stretch vibration, D will be relatively large for this system. In contrast, for the OD \cdots O_{latt} the potential energy curve is dictated by *lattice* parameters; the OD \cdots O_{latt} distance is determined not by the electrostatic interaction between the deuterium and the O_{latt}, but by the geometry of the zeolite lattice. The rigidity of the zeolite lattice strongly disfavours a change in the oxygen-oxygen distance. As a result the potential is non-dissociative, and very similar for the ground and excited state of the O-D vibration. As a result D will be relatively small, resulting in a narrow homogeneous absorption line. From the observation that the linewidths and the temperature dependence are the same for the free O-D groups and the OD \cdots O_{latt} groups (Fig. 5.4), we deduce that the homogeneous linewidth broadening due to the interaction with the hydrogen bond is so small, that a different broadening mechanism dominates. The observation of the $200 \pm 70 \text{ cm}^{-1}$ activation energy is most likely due to the involvement of the 260 cm^{-1} zeolite (oxygen) lattice mode in the dephasing process (there are no other low-frequency modes between 100 and 300 cm^{-1}). [111] This 260 cm^{-1} mode involves the cooperative motion of zeolite oxygen atoms[111]. The observation of an apparent activation energy is in good agreement with the Shelby-Harris theory in the limit of slow modulation. Hence we conclude that, for the LF OD \cdots O_{latt} groups, the coupling is properly accounted for by the Shelby-Harris theory, and that dephasing occurs by coupling to the 260 cm^{-1} zeolite (oxygen) lattice mode.

Another difference between the two differently hydrogen-bonded groups can be observed in the so-called hot-band absorption depicted in Fig. 5.6. From Fig. 5.6 it is clear that the hot-band absorption for the OD \cdots O_{latt} groups has approximately the

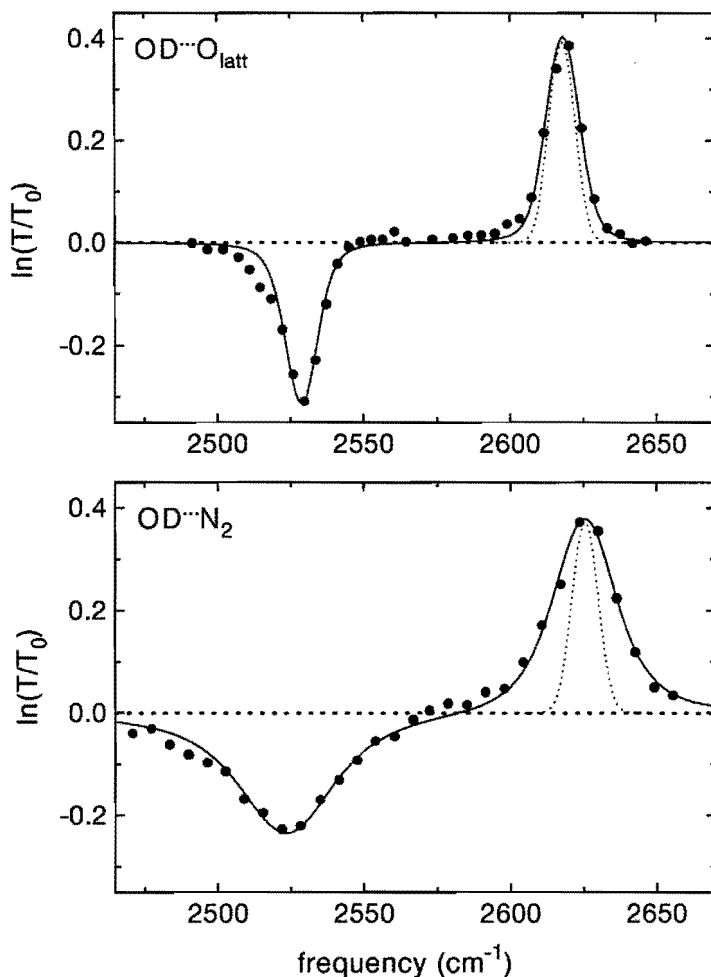


Figure 5.6: Transient absorption spectra after excitation of the O–D stretch vibration for the $\text{OD}\cdots\text{O}_{\text{latt}}$ hydroxyls at 200 K (upper panel) and the $\text{OD}\cdots\text{N}_2$ hydroxyls at 100 K (lower panel). For the $\text{OD}\cdots\text{O}_{\text{latt}}$ the induced hot band absorption (negative $\ln[T(t)/T_0]$) associated with the $1\rightarrow 2$ transition has the same width as the hole (positive $\ln[T(t)/T_0]$) due to the bleaching of the $0\rightarrow 1$ transition. For the $\text{OD}\cdots\text{N}_2$ groups the hot band is significantly broader than the hole. Solid lines are calculations explained in the text, dotted lines denote the instrumental function (convolution of the 6 cm^{-1} laser pump and probe pulses).

same width as the hole, whereas the hot band is much broader than the hole for the OD··N₂ groups. These transient spectra were recorded at temperatures of 200 K and 100 K for the OD··O_{latt} and the OD··N₂ groups, respectively.

The solid line through the data is a calculation for which each of the bleached Lorentzians constituting the absorption band are $\tilde{\nu}_{\text{anh}}$ anharmonically shifted from the original absorption band to form the hot band. In this calculation we assume that the 1→2 transition frequency of an oscillator is correlated to the 0→1 transition, in the sense that a transition corresponding to one of the Lorentzian lines on the red side of the absorption band will appear on the red side of the hot band: Each Lorentzian is exactly $\tilde{\nu}_{\text{anh}}$ cm⁻¹ shifted. The excited spectrum then reads:

$$A_{\text{exc}}(\tilde{\nu}, t) = \sum_i [1 - 2f_i^0 e^{(-t/T_1)}] \mathcal{L}_i(\tilde{\nu}, \Gamma_{\text{hom}}^{0 \rightarrow 1}) + \beta \sum_i f_i^0 e^{(-t/T_1)} \mathcal{L}_i(\tilde{\nu} + \tilde{\nu}_{\text{anh}}, \Gamma_{\text{hom}}^{1 \rightarrow 2}) \quad (5.5)$$

The first term corresponds to Eq. (5.4), and is due to the bleaching of the original absorption band, and the second term is the hot-band absorption. β is the ratio between the 1→2 and the 0→1 cross-sections (=2 for an harmonic oscillator). This straightforward procedure describes the data for the OD··O_{latt} groups quite well, with $\Gamma_{\text{hom}}^{0 \rightarrow 1} = 2.2 \pm 1$ cm⁻¹, $\tilde{\nu}_{\text{anh}} = 90 \pm 2$ cm⁻¹ and $\beta = 1.85$. In this calculation $\Gamma_{\text{hom}}^{1 \rightarrow 2} = 2.7 \pm 1$ cm⁻¹: $\Gamma_{\text{hom}}^{1 \rightarrow 2}$ is additionally broadened by ≈ 0.5 cm⁻¹ due to the 10 ps lifetime of the second excited state (see below). For the OD··N₂ groups the width of the Lorentzians constituting the hot band, $\Gamma_{\text{hom}}^{1 \rightarrow 2}$, has to be as large as 30 ± 4 cm⁻¹ ($\Gamma_{\text{hom}}^{0 \rightarrow 1} = 13 \pm 1$ cm⁻¹) to describe the experimental data, and $\beta = 1.95$. The anharmonicity, $\tilde{\nu}_{\text{anh}} = 100 \pm 2$ cm⁻¹ is significantly larger than that of the OD··O_{latt} groups. On the low-frequency side of both the hole and the hot band the calculations deviate slightly from the data, implying that the homogeneous linewidth varies slightly within the inhomogeneously broadened absorption band, as was found previously[22]. Hot bands with widths larger than the fundamental transition have been observed before in hydrogen-bonded systems [103, 104]. In fact, in all of these experiments a similar ratio of $\Gamma_{\text{hom}}^{1 \rightarrow 2} / \Gamma_{\text{hom}}^{0 \rightarrow 1}$ of 2-3 was observed. In our calculations we assume that the 1→2 transition center frequency of an oscillator is correlated to its 0→1 transition. In principle this need not be the case; an 'inhomogeneous' broadening mechanism for the 1→2 transition could be the cause of the large width of the hot band. However, this is not very likely due to the fact that this broadening is not observed for the LF OD··O_{latt} and the HF O-D groups (without adsorbed nitrogen), and that the same *relative* width of the hot band is observed for methane absorption (see below). Therefore, the relatively large $\Gamma_{\text{hom}}^{1 \rightarrow 2}$ associated with the 1→2 transition for the OD··N₂ groups is caused by either a much shorter population lifetime $T_1^{2 \rightarrow 1}$ for the $v=2$ state, or a faster dephasing of the 1→2

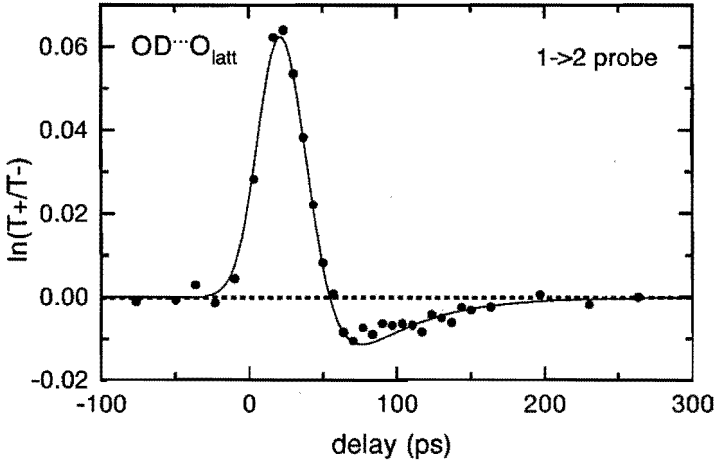


Figure 5.7: Results of the pump-pump-probe experiments for the $\text{OD}\cdots\text{O}_{\text{latt}}$ groups. Transmission changes at the hot band frequency ($1\rightarrow 2$ transition) due to the second pump pulse tuned to the $1\rightarrow 2$ transition ($T+$ denotes transmission with, and $T-$ without second pump pulse) versus delay between the probe pulse and the pump pulses. The solid line is the result of calculations assuming decay from the second excited state $v=2$ to the ground state via $v=1$.

transition (shorter $T_2^* 1\rightarrow 2$), since $\Gamma_{\text{hom}}^{1\rightarrow 2}$ is determined by [112]:

$$2\pi\Gamma_{\text{hom}}^{1\rightarrow 2} = \frac{1}{T_1^{1\rightarrow 0}} + \frac{1}{T_1^{2\rightarrow 1}} + \frac{2}{T_2^* 1\rightarrow 2}, \quad (5.6)$$

where $T_1^{1\rightarrow 0}$ and $T_1^{2\rightarrow 1}$ are the population lifetimes of the first and second excited states, and $T_2^* 1\rightarrow 2$ is the pure dephasing time for the $1\rightarrow 2$ transition. To check whether the $v=2$ population lifetime is the cause of the broadening, we measured this lifetime with pump-pump-probe experiments[113].

For the pump-pump-probe experiments, the delay between the $(1\rightarrow 2)$ -pump and the $(0\rightarrow 1)$ -pump was fixed at 16 ps (the time at which the $v=1$ state population due to the $(0\rightarrow 1)$ -pump is maximal). The delay of the probe pulse, of the same frequency as one of the two pump pulses, is varied. In Fig. 5.7 the results of a pump-pump-probe experiments are shown for the $\text{OD}\cdots\text{O}_{\text{latt}}$ groups, with the probe frequency tuned to the $1\rightarrow 2$ transition. In this Figure, the transmission changes induced by the second pump pulse are plotted vs. delay with respect to the first pump pulse. Clearly, the $(1\rightarrow 2)$ -pump excites a significant amount of oscillators to their second excited state, i.e.

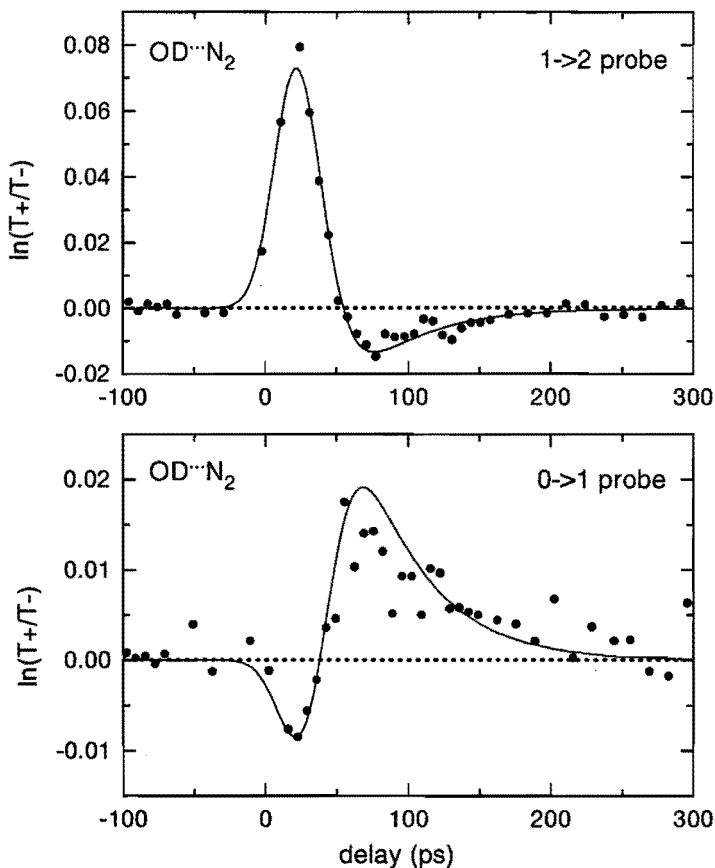


Figure 5.8: Results of the pump-pump-probe experiments for the $OD \cdots N_2$ groups. Upper panel: Transmission changes at the hot band frequency ($1 \rightarrow 2$ transition) due to the second pump pulse ($T+$ denotes transmission with, and $T-$ without second pump pulse). Lower panel: Transmission changes at the ground state absorption frequency ($0 \rightarrow 1$ transition) due to the second pump pulse. The solid lines are the results of calculations assuming decay from the second excited state $v=2$ to the ground state via $v=1$. Note that both data sets can be well accounted for by one calculation.

the hot-band absorption is bleached, causing the positive $\ln(T+/T-)$. With the (0→1)-pump blocked, no signal was observed, confirming that the transmission changes due to the (1→2)-pump result from up-pumping of the O–D oscillators to their second vibrationally excited state. The fact that after the transmission *increase* (bleaching), a transmission *decrease* is observed can be understood as follows: the probe pulse is monitoring the population difference between the $v=1$ and $v=2$ levels. If the oscillators in $v=2$ decay to $v=1$, then the long-time effect of the second pump pulse will be that there are more oscillators in $v=1$ than without the second pump pulse; the oscillators have been put 'on hold' in the $v=2$ state for a time $T_1^{2\rightarrow 1}$, so that the hot band (1→2 absorption) will effectively live somewhat longer with than without the second pump pulse. The experimentally observed signals were calculated by numerically solving the appropriate set of coupled rate equations for a three level system (See e.g. Chapter 6), rendering the time-dependent population distribution. Subsequently, the transmission of the probe pulse is evaluated. Input parameters are pulse (intensities, duration and shape) and sample (absorption cross sections, oscillator density and sample length) characteristics. The result using a lifetime $T_1^{2\rightarrow 1}$ of 10 ps is shown in Fig. 5.7 as a solid line. Although this lifetime is shorter than the duration of our pulses, we can deduce that the error in this value is not larger than 5 ps from both the amplitude and width of the signal. Decay from $v=2$ directly to the ground state has been observed in this type of experiment (see Chapter 8), but is not significantly occurring in this system, since in the case of direct relaxation, the signal would have a distinctly different shape (see Chapter 8): In case of direct decay to the ground state, the overshoot of the transmission after the bleaching of the hot band is not observed.

In Fig. 5.8 the results are shown for the OD··N₂ groups, with the probe tuned to the 1→2 transition, and the 0→1 transition, respectively. The results of the same calculations with exactly the same input parameters were used to describe both data sets, and a again a lifetime $T_1^{2\rightarrow 1}$ of 10 ps was found. Obviously, this value is too large to account for the observed width of the hot band of 30 cm⁻¹. We therefore conclude that the observation of the large hot-band width must be due to a faster pure dephasing for the 1→2 transition ($T_2^{* 1\rightarrow 2}=0.35\pm 0.05$ ps) compared to that of the 0→1 transition ($T_2^{* 0\rightarrow 1}=0.82\pm 0.1$ ps) for the OD··N₂ groups.

5.6 Coupling mechanism for hydrogen-bond induced dephasing

We have shown in the previous section that for the OD··O_{latt} groups the dephasing mechanism can be described by the Shelby-Harris coupling model. However, in that

case the homogeneous linewidth is not caused by coupling to the hydrogen-bond mode. In contrast, for the O–D groups with adsorbates coupling to the hydrogen bond is responsible for the observed linewidths. In this section we will investigate the coupling mechanism for this system.

The temperature dependence of the homogeneous linewidth of the OD \cdots N₂ groups does not provide conclusive information on the type of coupling between the high-frequency and the hydrogen-bond stretching modes. The absence of a significant temperature dependence (the same observation was made for other adsorbates) can be explained by both the Shelby-Harris and the Robertson-Yarwood model. The temperature-activated behavior predicted by the Shelby-Harris model is valid only in the low-temperature (slow modulation) limit and therefore the absence of temperature dependence might be due to the possibility that for this system the modulation is intermediate or fast. As far as the Robertson-Yarwood model is concerned, it does not predict a significant dependence of the linewidth on temperature. It is clear, however, that in the Robertson-Yarwood type of coupling the temperature dependence can be very complicated: Increasing the temperature will lead to an increase of the spectral distribution D due to an increase in the rms displacement of r_σ , $(r_\sigma^2)^{1/2}$. Furthermore, this theory would also predict a temperature dependent τ_c , if the low-frequency mode were treated quantum-mechanically [114, 115]: In a quantum-mechanical description, the stochastic modulation of the high-frequency mode is a result of ongoing energy exchange between the quantum levels of the hydrogen bond and the bath. With increasing temperature the rate of exchange will increase leading to a decrease of τ_c . On the other hand, with increasing temperature the hydrogen bond stretching frequency may decrease due to the strong anharmonicity of the hydrogen bond, leading to an increase of τ_c . In conclusion, a change in temperature can have very different, counteracting, effects on the linewidth. Hence, it is clear that temperature is not a suitable parameter to investigate the nature of the coupling between the high-frequency and the hydrogen-bond mode.

It is interesting to note that the theoretical models of Shelby-Harris and Robertson-Yarwood make diametrically opposed predictions concerning the linewidth upon changing the *frequency* of the $\nu_\sigma(\text{XH}\cdots\text{Y})$ hydrogen bond stretch vibration. The Shelby-Harris model predicts the following: An increase of the $\nu_\sigma(\text{XH}\cdots\text{Y})$ frequency will result in a slower exchange with the bath, and hence a slower modulation (larger τ_c) of the high-frequency vibration. The absence of a temperature dependence for the homogeneous linewidth of the O–D groups with adsorbates implies that the frequency modulation of the high-frequency O–D mode does not occur in the regime of slow modulation. In the regime of intermediate or fast modulation, a slower modulation

will result in a broadening of the line, since less motional narrowing will occur. In contrast, the Robertson and Yarwood model predicts a narrowing of the line, since in this model the coordinate r_σ determines the dephasing directly and $r_\sigma(t)$ will fluctuate more rapidly with increasing $\nu_\sigma(\text{XH}\cdots\text{Y})$ frequency. The faster modulation will lead to more motional narrowing, since $\tau_c = \gamma/\nu_\sigma^2$, and therefore the absorption linewidth will become smaller. Hence it is clear that the decisive test between the two theoretical models is a change of the ν_σ hydrogen bond stretching frequency. By adsorbing a molecule different from nitrogen, a change in ν_σ can easily be achieved. For a meaningful comparison between the theories, a requirement is that the shape of the $v=0$ and $v=1$ potentials (determining the spectral distribution D) and thus the adsorption energy remains the same. A good candidate is methane. Methane produces the same shift of the O–D stretching frequency (and a very similar absorption line)[108] but has only half the mass of nitrogen, and hence ν_σ will increase by approximately a factor of $\sqrt{2}$, since the reduced mass of this vibration will be determined predominantly by the mass of the adsorbate.

As shown in Fig. 5.9, the homogeneous linewidth decreases significantly from 13 ± 1 cm^{-1} for O–D $\cdots\text{N}_2$ to 8 ± 1 cm^{-1} for O–D $\cdots\text{CH}_4$, demonstrating the validity of the Robertson-Yarwood model for this system. The vibrational population lifetime for the O–D $\cdots\text{CH}_4$ groups was the same as for the O–D $\cdots\text{N}_2$ groups (~ 15 ps) and therefore does not contribute to the width of the homogeneous line. Nitrogen and methane were both adsorbed to deuterated mordenite zeolite (methane adsorbs poorly to Y zeolite). For the calculation for nitrogen adsorption, shown as a solid line in Fig. 5.9, exactly the same parameters were employed as those describing adsorption to Y zeolite: a homogeneous linewidth of 13 cm^{-1} , an excited state linewidth of 30 cm^{-1} , and $\beta=1.95$. Only the anharmonicity was found to be different (120 ± 2 cm^{-1} for Mordenite, as opposed to 100 ± 2 cm^{-1} for Y-zeolite). This means that, despite the different contributions from inhomogeneous broadening, the homogeneous linewidth is independent of zeolite structure. For methane the calculations show that $\Gamma_{\text{hom}}^{0\rightarrow 1}=8\pm 1$ cm^{-1} , $\Gamma_{\text{hom}}^{1\rightarrow 2}=20\pm 3$ cm^{-1} , $\tilde{\nu}_{\text{anh}}=115\pm 2$ and $\beta=2.0$; Again, the hot band is much broader than the fundamental transition as also observed for O–D $\cdots\text{N}_2$.

In Fig. 5.10 the transient spectra resulting from adsorption of xenon and carbon-monoxide are shown. For xenon adsorption, almost the whole absorption band is bleached, indicating that the homogeneous linewidth is very large. The solid line shows the absorption spectrum as recorded by the laser probe pulses. Obviously, this absorption line is almost completely homogeneously broadened. The spike at exactly the pump frequency is due to (LF) O–D groups to which no xenon is adsorbed. These free O–D groups have a very narrow homogeneous linewidth. The decreased transmission

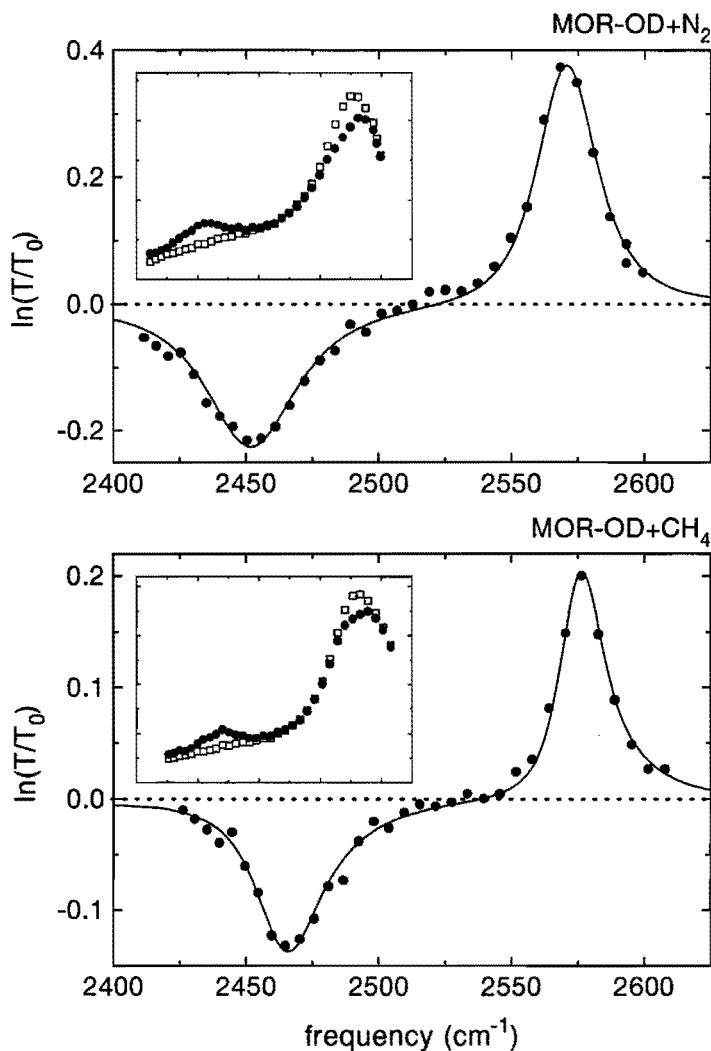


Figure 5.9: Transient absorption spectra after excitation of the O–D stretch vibration for the OD···N₂ hydroxyls at 100 K (upper panel) and the OD···CH₄ hydroxyls at 120 K (lower panel). The O–D groups are situated in zeolite Mordenite. Insets show the absorption spectra with (●) and without (□) the pump pulse, as recorded by the laser probe pulses. Although the overall absorption spectra are very similar, the bleaching (and therefore the homogeneous linewidth) is significantly narrower for the OD···CH₄ hydroxyls. Lines are calculations explained in the text.

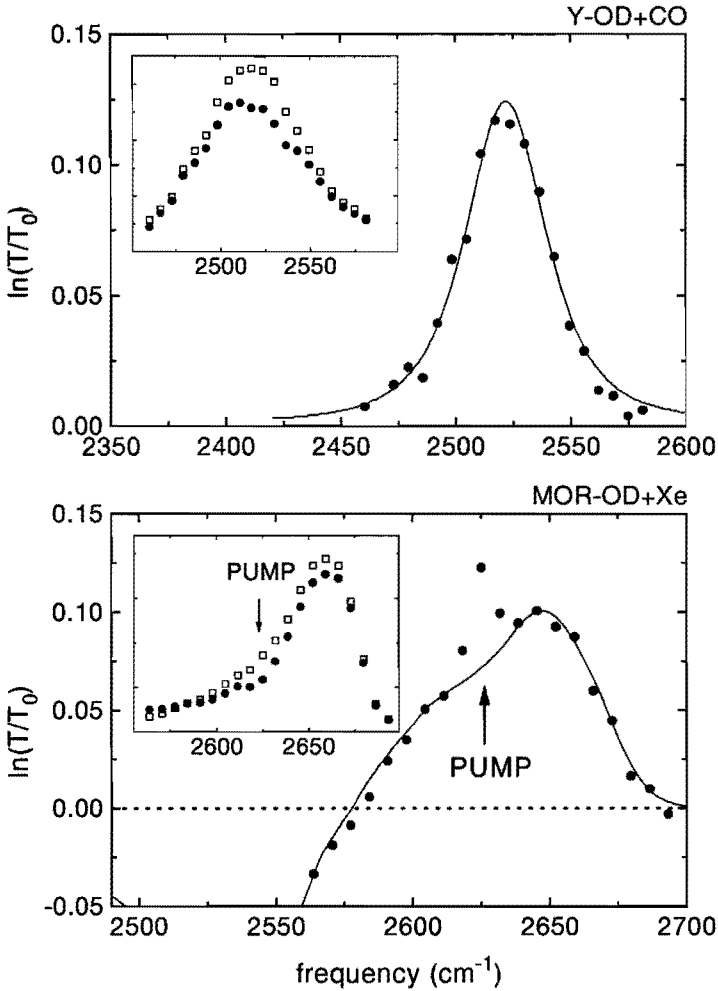


Figure 5.10: Transient absorption spectra after excitation of the O–D stretch vibration for the OD···Xe hydroxyls in D-Mordenite at 170 K (upper panel) and the OD···CO hydroxyls (lower panel) in NaD_{0.05}Y at 100 K. Insets show the absorption spectra with (●) and without (□) the pump pulse, as recorded by the laser probe pulses. For xenon adsorption the small spike at the pump frequency is due to O–D groups without adsorbed Xe (with a very narrow homogeneous line), and on the red side excited state absorption sets in. Lines are calculations explained in the text.

on the red side is due to excited state absorption. For the O-D groups with carbon-monoxide adsorbed, a homogeneous linewidth of $22 \pm 2 \text{ cm}^{-1}$ is observed. The results of the experiments are summarized in Table 5.1 .

The Robertson-Yarwood expression for τ_c provides a quantitatively correct description of the data for all adsorbates. Assuming a damping parameter γ of 50 cm^{-1} in accordance with Refs.[100–102], and a $\nu_\sigma(\text{OD} \cdots \text{X})$ frequency of 100 cm^{-1} for $\text{X}=\text{N}_2$ [64], we find that a value of 46 cm^{-1} for D is required to account for the observed hole of 14 cm^{-1} . This implies that $D\tau_c=0.23$, i.e. the modulation is in the intermediate modulation regime and motional narrowing is important in the description of the linewidth.² We take this set as a reference to calculate the linewidths for the other adsorbates. We approximate $V(r_\sigma)$ by a Morse potential: $V(r_\sigma) = E_{\text{ads}}(1 - e^{-a(r_\sigma - r_0)})^2$, where E_{ads} is the absorption energy (and hence dissociation energy), and a determines the degree of anharmonicity of the hydrogen-bond potential. This anharmonicity parameter a is determined from the $0 \rightarrow 1$ transition frequency (100 cm^{-1} for $\text{X}=\text{N}_2$ [64]) and the adsorption energy. If the degree of anharmonicity of the $(\text{OD} \cdots \text{X})$ potential remains the same for the different adsorbates, then for the other adsorbates the $\nu_\sigma(\text{OD} \cdots \text{X})$ frequency is readily calculated as a function of adsorption energy E_{ads} and adsorbate mass M_{ads} (*viz.* the reduced mass of this vibration):

$$\tilde{\nu}_\sigma(E_{\text{ads}}, M_{\text{ads}}) = \tilde{\nu}_\sigma^{\text{N}_2} \frac{M_{\text{N}_2} [2\sqrt{2}M_{\text{ads}} \sqrt{\frac{E_{\text{ads}}}{M_{\text{ads}}} \pi - ah}]}{M_{\text{ads}} [2\sqrt{2}M_{\text{N}_2} \sqrt{\frac{E_{\text{N}_2}}{M_{\text{N}_2}} \pi - ah}]}, \quad (5.7)$$

with h Planck's constant. If γ is independent of adsorbate, we obtain τ_c , also shown in Table 5.1. We assume that D , determined by the difference between the ground-state and excited-state potential, scales linearly with the heat of adsorption. The calculated linewidths resulting from numerically solving the integral of Eq. (5.2) are shown in Table 5.1.

The agreement with the data is excellent, and it should be noted that the results depend only weakly on the assumed reference values for γ and ν_σ for nitrogen, as long as these values reproduce the observed linewidth of 13 cm^{-1} for nitrogen.

It is clear that for the O-D \cdots CH₄ groups the small homogeneous linewidth as

²The fact that the product $D\tau_c \approx 1$, means that the homogeneous lineshape is *not* Lorentzian, as was assumed in the fits to our data (Eq. 5.4). In principle, the transient spectra should be calculated with an inhomogeneous line composed of profiles intermediate between Gaussian and Lorentzian. The problem is that the value of $D\tau_c$ is not precisely known, and therefore we approximate the lines by Lorentzians. Experimentally, the deviation from a Lorentzian-shaped homogeneous linewidth is very difficult to observe, since the deviation will manifest itself in the wings of the homogeneous lines, where the signal is small.

Table 5.1: Characteristics and effects of different adsorbates on zeolites Y and Mordenite: The shift from the original O-D stretch frequency by the adsorbate $\Delta\tilde{\nu}_{OD}$, the width of this line Γ_{OD} , the heat of adsorption E_{ads} , the experimentally observed homogeneous linewidth Γ_{hom}^{exp} , calculated spectral distributions D , calculated correlation times τ_c , and the calculated homogeneous linewidth Γ_{hom}^{calc} . All widths are FWHM and errors denote 2σ .

adsorbate		N ₂	N ₂	CH ₄	CO	Xe
zeolite		D-Mor	D-Y	D-Mor	D-Y	D-Mor
M_{ads}	(a.m.u.)	32	32	16	32	131.3
$\Delta\tilde{\nu}_{OD}$	(cm ⁻¹)	65 (±3)	60 (±3)	60 (±3)	168 (±5)	45 (±6)
Γ_{OD}	(cm ⁻¹)	61 (±3)	42 (±3)	50 (±3)	65 (±3)	30 (±6)
E_{ads}^a	(eV)	0.16	0.16	0.15	0.23	0.12
Γ_{hom}^{exp}	(cm ⁻¹)	13 (±1)	13 (±1)	8 (±1)	22 (±2)	28 (±4)
D	(cm ⁻¹)	51	51	47.5	73	38
τ_c	(10 ⁻¹³ s)	1.66	1.66	1.14	1.12	11.8
$D \times \tau_c$		0.25	0.25	0.16	0.24	1.34
Γ_{hom}^{calc}	(cm ⁻¹)	13 (ref.)	13 (ref.)	7.5	19.5	29.8

^a Heats of adsorption for CO and N₂ obtained from Ref. [116], others are estimated from $\Delta\tilde{\nu}_{OD}$ (see Ref. [64]).

compared to the O-D...N₂ is due to the increased effect of motional narrowing: the frequency of the ν_σ mode is increased, whereas D remains practically unaltered. For xenon the ν_σ (OD...Xe) frequency is relatively low due to the high mass of xenon. Hence τ_c is relatively large, and in this case *less* motional narrowing will occur. Indeed, despite the smaller adsorption energy and hence smaller D , a very broad homogeneous line is observed. For CO, its relatively strong adsorption results in both a large D and a small τ_c compared to nitrogen. The correlation time is very similar to that of methane: although the relatively strong hydrogen bond will lead to an increase of the frequency of the ν_σ mode, the higher reduced mass of the O-D...CO compared to O-D...CH₄ will lower this frequency.

It is clear that for the zeolite-adsorbate system the data can be very well described by a Robertson-Yarwood type of coupling between the modes. In general, the anharmonic coupling term can be expanded as a power series of the normal coordinates r_s and r_σ as:

$$V_{anh}(r_s, r_\sigma) = \mathcal{F}(r_\sigma) (a r_s + b r_s^2 + c r_s^3 + \dots) \quad (5.8)$$

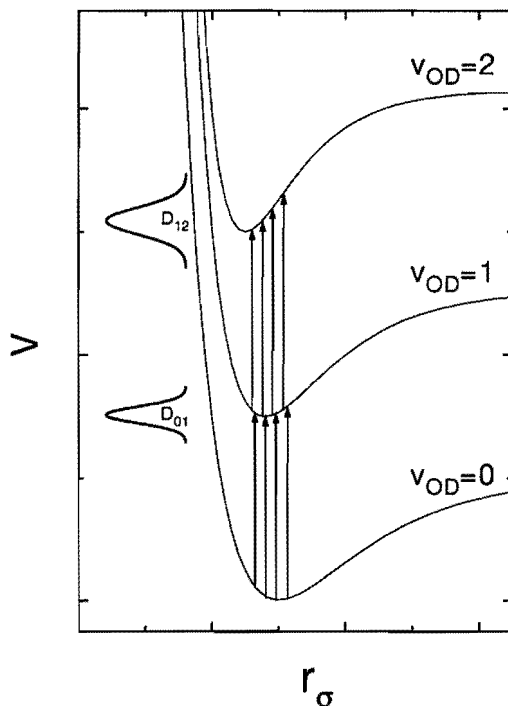


Figure 5.11: Schematic r_σ potentials for the hydrogen bonded OD...Adsorbate system for the $\nu_s(\text{O-D})$ in the ground, first and second excited state. The $1 \rightarrow 2$ transition is broadened compared to the $0 \rightarrow 1$ transition, indicating third- or higher-order terms in r_s contribute significantly to the anharmonic coupling term V_{anh} .

Since the Robertson-Yarwood model works so well for the O-D groups with adsorbates, this means that the coupling is first-order in r_σ . Hence, it must be that $\mathcal{F}(r_\sigma) \propto r_\sigma$. What is equally interesting, is the fact that the hot band is broader than the hole, i.e. $\Gamma_{\text{hom}}^{1 \rightarrow 2}$ is larger than $\Gamma_{\text{hom}}^{0 \rightarrow 1}$. This implies that *third-order* coupling terms in r_s are important in the anharmonic coupling term. This can be understood as follows: Consider a potential with negligible anharmonicity in the O-D distance r_s , i.e. the potential $V(r_s; r_\sigma)$ which depends parametrically on the hydrogen-bond coordinate r_σ in the Born-Oppenheimer approximation. Then for a given value of r_σ , the potential $V(r_s; r_\sigma)$ is the sum of a term quadratic in r_s and V_{anh} : $V(r_s; r_\sigma) = \alpha r_s^2 + V_{\text{anh}}(r_s, r_\sigma)$. If only

linear terms in r_s in Eq. (5.8) contribute to the anharmonic coupling term $V_{\text{anh}}(r_s, r_\sigma)$, then the $V(r_s; r_\sigma)$ potential is still completely harmonic, the spacing between the energy levels is constant and independent of r_σ . This means that the transition frequencies between the energy levels are the same and that these cannot be broadened due to the hydrogen bond. Another way of understanding this is that, in case only linear terms in r_s contribute to V_{anh} , the hydrogen bond potentials $V(r_\sigma)$ for the ground state ($v_{\text{OD}}=0$) and the excited states ($v_{\text{OD}}=1, 2, \text{etc.}$) are exactly the same. Indeed, none of the transitions will be broadened, since the spectral distribution D is determined by the *difference* between the potentials. In this case the absorption line as well as the hot band would be infinitely narrow. If the r_s^2 -terms become important, the $0 \rightarrow 1$ and the $1 \rightarrow 2$ transitions will both be equally broadened.[112, 117, 118] In this case, a change in r_σ induces a difference between the ($v_{\text{OD}}=0$) and ($v_{\text{OD}}=1$) hydrogen-bond potentials, that is equal to the difference between the ($v_{\text{OD}}=1$) and ($v_{\text{OD}}=2$) potentials: The hole and the hot band will both have the same, non-zero width. It is only when third -or higher- order terms become significant that the width of the $0 \rightarrow 1$ will be different from that of the $1 \rightarrow 2$. In this case, the difference between the $V(r_\sigma)$ hydrogen bond potentials for $v_{\text{OD}}=1$ and $v_{\text{OD}}=2$ will be larger than the difference between $v_{\text{OD}}=0$ and $v_{\text{OD}}=1$ potentials. This situation is schematically depicted in Fig. 5.11. The spectral distribution associated with the $1 \rightarrow 2$ transition $D_{1 \rightarrow 2}$ is broader than that of the $0 \rightarrow 1$ transition $D_{0 \rightarrow 1}$, accounting for the broader hot band. Hence it is concluded that the coupling between the ν_s and the ν_σ mode is *linear* in the hydrogen bond coordinate r_σ , and that third -or higher- order terms in r_s contribute significantly to the anharmonic coupling term.

For the $\text{OD} \cdots \text{O}_{\text{latt}}$ groups, for which the hole and the hot band have the same width, it is clear that anharmonic coupling terms of higher than second-order in r_s do not significantly contribute. This is in agreement with the Shelby-Harris model that states that the predominant terms are of second-order in both the low- and high- frequency coordinate.

The relative importance of different anharmonic coupling terms for the $\text{OD} \cdots \text{O}_{\text{latt}}$ and the $\text{OD} \cdots \text{N}_2$ groups also explain the different anharmonicities of 92 and 100 cm^{-1} , respectively. The third-order r_s -term in the V_{anh} of the $\text{OD} \cdots \text{N}_2$ groups will lead to an increase of the anharmonicity of the effective potential in r_s of the O-D stretching vibration, whereas the second-order terms in r_s for the $\text{OD} \cdots \text{O}_{\text{latt}}$ groups will not.

5.7 Conclusions

We have shown that the effect of a hydrogen bond on the vibrational lineshape depends critically on the nature of the hydrogen bond. If the potential energy as a function of the hydrogen bond coordinate is solely determined by the electrostatic interaction between the hydrogen atom and the hydrogen bonding partner, this will result in broad homogeneous lines, as observed for O–D groups to which simple molecules are adsorbed. In the case that the structure is rigid, however, it is not the hydrogen bond that determines the homogeneous linewidth, and we observe that the linewidth is determined by coupling to a $\sim 200\text{ cm}^{-1}$ lattice mode. If the homogeneous linewidth is determined by the hydrogen bond (in case of the adsorbates), we find that variation of the adsorbates allows us to investigate the coupling between the high-frequency ν_s (O–D) stretching mode and the low-frequency ν_σ (OD \cdots X) stretching mode. From the variation of adsorbate, we find strong evidence that this coupling is linear in the r_σ coordinate. From the fact that the 1 \rightarrow 2 transition is broadened compared to the 0 \rightarrow 1 transition, we deduce that third- or higher-order terms in r , contribute significantly to the coupling term.

Chapter 6

The dynamics of infrared photodissociation of methanol in zeolites and in solution

We have investigated the dynamics of the O–H stretch vibration of methanol in solution and adsorbed to sodium forms of Y zeolite with non-linear picosecond infrared spectroscopy. Both in solution and adsorbed to NaY, methanol is present as hydrogen-bonded clusters. After resonant IR excitation, vibrational relaxation occurs by breaking the hydrogen bond between the methanol molecules, resulting in a dissociation of the clusters. This process occurs much faster in solution ($T_1 \leq 3$ ps) than inside the sodium zeolite ($T_1 = 10 \pm 3$ ps). A second remarkable difference is that whereas in solution a rapid hydrogen-bond re-association occurs, ($\tau_r = 25 \pm 3$ ps), in the zeolite this process takes considerably longer ($\tau_r \gg 2$ ns). The differences can be understood by considering the different microscopic environments of the methanol clusters.

6.1 Introduction

Vibrational energy transfer processes have been studied extensively in the condensed phase (for a review, see e.g. Ref. [119]), since the redistribution of vibrational energy is an important factor in chemical reaction kinetics. The rate of vibrational (energy) relaxation relative to the rate for coupling into the reaction coordinate may dictate reaction rates and pathways. A frequently employed tool in these investigations is time-resolved (picosecond) IR spectroscopy, since this technique allows for the direct observation of energy relaxation times. The relaxation times cannot be extracted from linewidth data, since linewidths in the condensed phase are generally determined by pure dephasing processes. Clearly, relaxation rates of molecules incorporated in zeolites can provide information concerning the interaction between reactant and catalyst, more specifically, on the energy transfer dynamics between the two. In this Chapter, we report on conventional (linear) and time-resolved (picosecond) non-linear infrared spectroscopic experiments performed on methanol in solution and adsorbed to the sodium forms of Y-zeolite, to investigate the dynamics of vibrational energy flow in these systems. It is shown that, although the linear absorption spectra for the two systems are very similar, the vibrational *dynamics* of the methanol molecules are markedly different. We obtain novel information on the dynamic behaviour of molecules incorporated in zeolites and their interaction with the cationic zeolite sites, which cannot be obtained with conventional linear spectroscopy.

6.2 Infrared dynamics of methanol clusters in solution and adsorbed to NaY

In Figure 6.1 two absorption spectra in the O–H stretching region are depicted. The upper panel shows the absorption of a 2 mm thick sample of a solution of 0.25 M methanol in carbontetrachloride. The spectrum consists of three spectral components at 3645, 3520 and 3350 cm^{-1} . These are known [66,120,121] to be due to absorption by (i) isolated methanol molecules and methanol molecules terminating clusters/chains by accepting an H-bond (both $\tilde{\nu}_{\text{OH}} \approx 3645 \text{ cm}^{-1}$), (ii) methanol molecules terminating chains/clusters by donating an H-bond (singly hydrogen-bonded) ($\tilde{\nu}_{\text{OH}} \approx 3520 \text{ cm}^{-1}$), and (iii) internal doubly hydrogen-bonded methanol molecules inside the cluster ($\tilde{\nu}_{\text{OH}} \approx 3350 \text{ cm}^{-1}$). Hence, the integrated absorption of the 3520 cm^{-1} peak is a measure for the number of clusters and the integrated absorption of the 3350 cm^{-1} peak is a measure for the size of the methanol clusters.

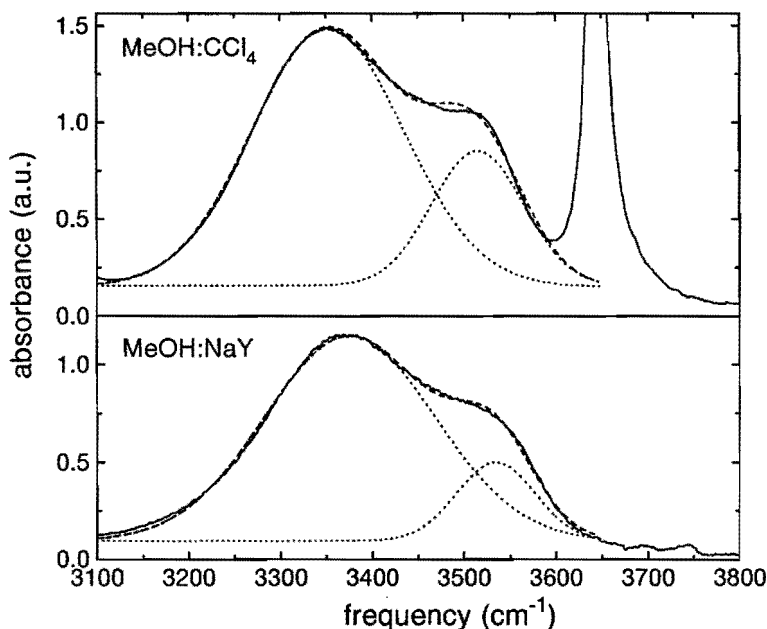


Figure 6.1: Linear absorption spectra of (i) a 2 mm thick solution of 0.25 M methanol in carbontetrachloride (offset by 1.2 absorbance units), and (ii) methanol adsorbed to $\text{Na}_{0.27}\text{Y}$ both at 298 K. The spectra are deconvoluted into two Gaussian lines (dotted lines) the sums of which are shown as a dashed line. Note the similarities between the absorption spectra.

The lower panel of Fig. 6.1 shows the spectrum of methanol adsorbed to NaY, characterized by a silicon-aluminum ratio of $\text{Si}/\text{Al}=2.4$. The ~ 10 mg zeolite sample was pressed into a self-supporting disc and water was removed by heating to 700 K *in vacuo* for 1 hour. Interestingly, apart from the absence of the 3645 cm^{-1} peak, the absorption spectrum looks very similar to that of methanol in solution. The two absorption bands have been observed previously for methanol adsorbed to NaK-ERIO-75 zeolite.[122] This indicates that also in the zeolite clustering of the methanol occurs, presumably around the favored adsorption sites, the Na^+ atoms; it has been established that the heat of adsorption of methanol to these sites is much higher than to the bare zeolite pore walls or silanol groups.[123] Indeed, upon increasing the methanol pressure, both peaks increase in intensity, but at some point the $\sim 3530\text{ cm}^{-1}$ peak stops growing

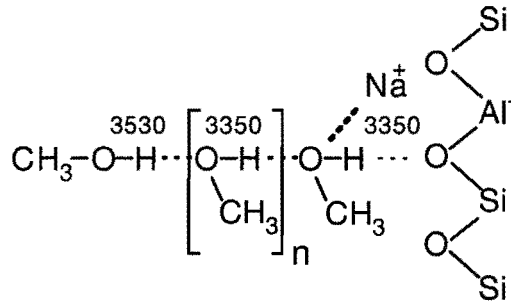


Figure 6.2: Microscopic configuration of the methanol cluster adsorbed to the sodium ion inside the zeolite. In solution, the cluster is terminated by a hydrogen-bond accepting methanol molecule instead of the sodium atom. Multiple adsorption to one Na^+ site, the formation of cyclic (sub-)structures, or multiple bonding within the cluster cannot be excluded.

(also observed in Ref. [122]), suggesting that no more clusters can be formed. The 3350 cm^{-1} peak grows continuously with methanol-pressure, indicating that the size of the clusters increases. Evacuating the zeolite sample after adsorption removes all methanol, indicating the absence of chemisorption. Thus we conclude that both in solution and in the zeolite the methanol is present as hydrogen-bonded clusters.

The microscopic picture of the methanol with the associated transition frequencies that emerges[66, 77, 120, 121] is shown in Fig. 6.2, where we cannot exclude multiple adsorption to one Na^+ site, the formation of cyclic (sub-)structures, or multiple bonding within the cluster. Also, due to the high density of sodium atoms, it is possible that within one cluster different methanol molecules are bound to different sodium atoms. In the zeolite the chain is terminated on one side by the sodium atom and on the other by a methanol molecule with $\tilde{\nu}_{\text{OH}}=3530\text{ cm}^{-1}$. From the absorption cross-sections[66], we estimate that the number of internal methanol molecules $n \approx 2$ for the absorption spectrum in Fig. 6.1. In solution the same picture applies[66, 77] with a methanol molecule taking the place of the sodium atom.

For the time-resolved experiments intense picosecond (18 ps) tunable infrared ($2200\text{--}4500\text{ cm}^{-1}$) pulses are generated by downconversion of 1064 nm Nd:YAG pulses in LiNbO_3 crystals (for details, see Chapter 1). Our set-up generates independently tunable, parallel polarized infrared pump ($\sim 100\text{ }\mu\text{J}$) and probe ($\sim 1\text{ }\mu\text{J}$) pulses, allowing for two-color experiments. For the experiments described in this section, the 5 Hz pump pulse was tuned to 3350 cm^{-1} , the frequency of the O-H stretch vibration of methanol

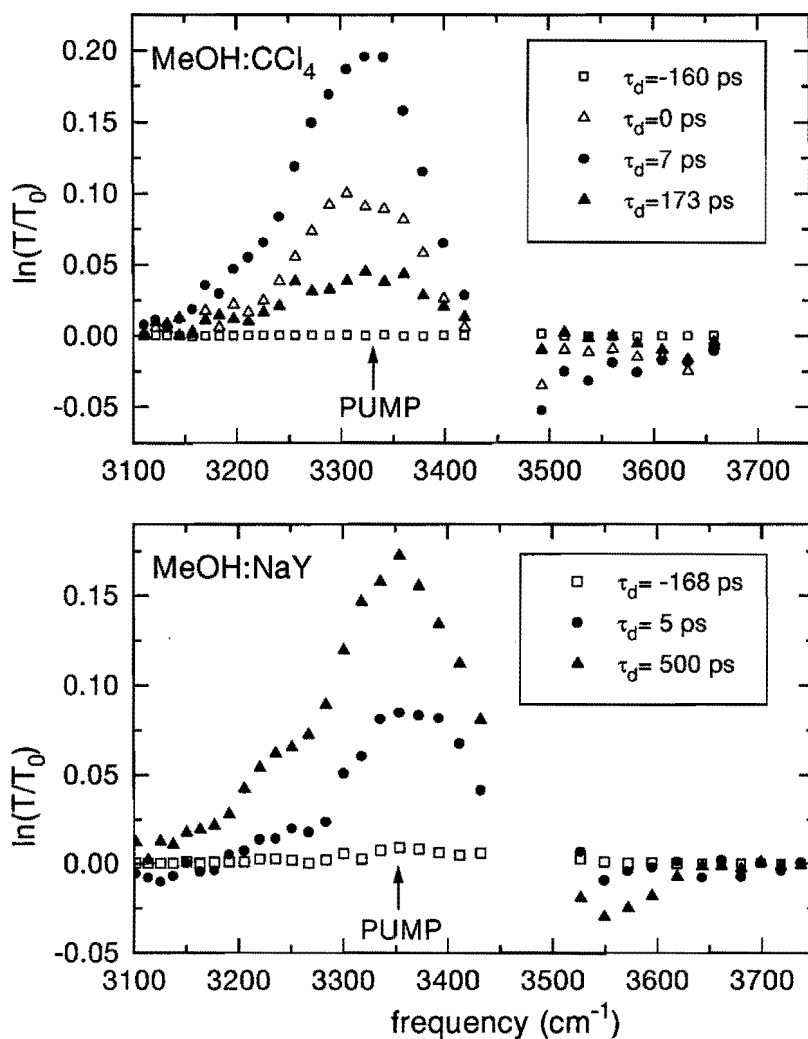


Figure 6.3: Transient spectra after excitation at 3350 cm^{-1} (arrows denote pump frequency): Pump-induced transmission changes ($\ln[T/T_0]$) of the probe pulses as a function of probe frequency at different delay times between pump and probe pulses (denoted in the graph). T and T_0 denote the transmission of the probe pulse in presence and in absence of the pump pulse, respectively.

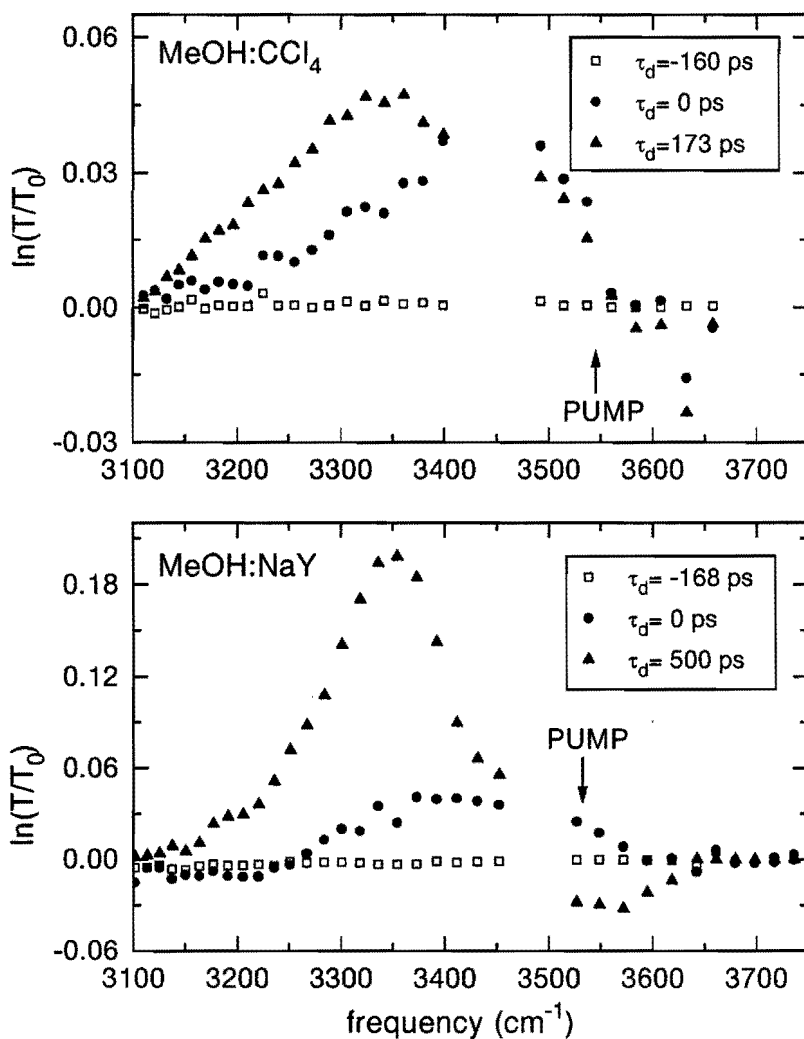


Figure 6.4: Transient spectra after excitation at 3530 cm^{-1} (arrows denote pump frequency): Relative transmission ($\ln[T/T_0]$) of probe pulses as a function of probe frequency at different delay times with respect to the pump pulse. Delay times are denoted in the graph. T and T_0 denote the transmission of the probe pulse in presence and in absence of the pump pulse, respectively.

molecules inside the clusters, and 3530 cm^{-1} , the frequency of the O–H stretch vibration of methanol molecules terminating the clusters. The pump pulse (focused onto the sample, focus diameter 0.4 mm) excites a significant fraction (typically 10%) of these molecules to the first vibrationally excited state of the O–H stretch vibration. The subsequent relaxation is followed with the 10 Hz probe pulse (focused onto the same spot as the pump, every other shot is used for reference): With the probe pulse the pump-induced transmission changes are monitored as a function of probe frequency and delay between pump and probe. The spectral full width at half maximum of the pulses is typically 20 cm^{-1} .

Transient spectra for several delay times are depicted in Figures 6.3 ($\tilde{\nu}_{\text{pump}} = 3350\text{ cm}^{-1}$) and 6.4 ($\tilde{\nu}_{\text{pump}} = 3530\text{ cm}^{-1}$). Due to water absorption in the LiNbO_3 crystals (used in the generation of the infrared pulses, see Chapter 1), infrared probe pulses cannot be generated around 3480 cm^{-1} . Pumping at 3350 cm^{-1} (Fig. 6.3), for both samples a transmission increase at 3350 cm^{-1} , and a transmission *decrease* around 3530 cm^{-1} is observed. A striking difference is that whereas in solution the pump-induced transmission changes exhibit decay, in the zeolite they are long-lived. Furthermore, in the zeolite a transmission *decrease* around 3150 cm^{-1} is observed, not present in solution. Pumping at 3530 cm^{-1} (Fig. 6.4) reveals similar transient effects. In solution monomer absorption around 3640 cm^{-1} appears. In the zeolite the transmission at the pump frequency is increased, before the long-lived transmission decrease sets in. Again in the zeolite an induced absorption is observed around 3200 cm^{-1} , in contrast to the solution. In solution the long-time transmission changes can be fully accounted for by thermal effects (temperature increases are typically 10 K), in contrast to the zeolite. For the zeolite, an increase in temperature would lead to an increased transmission at all frequencies; hence the observed negative $\ln(T/T_0)$ around 3550 cm^{-1} for both pump frequencies, can not be caused by an increased temperature after relaxation. It should be noted that in none of the experiments on the zeolite transmission changes were observed around $\sim 3650\text{ cm}^{-1}$, *viz.* the frequency of isolated methanol molecules.

To investigate the dynamics of the transmission changes due to the 3350 cm^{-1} pump, we performed the pump-probe experiments at fixed probe frequencies, as a function of delay. Three probe frequencies were employed: 3100 cm^{-1} (excited state absorption frequency: $v=1\rightarrow v=2$, see below), 3350 cm^{-1} and 3530 cm^{-1} .

The results of the time-resolved experiments for methanol in solution pumping at 3350 cm^{-1} are shown in upper panel of Fig. 6.5. Probing at 3350 cm^{-1} (Δ) a transmission increase is observed, with a subsequent decay with a 25 ps time constant. Probing at 3100 cm^{-1} (\bullet), the same signal (of smaller amplitude) is observed. Prob-

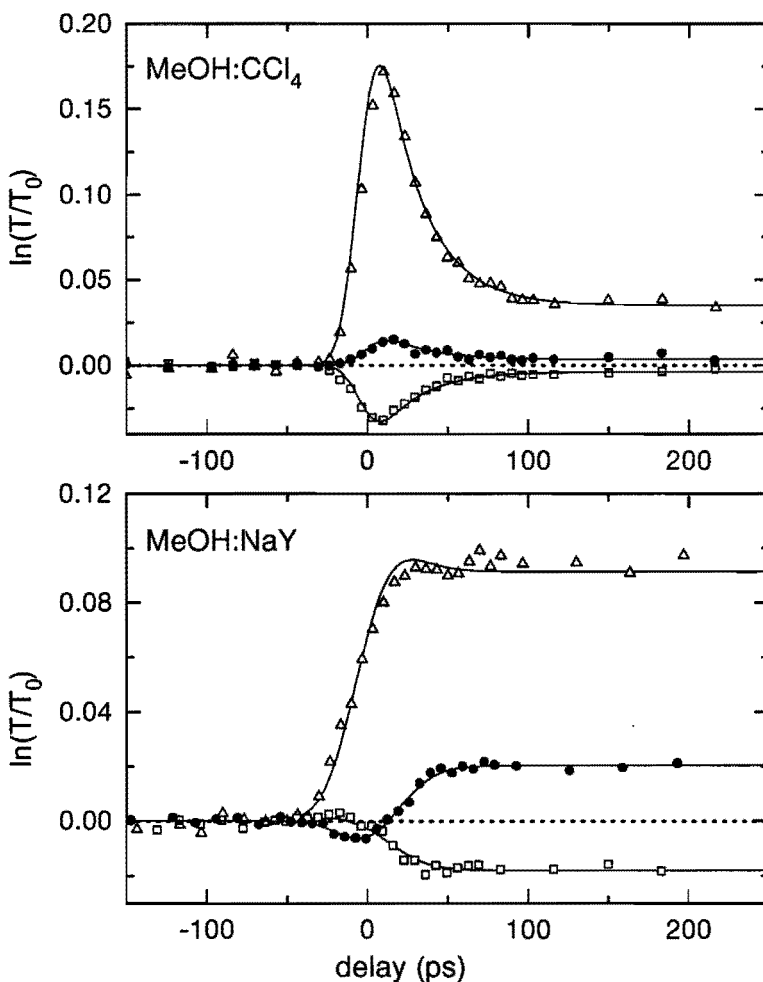


Figure 6.5: Results of the time-resolved pump-probe experiments for the two systems: Relative transmission of probe pulses at 3350 (Δ), 3530 (\square) and 3100 (\bullet) cm^{-1} as a function of delay with respect to the pump pulse. The pump pulse is tuned to 3350 cm^{-1} in these experiments. T and T_0 denote the transmission of the probe pulse in presence and in absence of the pump pulse, respectively. Probing at 3100 cm^{-1} (\bullet), an induced absorption (negative $\ln(T/T_0)$) is observed for the zeolite, not present in solution. Lines are calculations with $T_1=2$, $\tau_r=25$ ps and τ_t is infinite for MeOH:CCl₄ and $T_1=10$ ps and both τ_r and $\tau_t=\infty$ for MeOH:NaY.

ing at 3530 cm^{-1} (\square) an *absorption* increase is observed, decaying with exactly the same time-constant as the signal at 3350 cm^{-1} . These results are equivalent to corresponding measurements by Graener *et al.*[66] on ethanol dissolved in CCl_4 . It was shown that the observed signals can be accounted for by noting that a very effective way for the methanol molecule to get rid of its excess vibrational energy, is by breaking its hydrogen bond ($E_{\text{H-bond}} \approx 2000\text{ cm}^{-1}$)[66]: Vibrational relaxation occurs by breaking the hydrogen bond, and this process occurs very rapidly (for ethanol in solution $T_1 = 5 \pm 3\text{ ps}$ [66]). In the picture in Fig. 6.2 this means that the methanol chain is broken, thus creating new end-groups (absorbing at $\tilde{\nu}_{\text{OH}} = 3530\text{ cm}^{-1}$) at the expense of internal methanol molecules ($\tilde{\nu}_{\text{OH}} = 3350\text{ cm}^{-1}$). The observed decay-time of 25 ps at both frequencies is therefore not the vibrational lifetime T_1 , but rather the hydrogen-bond re-association lifetime τ_r . This value is in good agreement with the $20 \pm 5\text{ ps}$ re-association time of ethanol.[66] A similar vibrational pre-dissociation process by one IR photon has been observed for gas-phase methanol clusters[120] and methanol clusters in a nitrogen matrix[121].

For a sufficiently long vibrational (pre-dissociation) lifetime T_1 , one would expect (i) an excited state $v=1 \rightarrow v=2$ absorption redshifted to about 3100 cm^{-1} due to the anharmonicity of the vibration [66] and (ii) a time delay between the transmission rise at 3350 cm^{-1} and the absorption rise at 3530 cm^{-1} , since T_1 is simply the time it takes to break the hydrogen bond resulting in the formation of 3530 cm^{-1} species. The absence of both the pump-induced absorption (negative $\ln(T/T_0)$) at 3100 cm^{-1} and no significant time delay between the other two signals indicates that the vibrational lifetime is very short compared to the duration of our pulses (18 ps). The signal observed at 3100 cm^{-1} is identical -albeit of smaller amplitude- to that at 3350 cm^{-1} due to the spectrally broad induced transmission changes when pumping the $\tilde{\nu}_{\text{OH}} = 3350\text{ cm}^{-1}$ transition.

For methanol in NaY, the results (depicted in lower panel of Fig. 6.5) are strikingly different. Although initially the same behavior is observed, i.e. a transmission increase around 3350 cm^{-1} (Δ) and a transmission decrease around 3530 cm^{-1} (\square), the subsequent relaxation is absent. *Apparently, the rapid re-association does not occur in the zeolite.* A second difference is that (i) at 3100 cm^{-1} (\bullet) an induced absorption is observed and (ii) the 3530 cm^{-1} data (\square) show a delayed rise of absorption compared to 3350 cm^{-1} (Δ), both demonstrating that the vibrational lifetime T_1 is relatively long. At 3100 cm^{-1} the induced transmission subsequent to the induced absorption is again caused by spectral overlap of the 3100 cm^{-1} probe pulse with the 3350 cm^{-1} absorption line. For both systems we established that the transmission changes after relaxation showed no changes for delay times up to 2 ns.

The time-resolved data pumping at 3530 cm^{-1} are shown in Fig. 6.6. Vibrationally exciting the end-groups, these are expected to dissociate from the cluster upon relaxation. In this process an internal methanol molecule is converted to a terminal group, absorbing around 3530 cm^{-1} , and the excited methanol molecule becomes an isolated monomer. The overall effect is that an internal methanol molecule is converted to a monomer. In solution, pumping and probing at 3530 cm^{-1} results in a pulse-duration limited transient transmission increase, determined by the lifetime of the vibration. The transmission increase is due to excitation of end-groups, the decay due to vibrational relaxation. For the zeolite, also an induced transmission is observed at 3530 cm^{-1} , but the transmission relaxes to negative $\ln(T/T_0)$: Excitation at 3530 cm^{-1} leads to a long-time increase in absorption at this frequency. Probing at 3200 cm^{-1} , excited state ($v=1\rightarrow v=2$) absorption is observed (negative $\ln(T/T_0)$), again indicative of a lifetime that is long compared to that in solution. The subsequent transmission increase is caused by spectral overlap between the probe pulse at this frequency and the 3350 cm^{-1} absorption band.

Summarizing our data, it is clear that for both systems excitation of hydrogen-bonded O–H stretch vibrations (at 3350 and 3530 cm^{-1}) results in the dissociation of hydrogen bonds. This process occurs more rapidly in solution than in the zeolite, due to the shorter lifetime in solution. Subsequently, in solution a re-association takes place, equilibrating to a somewhat elevated temperature. In the laser focus, this temperature remains constant on the largest experimental timescale of 2 ns.[66, 77] In the zeolite re-association does not take place within 2 ns, resulting in a situation where the energy has thermalized within the clusters, but the methanol cluster distribution is non-thermal. Also here, temperature diffusion out of the laser focus is slow.[69]

The salient features of the infrared photo-dissociation are contained in the time-resolved data, which we will attempt to simulate to extract the relevant lifetimes. The appropriate level scheme for the systems is shown in Figure 6.7. After excitation with the pump pulse ($\tilde{\nu}=3350\text{ cm}^{-1}$, thick, dashed arrow) from $v=0$ (N_0) to $v=1$ (N_1), excited state absorption from $v=1$ to $v=2$ becomes possible ($\tilde{\nu}\approx 3100\text{ cm}^{-1}$). Vibrational relaxation with time constant T_1 results in a change of the O–H absorption spectrum due to the breaking of hydrogen bonds [e.g. $\tilde{\nu}=3350\rightarrow 3530\text{ cm}^{-1}(N_A)$]. Re-association of the hydrogen bonds occurs with time constant τ_r resulting in a new equilibrium state at higher temperature (N_B), from which relaxation with time constant τ_t back to the original ground state occurs (infinite compared to experimental time-scales). The associated rate equations for the four populated levels read:

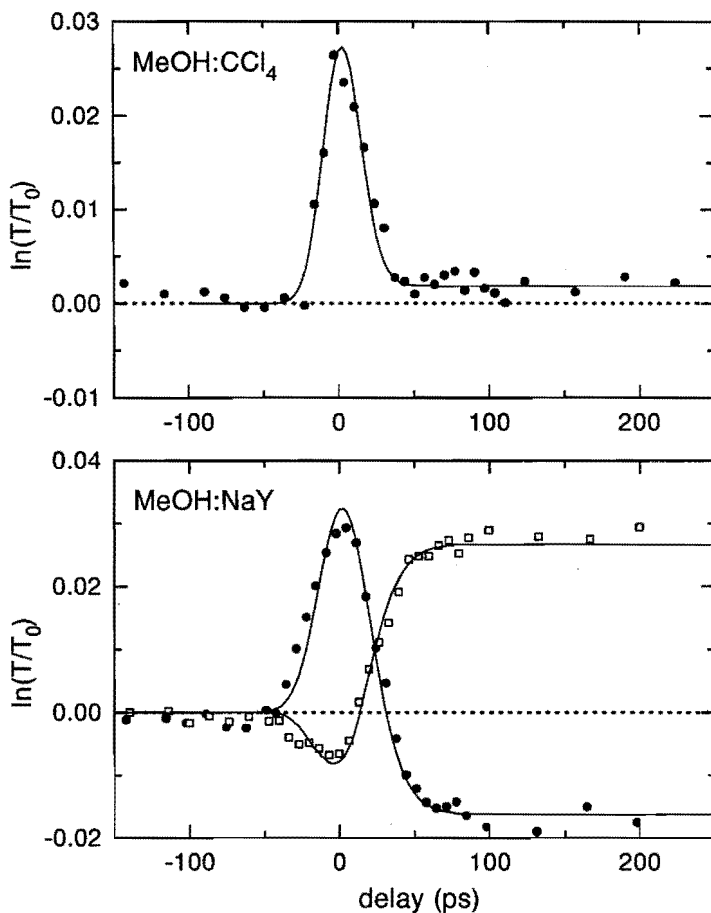


Figure 6.6: Results of the time-resolved pump-probe experiments for the two systems: Relative transmission of probe pulses at 3530 (●) and 3200 (□) cm^{-1} as a function of delay with respect to the pump pulse. The pump pulse is tuned to 3530 cm^{-1} in these experiments. T and T_0 denote the transmission of the probe pulse in presence and in absence of the pump pulse, respectively. Probing at 3200 cm^{-1} (□), an induced absorption (negative $\ln(T/T_0)$) is observed for the zeolite, not present in solution. Lines are calculations with $T_1=4$ ps for MeOH:CCl₄ and $T_1=15$ ps for MeOH:NaY.

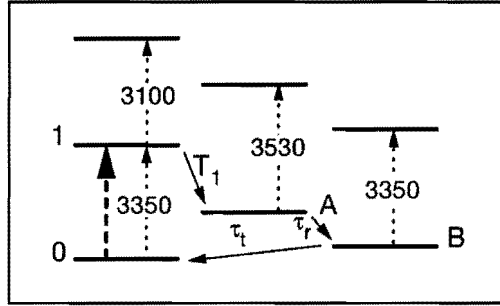


Figure 6.7: 7-level system used in the calculations to describe the 3350 cm^{-1} -pump data: After excitation with the pump pulse (thick, dashed arrow) from $v=0$ to $v=1$ excited state absorption from $v=1$ to $v=2$ becomes possible ($\tilde{\nu}\approx 3100\text{ cm}^{-1}$). Relaxation with time constant T_1 results in a change in absorption frequency due to the breaking of hydrogen bonds. Re-association of the hydrogen bonds occurs with time constant τ_r resulting in a thermal non-equilibrium state, from which relaxation with time constant τ_t back to the original ground state occurs. τ_t is long ($\tau_t\gg 2\text{ ns}$) compared to the experimental time-scale.

$$\begin{aligned}
 \frac{\partial N_0(z, t_p)}{\partial t_p} &= \frac{-\sigma_{01}}{h\nu} I_{\text{pump}}(z, t_p) [N_0(z, t_p) - N_1(z, t_p)] + (1/\tau_t) N_B(z, t_p) \\
 \frac{\partial N_1(z, t_p)}{\partial t_p} &= \frac{\sigma_{01}}{h\nu} I_{\text{pump}}(z, t_p) [N_0(z, t_p) - N_1(z, t_p)] - (1/T_1) N_1(z, t_p) \\
 \frac{\partial N_A(z, t_p)}{\partial t_p} &= (1/T_1) N_1(z, t_p) - (1/\tau_r) N_A(z, t_p) \\
 \frac{\partial N_B(z, t_p)}{\partial t_p} &= (1/\tau_r) N_A(z, t_p) - (1/\tau_t) N_B(z, t_p) \\
 \frac{\partial I_{\text{pump}}(z, t_p)}{\partial z} &= -\frac{\sigma_{01}}{V} [N_0(z, t_p) - N_1(z, t_p)] I_{\text{pump}}(z, t_p)
 \end{aligned}$$

N_x denotes the population in level x , z the coordinate perpendicular to the sample surface, t_p the time coordinate in a moving frame[20], σ_{01} the cross section for the $0\rightarrow 1$ transition, $h\nu$ the IR photon energy, $I_{\text{pump}}(z, t_p)$ the space- and time dependent pump intensity and V the irradiated volume. The radial profile of the laser pulse was not considered, since this results in only very minor changes in the transients. These equations were solved numerically, after which the transmission of the probe at the

three frequencies was evaluated. The amount of transmitted probe is determined by the population difference between the two levels associated with the appropriate transition. These calculations require as input laser pulse parameters (duration, energy and frequency) and sample parameters (cross-sections[66], density, sample length and relaxation times). Apart from the relaxation times all these parameters can be determined independently. Care has to be taken to consider the spectral overlap between the probe pulse and the different contributions to the overall (transient) absorption spectrum; e.g. part of the observed signal at 3530 cm^{-1} is due to changes in the absorption peak centered around 3350 cm^{-1} . The results are shown as lines in Figure 6.5. It should be stressed that for each system the three kinetic fits result from one single calculation. The results of the calculations were scaled vertically to coincide with experimental signal amplitude (with scaling factors varying only from 0.6 to 1.4, confirming the good agreement between data and calculations). For methanol in solution, the calculations yield an upper limit for the vibrational lifetime of 3 ps. This is concluded not only from the absence of induced absorption around 3100 cm^{-1} (which the calculations predict to be significant for $T_1 > 4$ ps), but, more convincingly, from the observation that experimentally there is no detectable delay between the maximum in transmission around 3350 cm^{-1} and the maximum absorption around 3530 cm^{-1} . This implies that the excited 3350 cm^{-1} -groups are almost instantaneously converted into 3530 cm^{-1} groups. A T_1 lifetime of 0.5 ps was used in the calculations, reproducing the data very well. This value is smaller than the lifetime of 5 ± 3 ps estimated for ethanol in CCl_4 by Graener *et al.* [66], but in excellent agreement with recent femtosecond infrared experiments by Woutersen *et al.*[124], in which a hydrogen-bond pre-dissociation lifetime of ~ 500 fs was observed for ethanol in CCl_4 .

The re-association time τ_r is found to be 25 ± 3 ps. For methanol in the zeolite the data are reproduced theoretically with an infinite re-association time τ_r (implying $\tau_r \gg 2$ ns) and $T_1 = 10 \pm 3$ ps. For larger T_1 lifetimes one would expect to observe transient bleaching of the 3350 cm^{-1} transition decaying with T_1 and shorter lifetimes defy the observation of the induced absorption around 3100 cm^{-1} and the delay in rise between the 3350 and 3530 cm^{-1} signals. The methanol has re-associated when the next probe pulse hits the sample (implying $\tau_r \ll 100$ ns, since the repetition rate of our laser system is 10 Hz). Modeling the 3530 cm^{-1} -data is less straightforward, since at this frequency not a similar complete data set is available as for the 3350 cm^{-1} -data. However, from the observation of the hot band in the zeolite, and its absence in solution, it is clear that the vibrational lifetime of the 3530 cm^{-1} -species is substantially longer in the zeolite than in solution. The lines in Fig. 6.6 are results of calculations with $T_1 = 4$ ps in solution and $T_1 = 15$ ps for the zeolite. While the 4 ps lifetime in solution is an

upper limit (for longer lifetimes the hot band should be observed), the lifetime in the zeolite lies between $12 \text{ ps} \leq T_1 \leq 25 \text{ ps}$. The 12 ps lower limit is set by the hot-band absorption, the upper limit by the pulse-duration limited decay of the transmission at 3550 cm^{-1}

It was shown by Graener *et al.* that for ethanol in solution, the hydrogen-bond re-association lifetime τ_r does not depend on the ethanol concentration.[66] This implies that in solution the sequential hydrogen-bond dissociation and re-association occurs between the same O-H groups. It is most likely that the solvent plays a crucial role in keeping the dissociated fragments in each others vicinity; the solvent acts as a cage, keeping the dissociated fragments together sufficiently long to re-associate. In the zeolite such a caging effect is not very likely to occur, since in the zeolite experiments the methanol dosage was kept well below complete saturation of the zeolite, implying the pores and cages were not completely filled. This means that after dissociation, the fragments are free to move away from each other. Moreover, stabilization of the fragments can occur through association of the methanol fragments with other zeolite oxygen lattice atoms. This association leads to a persistent increase of absorption of the terminal O-H groups absorbing at 3530 cm^{-1} due to methanol molecules hydrogen-bonded to zeolite oxygen atoms, the associated persistent decrease of the absorption at 3350 cm^{-1} , and explains the absence of any spectral changes around 3645 cm^{-1} in the zeolite. Hence the re-association rate will be determined by diffusion of methanol along the zeolite pore, indeed probably slow on our experimental time-scales[125]. This interpretation is corroborated by the 3530 cm^{-1} -pump data: For the zeolite a persistent increase of absorption of the terminal O-H groups absorbing at 3530 cm^{-1} due to methanol molecules hydrogen-bonded to zeolite oxygen atoms is also observed.

It is clear that vibrational relaxation is substantially faster in the zeolite than in solution; for the 3350 cm^{-1} molecules relaxation occurs at least twice as fast for the methanol in solution ($T_1 \leq 3 \text{ ps}$) than for methanol adsorbed in the zeolite ($T_1 = 10 \pm 3 \text{ ps}$). This is most likely due to energy mismatch compensation, which can be readily provided by the solvent CCl_4 , but is not as likely in the zeolite. In solution, the methanol cluster is surrounded by solvent molecules and therefore part of the excess energy can be transferred to solvent degrees of freedom, allowing for a more rapid vibrational relaxation. In the zeolite, the cluster adsorbed to the sodium site is indirectly coupled to the zeolite lattice, so that the excess energy ($E_{\text{excitation}} - E_{\text{H-bond}}$) can only be converted into excitations of low-frequency methanol vibrations and kinetic energy of the fragments[126].

6.3 Conclusion

We have investigated the vibrational dynamics of methanol in solution and in sodium zeolites. We deduce from the similarities of the linear absorption spectra, that in both cases clustering of the methanol molecules occurs through hydrogen-bonding. With non-linear spectroscopy, we find that for both systems excitation with resonant infrared pulses leads to breaking of the H-bonds and fragmentation of the clusters. However, the dynamics of this infrared photo-dissociation process differ greatly in two respects. Firstly, the vibrational population relaxation times (i.e. the vibrational pre-dissociation times) are markedly different, $T_1 \leq 3$ ps for methanol in solution and $T_1 = 10 \pm 3$ ps for methanol inside the zeolite. This is explained by noting that, in contrast to the zeolite, in solution the solvent provides an additional relaxation channel. Secondly, the re-association of methanol molecules, after dissociation due to vibrational relaxation, occurring in the liquid phase with a time-constant of 25 ps, is absent on our experimental timescales for the methanol clusters in the zeolite. This is attributed to a caging effect in solution, and, in the zeolite, a stabilization of the fragments by interaction with the lattice.

Chapter 7

Infrared induced conversion of methanol in acid zeolites

In the reactive system of methanol physisorbed to the acid zeolite HY, the equilibrium between two adsorption structures can be temporarily shifted towards the more reactive of the two complexes by excitation with picosecond infrared pulses. The picosecond dynamics of the conversion demonstrate a non-linear dependence of this process on the energy inserted into the system. This behavior is explained by the large anharmonicity of the hydrogen bond between the methanol and the reactive (Brønsted) site.

7.1 Introduction

With the recent advent of ultra-short laser pulses, it has become possible to follow reaction dynamics 'real-time'. Ultra-short laser pulses can be used to initiate a chemical reaction and subsequently probe (and even control) its time evolution[127]. Not only the disappearance of reactants and appearance of products, but even short-lived reaction intermediates and transition states can be observed in a time-resolved manner[128]. In this Chapter, we employ picosecond infrared pulses to investigate the dynamics of methanol adsorbed to the active sites in acid zeolites catalysts. One of the more important chemical reactions catalyzed by acid zeolites is the reaction of methanol, initially to dimethyl ether and subsequently to gasoline[129]. Methanol adsorption in zeolites has therefore received substantial attention the past decade. However, despite several experimental[122, 123, 130–135] and theoretical (ab initio) studies[136–145], substantial ambiguity remains concerning the microscopic structure of the adsorption complex and the interpretation of the associated infrared spectra. In this Chapter, we present new information concerning methanol adsorption structures and methanol-zeolite interaction dynamics obtained with time-resolved (picosecond) infrared spectroscopy.

7.2 Methanol adsorption structure and linear infrared spectra

The infrared absorption spectra of HY-zeolite with and without adsorbed methanol are depicted in Fig. 7.1. In vacuum, hydroxyls situated in the small and large cages give rise to the 3550 and 3645 cm^{-1} absorption bands, respectively.[49] Methanol adsorbs mainly to the hydroxyls in the easily accessible large cages.[134] This interaction is sufficiently strong to warrant a 1:1 adsorption complex, since adsorption of methanol to an already occupied site is energetically much less favorable (by ≈ 20 kJ/mole) than adsorption to an empty site (See e.g. Refs. [122, 130, 134, 143, 145]). The amount of dosed methanol was kept such, that 5% of the intensity of the HF-OH absorption peak ($\tilde{\nu}=3646 \text{ cm}^{-1}$) remained (adsorption of more methanol leads to the total disappearance of the HF-OH band), to avoid adsorption of multiple methanol molecules to one site.¹

In open-cage structures such as Y zeolite, there is general consensus that methanol is present as a doubly hydrogen-bonded complex, as shown in Fig. 7.2A.[135–142] The

¹In the time-resolved experiments, the methanol coverage is not exactly known, but is decidedly lower than 95%. Thermal desorption of part of the methanol occurs due to steady state heating effects caused by the laser pulses (these steady state thermal effects should not be confused with one-pulse thermal effects, see e.g. Chap. 4).

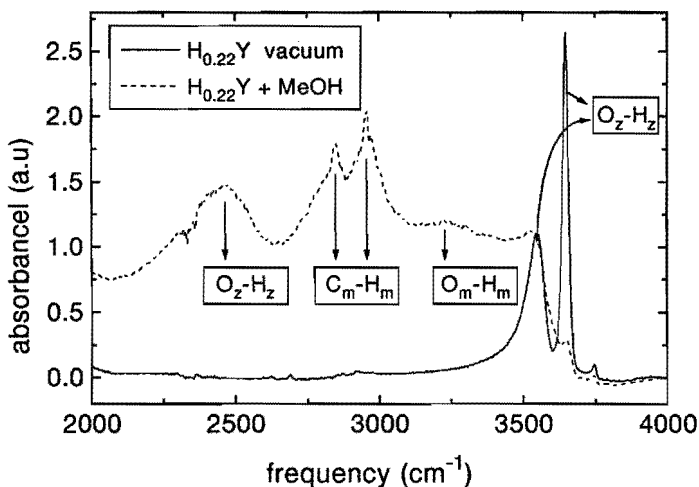


Figure 7.1: Absorption spectra of $H_{0.22}Y$ ($Si/Al=0.27$), in vacuum (solid line) and with adsorbed methanol (dashed line). The assignment of the different absorption peaks is indicated in the graph. The presence of 18% Na is of little consequence since these sites are located in the small cages, poorly accessible for the methanol. To avoid adsorption of multiple methanol molecules to one site, some 'free' zeolite hydroxyl groups ($\nu_{OH}=3645\text{ cm}^{-1}$) were left.

doubly-bound complex has also been referred to as the 'end-on'[138] or the 'bifurcated'[142] complex. The broad feature around 3250 cm^{-1} is attributed to the strongly perturbed O_m-H_m stretch vibration of methanol, in accordance with Refs. [133, 137, 138]. Somewhat lower[136] and higher[139, 141] values have been found in ab initio studies. The sharp peaks around 2900 cm^{-1} are due to the methanol C-H stretching vibrations.[123, 130–134, 136–139] The frequency of the zeolite O_z-H_z stretch vibration is strongly red-shifted (from 3645 to $\sim 2300\text{ cm}^{-1}$). Fermi resonances of this strongly redshifted but very broad O_z-H_z stretching mode with the overtone of the O_z-H_z in-plane bending result in an Evans transmission window around 2600 cm^{-1} [146], causing broad (quasi-)peaks around 2400 and 2900 cm^{-1} . [136, 138, 139, 141]

In the zeolite that is most widely applied to catalyze the methanol-to-gasoline process, zeolite HZSM-5, an absorption band appears around 3580 cm^{-1} , upon adsorption of methanol.[130, 131, 133, 134] This peak can indubitably be assigned to the O_m-H_m stretch vibration of methanol, by the shift induced by isotopic substitution of the methanol oxygen (^{16}O replaced by ^{18}O)[147], in analogy to isotopic substituted water[148]. Since there exists a strong correlation between the hydrogen bond strength and the

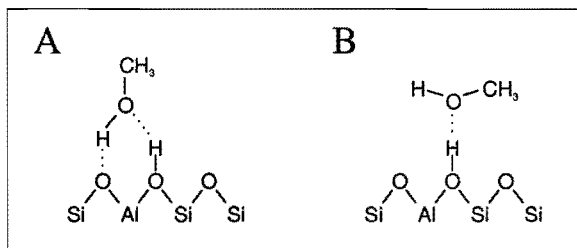


Figure 7.2: Schematic representations of methanol interacting with a zeolite acid site. A: Doubly hydrogen-bonded interaction. B: Singly hydrogen-bonded interaction.

vibrational frequency of an OH group[64], the high O_m-H_m frequency for methanol adsorbed to HZSM-5 indicates that the hydrogen bond between the methanol hydrogen and the zeolite oxygen is much weaker in HZSM-5 than in HY (or even absent). This suggests that in HZSM-5 the *singly-bound* adsorption structure depicted in Fig. 7.2B is the equilibrium adsorption structure, in contrast to HY. The singly-bound complex has also been referred to as the 'side-on'[138] or the 'monodentate'[142] complex.

Apparently, the exact position in the equilibrium between singly- and doubly bound methanol depends strongly on the type of zeolite. The effect of zeolite *structure* on the adsorption complex was illustrated recently[140,141]. In these ab initio studies, the doubly H-bonded structure was predicted for methanol adsorbed to large pore zeolites, whereas methanol adsorbed to a small pore system was found to be protonated. The difference in adsorption structures between the zeolites Y and ZSM-5, can be explained by the different Si/Al-ratios, rather than structural differences. The strongly basic oxygen atom (next to the aluminum) in the high-aluminum Y zeolite will favor interaction with the methanol hydroxyl, whereas the a-polar, hydrophobic lattice in ZSM-5[130,149] will preferentially interact with the methyl group, as was surmised previously.[133]

It has been demonstrated that the dehydrogenation reaction of methanol at the acid site is the first step in the methanol-to-gasoline process. Before dehydrogenation of the methanol at the acid site can occur, however, the doubly-bound methanol (Fig. 7.2A.) has to be converted to the more reactive singly-bound structure (Fig. 7.2B).[143] The fact that in ZSM-5 the more reactive singly-bound complex is the equilibrium adsorption structure, indicates a higher catalytic activity with respect to methanol conversion for this zeolite compared to Y, as indeed has been observed[150].

In the following, we will discuss the results of time-resolved infrared experiments on zeolite HY.

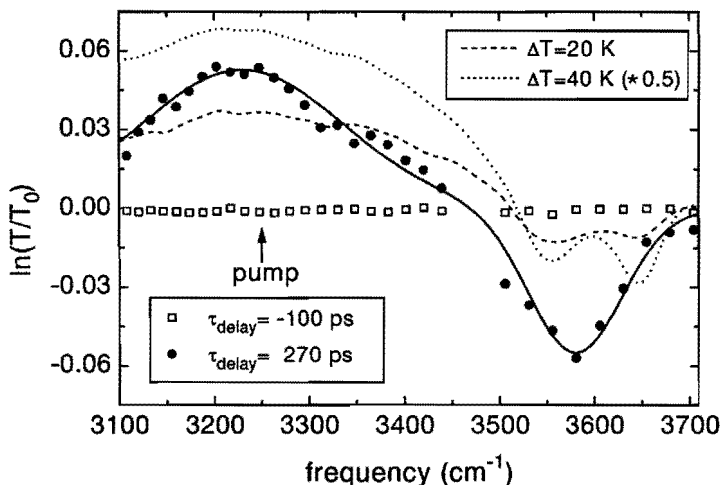


Figure 7.3: Transmission changes after excitation at 3250 cm^{-1} of the methanol:HY system corresponding to the dashed absorption spectrum in the upper panel of Figure 7.1. For negative delay between excitation and probe pulse, ($\tau_{\text{delay}} = -100\text{ ps}$), the probe hits the sample before the excitation (no absorption changes). For longer delays ($\bullet\ \tau_{\text{delay}} = 270\text{ ps}$) the absorption decreases at the excitation frequency (3250 cm^{-1}), while simultaneously an induced absorption is observed around 3580 cm^{-1} . Lines are the results of calculations described in the text.

7.3 The infrared conversion of methanol in acidic Y zeolite

For the time-resolved experiments picosecond (25 ps) tunable infrared ($2500\text{--}4000\text{ cm}^{-1}$) pulses of $\sim 150\ \mu\text{J}$ energy (bandwidth $\sim 20\text{ cm}^{-1}$) are generated by downconversion of 1064 nm pulses from a Nd:YAG laser. The changes in the absorption spectrum (and the time evolution) due to excitation with an IR pulse are monitored by weak ($3\ \mu\text{J}$), independently tunable, infrared pulses. For details, see Chapter 1. The changes in the absorption spectrum, 270 ps after excitation at 3250 cm^{-1} , are depicted in Figure 7.3. At the excitation frequency ($\tilde{\nu} = 3250\text{ cm}^{-1}$) the absorption decreases, whereas around 3580 cm^{-1} an induced absorption is observed. These changes occur mostly very rapidly compared to the duration of our pulses (the next section contains a discussion of

the dynamics), and persist up to the largest experimental delay time of 1.5 ns. Apparently, the excitation causes the frequency of adsorbed methanol to change from 3250 to 3580 cm^{-1} . The solid line through the data is the result of a calculation with a disappearing absorption at 3230 cm^{-1} (width = 250 cm^{-1}), and a 100 cm^{-1} wide band appearing at 3580 cm^{-1} (ratio of cross-sections $\sigma_{3230}/\sigma_{3580}=2.9$). This means that the hydrogen bond between the methanol hydrogen and the zeolite oxygen is much weaker than before, suggesting the type of *singly-bound* adsorption structure depicted in Fig. 7.2B. This indicates that in Y zeolite the $\text{O}_m\text{-H}_m\cdots\text{O}'_z$ hydrogen bond² between the methanol hydrogen and the zeolite oxygen is dissociated due to the excitation: The infrared excitation induces a conversion of a considerable fraction of methanol from the doubly-bound structure (Fig. 7.2A.) to the singly-bound structure (Fig. 7.2B) in Y zeolite, which is the first step in the catalytic reaction of methanol at the acid site. From the absence of significant transmission changes around 3645 cm^{-1} it is clear that the second H-bond remains intact. It should be stressed that the observed absorption changes cannot be explained by a simple temperature increase: The effect of typical temperature increases[69] on the absorption spectrum are shown as dotted ($\Delta T=20$ K) and dashed lines ($\Delta T=40$ K) in Fig. 7.3. With increasing temperature thermal desorption of some methanol occurs, giving rise to increased absorption at $\text{O}_z\text{-H}_z$ frequencies (3550 and 3645 cm^{-1}), clearly different from the data.

Excitation of the zeolite $\text{O}_z\text{-H}_z$ stretch vibration at 3550 cm^{-1} (hydroxyls in small pores) results in similar long-time absorption changes as those observed for excitation at 3250 cm^{-1} . This transient spectrum is depicted in Fig. 7.4. The only difference is the presence of a second induced transmission around 3430 cm^{-1} . The fact that the long-time transient spectra are so similar implies that the new doubly:singly bound methanol equilibrium arises—at least partly—from a situation where the energy has flown out of excited high-frequency modes (i.e. vibrational relaxation has occurred), but the energy has not yet fully thermalized. Full thermalization would result in the desorption of a fraction of methanol molecules (dashed and dotted lines in Fig. 7.3), which is clearly not observed. From the data it is clear that the doubly-to-singly bound conversion is most efficient for excitation at 3250 cm^{-1} . Although there is overlap of several absorption bands at this frequency, excitation of the $\text{O}_m\text{-H}_m$ stretch vibration of methanol, is expected to lead to *direct* dissociation of the $\text{O}_m\text{-H}_m\cdots\text{O}'_z$ hydrogen bond directed along the excited $\text{O}_m\text{-H}_m$ bond ($E_{\text{H-bond}}\sim 3000$ cm^{-1} [138]), since this has been demonstrated to be a very effective relaxation channel for methanol[151] (and ethanol[66]) clusters in solution, adsorbed to NaY[151], gas-phase clusters[120] and hydrogen-bonded in a nitrogen-matrix[121].

²The prime in O'_z denotes that this zeolite oxygen atom is not part of the $\text{O}_z\text{-H}_z$ zeolite hydroxyl.

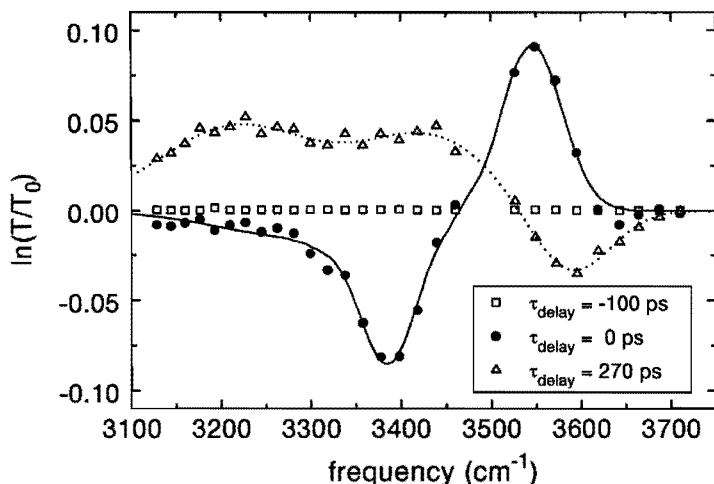


Figure 7.4: Transient spectrum after excitation of the zeolite $\text{O}_z\text{-H}_z$ groups in the small cages to which no methanol was adsorbed, $\nu_{\text{pump}}=3550\text{ cm}^{-1}$. For small delay, the bleaching of the fundamental transition ($0\rightarrow 1$) gives rise to the increased transmission around 3550 cm^{-1} . The hot band ($1\rightarrow 2$) is observed around 3400 cm^{-1} . Long-time transmission changes reveal an induced absorption around 3580 cm^{-1} and an increased transmission around 3250 cm^{-1} , similar to excitation at 3250 cm^{-1} . Here, also an increased transmission around 3430 cm^{-1} is observed. Lines are guides to the eye.

7.4 The dynamics of methanol conversion in acidic Y zeolite

To investigate the dynamics of the transmission changes, delay scans were performed probing at 3250 cm^{-1} and 3580 cm^{-1} , after excitation at 3250 cm^{-1} . The results are shown in Fig. 7.5. From these data it is clear that the disappearance of intensity at 3250 cm^{-1} and the appearance of the induced absorption around 3580 cm^{-1} are synchronous. Apparently, pumping the O-H groups at 3250 cm^{-1} converts these very rapidly to groups absorbing around 3580 cm^{-1} . One would expect vibrational relaxation to be much faster than our 20 ps pulses can resolve, due to the large perturbation of the methanol hydroxyl groups (the large redshift in absorption frequency) upon adsorption.[126] Although, indeed, the major part of the transmission changes sets in

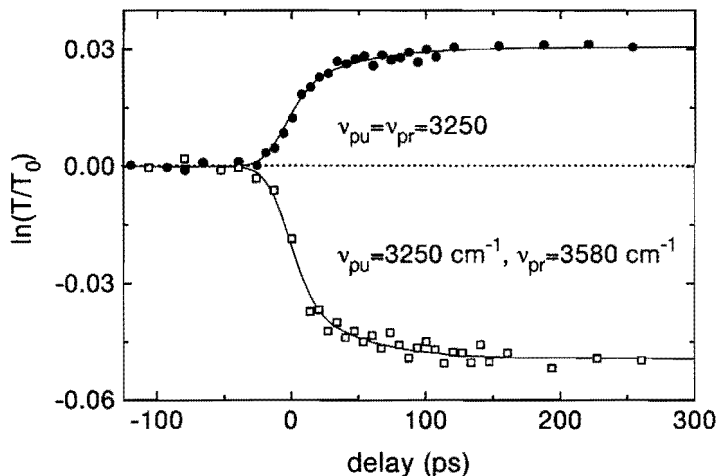


Figure 7.5: Results of one- and two-colour pump-probe experiments on MeOH:HY system. Upper panel: pumping and probing at 3250 cm^{-1} . Lower panel: pumping at 3250 cm^{-1} , probing at the induced absorption around 3580 cm^{-1} . The different signal amplitudes are due to the fact that the two curves were measured on different samples, on different days. Lines are guides to the eye.

very rapidly (pulse duration limited), the transients exhibit the puzzling feature that the transmission changes are protracted by a second, slower (time constant ~ 50 ps) process.

We performed the same experiment pumping the methanol C_m-H_m stretch vibration at 2956 cm^{-1} . The long-time transient spectrum is identical to the long-time spectrum after excitation at 3550 cm^{-1} (Fig. 7.4). The result of the time-resolved experiment, probing at 3250 cm^{-1} is depicted in Fig. 7.6. Surprisingly, although the same type of signal is observed, it is delayed by ~ 15 ps. This delay is not caused by an experimental artefact; replacing the sample by a LiIO_3 -crystal ($6 \times 6 \times 3$ mm, $\Theta = 20^\circ$), the sum frequency of pump and probe pulses can be generated as a function of delay. The inset of Fig. 7.6 shows that time zero does not nearly shift sufficiently (< 2 ps) to account for the different signals. This small shift in zero delay observed in the SFG experiment is probably due to dispersion in the optical components. The most likely cause for the delayed rise is the lifetime of the C_m-H_m stretch vibration. This leads to a temporary storage of the energy in this mode, before it is used for the conversion of

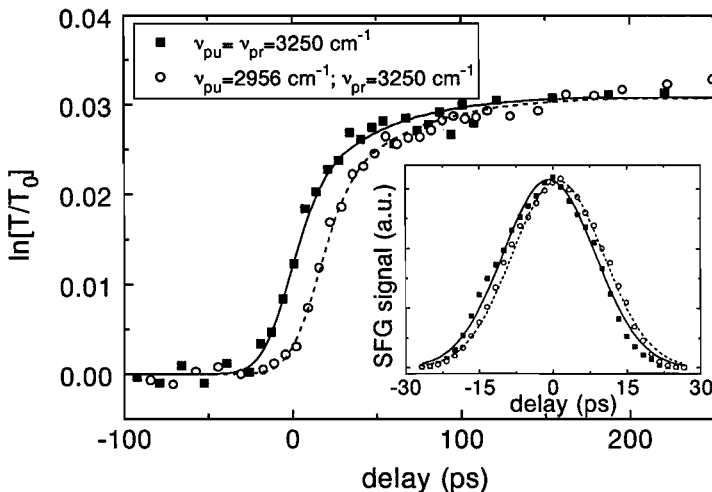


Figure 7.6: Time-resolved spectral changes at 3250 cm^{-1} with the pump pulse tuned to the methanol O_m-H_m stretch (3250 cm^{-1}), and the methanol C_m-H_m stretch (2956 cm^{-1}). The inset shows a cross-correlate between pump and probe (sum frequency generation in a LiIO_3 -crystal), which demonstrates that the $\sim 15 \text{ ps}$ delayed rise of the latter is not caused by dispersive effects in one of the optical components. Lines are guides to the eye.

doubly- to singly bound methanol. Indeed, the lifetime of the C_m-H_m stretch vibration of ethanol in solution was found to be $15 \pm 3 \text{ ps}$.^[76] Attempts to measure the lifetime of this mode of methanol adsorbed to the zeolite were unsuccessful, due to additional noise caused by frequency jitter, inevitable for parametrically generated infrared light, in combination with the sharp absorption peak.

It is highly unlikely that the double time behavior, observed for excitation at both 3250 and 2960 cm^{-1} , is due to the fact that two relaxation processes with different time-constants are driven by the excitation. The methanol:zeolite system is a strongly hydrogen-bonded system, and the vibrational relaxation rate is known to decrease rapidly with increasing hydrogen-bond strength. This has been observed for hydrogen-bonded complexes in both liquids^[152, 153] and solids^([44, 54–58] and Chapters 2 and 3 of this thesis). The strange temporal shape of the pump-induced transmission changes therefore seem to indicate that the response of the hydrogen-bonded system is non-linear with respect to the energy that is inserted into it: The effect of a fixed amount

of energy inserted into the system depends on how much energy preceded this amount: Energy in the late part of the laser pulse has a larger effect on the methanol conversion than the same amount in the beginning of the pulse. Since we do not know the exact shape of the pulses, it is very difficult to make quantitative statements concerning the possible non-linearity.

However, an interesting handle on the dynamics of the conversion of methanol from doubly- to singly bound comes from excitation of the zeolite O_z-H_z groups in the small cages to which no methanol was adsorbed, $\nu_{OH}=3550\text{ cm}^{-1}$. In this case, we can directly measure the decay of excited O_z-H_z groups (and thus the time-dependent amount of energy inserted into the system), and the time-dependence of the conversion, by probing at 3250 and 3580 cm^{-1} . The surprising results of these experiments are depicted in Fig. 7.7. The upper two panels of this Figure depict transmission changes at the fundamental ($0\rightarrow 1$) transition ($\tilde{\nu}_{OH}=3550\text{ cm}^{-1}$) and the induced hot band absorption ($1\rightarrow 2$, $\tilde{\nu}_{OH}=3400\text{ cm}^{-1}$). Both measurements can be very well described with a 44 ps lifetime of the excited state. In contrast, the disappearance of the 3250 cm^{-1} band, and the appearance of the 3580 cm^{-1} band, both occur significantly *faster*, as depicted in the lower two panels, and cannot be described by the calculations with a relaxation time of 44 ps (lines in Figure 7.7). In these calculations, it is assumed that the absorption changes at 3250 and 3580 cm^{-1} are linearly proportional to the amount decayed O_z-H_z groups (as for fundamental and hot-band absorption), and therefore linearly on the amount of energy released by these groups. The inability of these calculations to describe the data clearly substantiates the non-linearity of the process.

A clue to the cause of the non-linearity can be obtained by considering the potential of the $O_m-H_m\cdots O'_z$ hydrogen bond between the methanol hydrogen and the zeolite oxygen. This is the hydrogen bond that is dissociated upon conversion of doubly- to singly bound methanol. It is well-known that a strong correlation exists between this hydrogen bond coordinate and both the cross-section and the vibrational frequency of the O_m-H_m stretching mode.[64] Furthermore, this hydrogen-bond potential is strongly anharmonic.[64] One of the consequences of this strong anharmonicity is that the average $O_m-H_m\cdots O'_z$ distance (*viz.* the hydrogen-bond coordinate R), depends strongly non-linearly on the amount of energy inserted into this hydrogen bond. This is schematically shown in Fig. 7.8, where a Morse potential

$$V(R) = D_e[1 - e^{a(R-R_e)}]^2 \quad (7.1)$$

is depicted, with its eigenvalues. In this Equation, D_e is the dissociation energy, R_e the equilibrium (ground state) value of the hydrogen-bond coordinate R , and a a measure of the anharmonicity. The dotted line in Fig. 7.8 depicts the dependence of the average hydrogen-bond distance on the energy, and it is clear that starting from a low-energy

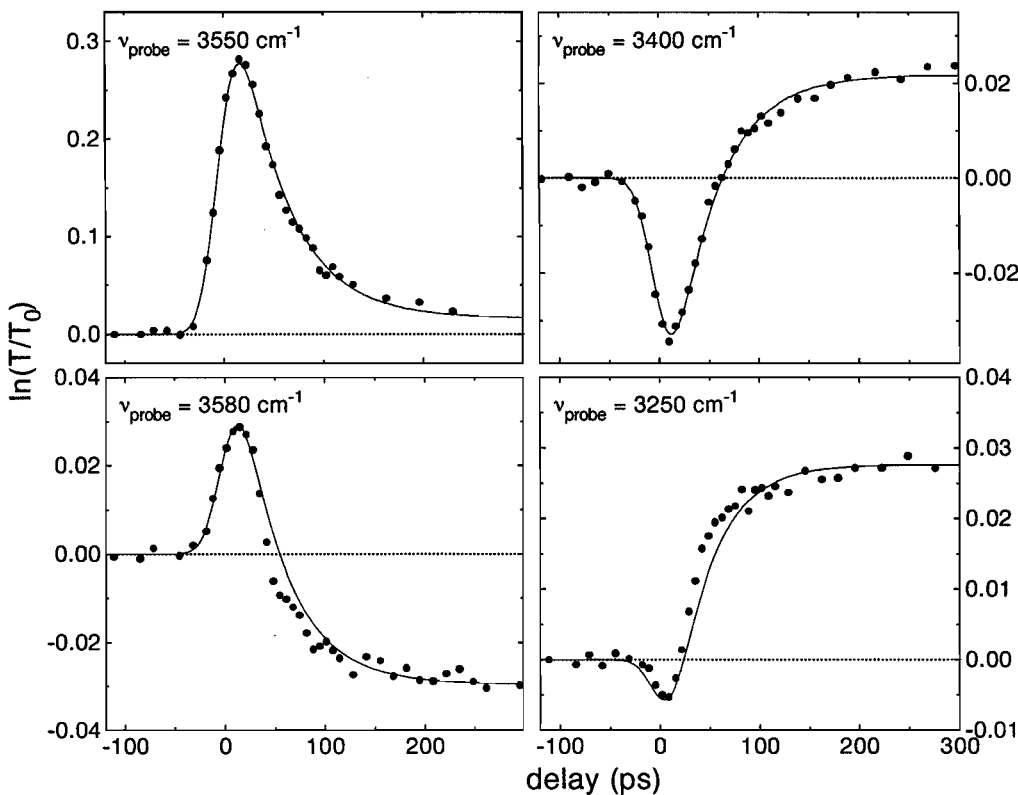


Figure 7.7: Time-resolved spectral changes after excitation of the zeolite O-H groups in the small cages to which no methanol was adsorbed, $\nu_{\text{pump}}=3550\text{ cm}^{-1}$, with calculations resulting from numerically solving the appropriate rate equations (lines). Upper Left: probing the induced transmission at the pump frequency, a lifetime of $44\pm 2\text{ ps}$ is observed. This measurement was performed at zero coverage, but the lifetime at this frequency was found to be independent of the amount of methanol adsorbed. Upper Right: probing the hot band (of the sample with adsorbed methanol), the induced absorption of the $\nu=1$ to $\nu=2$ transition, reveals the same lifetime. Lower Left: Probing the appearance of the shifted methanol $\text{O}_m\text{-H}_m$ band at 3580 cm^{-1} . The small increase in transmission is caused by spectral overlap with the bleaching at the pump frequency. The subsequent appearance of the 3580 cm^{-1} band is much faster than would be expected from the 44 ps lifetime. Lower Right: The same observation is even clearer for the disappearance of absorption around 3250 cm^{-1}

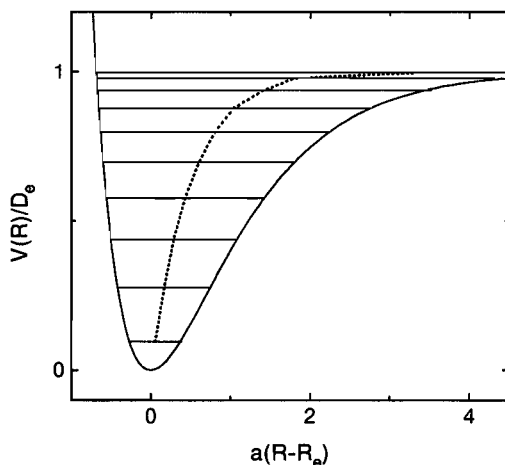


Figure 7.8: Morse potential and average displacements $\langle(R - R_e)\rangle$ as a function of energy. Note the non-linear dependence of the average displacement $\langle(R - R_e)\rangle$ on the energy.

situation, the effect of additional energy is much smaller than starting from higher initial energy.

The observed non-linear character of the conversion process induced by the infrared pulse is presumably closely related to the catalytic reactivity of the system. The essence of a catalyst is that it lowers activation barriers for chemical reactions, so that only a limited amount of energy is required to induce large changes in coordinates relevant for the reaction. This is indeed the type of behavior that we observe here.

7.5 Conclusions

We have demonstrated that an equilibrium exists between two adsorption structures, doubly- and singly bound, for methanol physisorbed to acidic zeolites. Although structural effects cannot be excluded, the position of the equilibrium is expected to depend mainly on zeolite composition, i.e. silicon-to-aluminum ratio. We demonstrate that the doubly bound adsorption structure predominantly observed in Y zeolite, can be temporarily converted into the more reactive singly bound complex by excitation with picosecond infrared pulses. The picosecond dynamics of the conversion shows anomalous behavior, which can be explained by the large anharmonicity of the hydrogen bond between the methanol and the reactive (Brønsted) site.

Chapter 8

Solvent-dependent vibrational relaxation pathways after successive resonant IR excitation to $v = 2$

With two subsequent, resonant intense picosecond infrared pulses we have succeeded in pumping a significant fraction of iodoform (CHI_3) molecules in solution to the second vibrationally excited state of the C–H stretching mode. Transient populations of the vibrational levels are monitored with weak probe pulses. From these pump-pump-probe experiments, we find that the subsequent relaxation route depends critically on the solvent. In a strongly polar solvent (acetone) relaxation from $v=2$ to $v=0$ occurs predominantly *via* the $v=1$ state, with time constants of $T_1^{2 \rightarrow 1} = 10 \pm 5$ and $T_1^{1 \rightarrow 0} = 60 \pm 5$ ps, respectively. In contrast, in a less polar solvent (chloroform) direct decay to the ground state is observed, with a time constant ($T_1^{2 \rightarrow 0} = 80 \pm 20$ ps), comparable to the energy lifetime of the first excited state ($T_1^{1 \rightarrow 0} = 125 \pm 5$ ps).

8.1 Introduction

A multitude of time-resolved experiments on small organic molecules in solution has provided great insight into vibrational energy flow and dissipation mechanisms in these molecules.[119] In these pump-probe experiments, the C–H stretch vibration is excited to its first excited state, either by a resonant infrared pulse or by (stimulated) Raman excitation. A second, weaker, delayed probe pulse monitors the decay of the excited level. Some of these experiments have shown that after excitation of the C–H vibration there are *two* consecutive relaxation processes (see e.g. Refs. [59, 77, 154]. First, intramolecular vibrational relaxation (IVR) occurs: the energy is transferred to other low-frequency vibrations within the molecule. In the second process, called intermolecular energy transfer (IET), the excess energy is transferred to solvent molecules. It was found that the solvent has a large influence on the vibrational dynamics of small organic molecules [154]; The solvent not only modifies the rate of energy transfer to the solvent after vibrational relaxation within the molecule (IET), it also affects the intramolecular vibrational relaxation process (IVR) itself. With increasing polarity of the solvent, both relaxation processes are accelerated.

These insights were obtained from an abundance of experiments that have been performed on the lifetime of the first vibrationally excited state. In contrast, little is known about the relaxation rates and pathways of higher excited states. Lifetimes of higher excited states have previously been reported for (i) the C–O stretch of $\text{W}(\text{CO})_6$ [79], where due to the small anharmonicity of the vibration several higher transitions lie within the laser bandwidth, (ii) the C–D stretch of DCN [155] where a distribution of vibrationally excited states was observed after photo-induced generation of the molecule, and (iii) the C–H stretch of CHBr_3 [156], where the $v = 2$ state was populated directly by overtone absorption and the subsequent relaxation was monitored by anti-Stokes Raman probe scattering. In all of these cases, the relaxation rate was seen to increase with increasing vibrational quantum number and decay always occurred to the level directly below.

In this Chapter, we report on the relaxation from the second vibrationally excited state of the C–H stretch vibration of CHI_3 , after resonant excitation from $v=0$ to $v=1$ and subsequent resonant excitation from $v=1$ to $v=2$. We find that the nature of the solvent not only determines the rate of the IVR process, but also controls the IVR pathways of the $v=2$ relaxation.

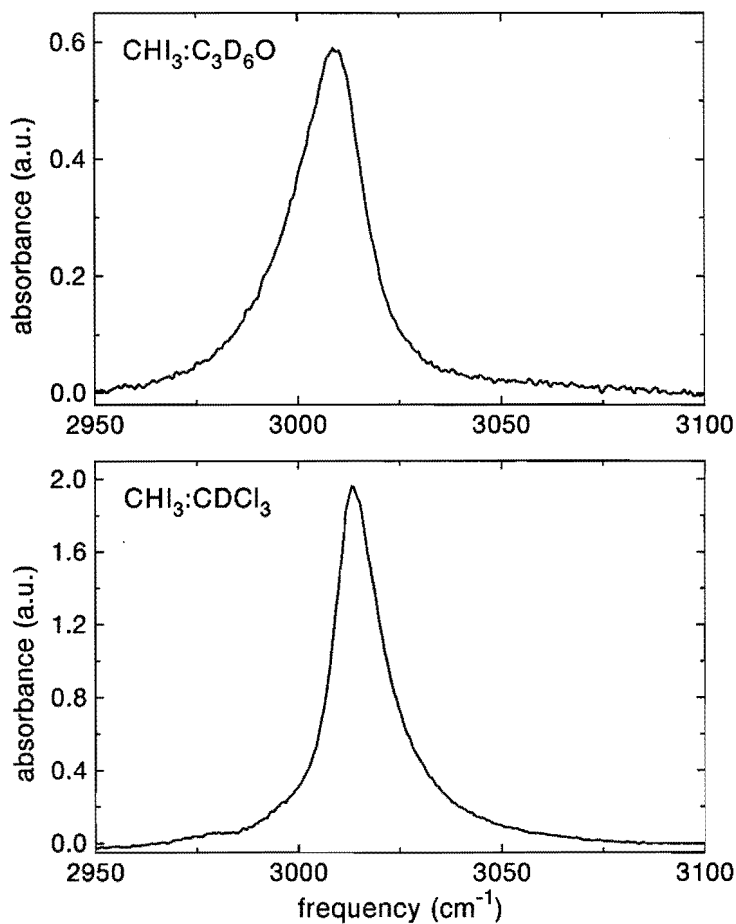


Figure 8.1: Conventional absorption spectra in the C–H stretch region of a) a 0.5 mm thick sample of a 0.045 M solution of iodoform in deuterated acetone ($\tilde{\nu}_{\text{center}}=3008 \text{ cm}^{-1}$) (upper panel) and b) a 1 mm thick sample of a 0.206 M solution of iodoform in deuterated chloroform ($\tilde{\nu}_{\text{center}}=3013 \text{ cm}^{-1}$) (lower panel).

8.2 Results and Discussion

The systems under investigation are 0.34 and 0.19 mol/l solutions of iodoform (CHI_3 , 99%, Merck) in deuterated acetone ($\text{C}_3\text{D}_6\text{O}$, 99.5 atom-% D, Aldrich) and deuterated chloroform (CDCl_3 , 99.8 atom-% D, Janssen Chimica), 200 and 1000 μm thick, respectively. The absorption spectra associated with the C–H stretch vibration of the iodoform in the two solvents is shown in Fig. 8.1.

Two independently tunable (2500–4000 cm^{-1} , bandwidth $\sim 10 \text{ cm}^{-1}$ at 3000 cm^{-1}) 25 ps infrared pulses (rep. rate of 10 Hz) with energies of $\sim 100 \mu\text{J}$ are generated through downconversion of 1064 nm Nd-YAG pulses in LiNbO_3 (an extensive description of the setup can be found in Chapter 1).

Transient spectra (showing the (0 \rightarrow 1)-pump-induced spectral changes with a delay between pump and probe of 35 ps) are shown in Fig. 8.2. At the 0 \rightarrow 1 transition around 3010 cm^{-1} the transmission increases due to the excitation of a considerable fraction of oscillators from 0 \rightarrow 1. For these excited oscillators absorption from 1 \rightarrow 2 becomes possible. This transient absorption band associated with the $v=1$ excited state absorption, the so-called hot band, is $\tilde{\nu}_{\text{anh}}$ shifted from the 0 \rightarrow 1 transition, and is observed around 2900 cm^{-1} . [157] For iodoform in chloroform-d the transmission is seen to dip slightly at the red side of the 0 \rightarrow 1 transition ($\sim 2980 \text{ cm}^{-1}$). This is due to an anharmonic shift: after excitation of the C–H stretch mode to $v=1$, IVR decay occurs to $v_{\text{CH}}=0^*$, where $v_{\text{CH}}=0^*$ stands for $v_{\text{CH}}=0$ with other modes within the molecule excited. [77] Anharmonic coupling between the C–H stretch mode and these other low-frequency intramolecular modes leads to a redshift of the ($v_{\text{CH}}=0^*$) \rightarrow ($v_{\text{CH}}=1^*$) compared to the ($v_{\text{CH}}=0$) \rightarrow ($v_{\text{CH}}=1$) transition [72, 77], as observed in Fig. 8.2b. Subsequent to decay from $v_{\text{CH}}=1$ to $v_{\text{CH}}=0^*$ (IVR), $v_{\text{CH}}=0^*$ will decay to $v_{\text{CH}}=0$ (IET). The anharmonic shift [difference between (0 \rightarrow 1) and (0 \rightarrow 1*)] was found to be $29 \pm 3 \text{ cm}^{-1}$ for the solvent CDCl_3 . For CHI_3 in $\text{C}_3\text{D}_6\text{O}$ this is not observed (Fig. 8.2a), since in this case the 0 \rightarrow 0 relaxation is much faster [72].

In the calculations (lines in Fig. 8.2) the transient spectrum is calculated: input parameters are the absorption band and the spectral profile of the pulses. The excited fraction of oscillators (typically 10%) is adjusted to the experimental 0 \rightarrow 1 signal amplitude. For the hot band, the width, the 1 \rightarrow 2 cross section and the anharmonicity are adjustable parameters. The *shape* of the hot band and the 0 \rightarrow 1* transition (for CHI_3 in CDCl_3) are assumed to be that of the 0 \rightarrow 1 absorption band. For both transients the hot band was found to be 1.65 ± 0.10 broader than the fundamental absorption band. The integrated cross-sections for 1 \rightarrow 2 were found to be 1.95 ± 0.10 times that of 0 \rightarrow 1, close to the value of 2 for a harmonic oscillator [158]. The anharmonicities are 118 ± 1.5 and $122 \pm 1.5 \text{ cm}^{-1}$ for CDCl_3 and $\text{C}_3\text{D}_6\text{O}$, respectively.

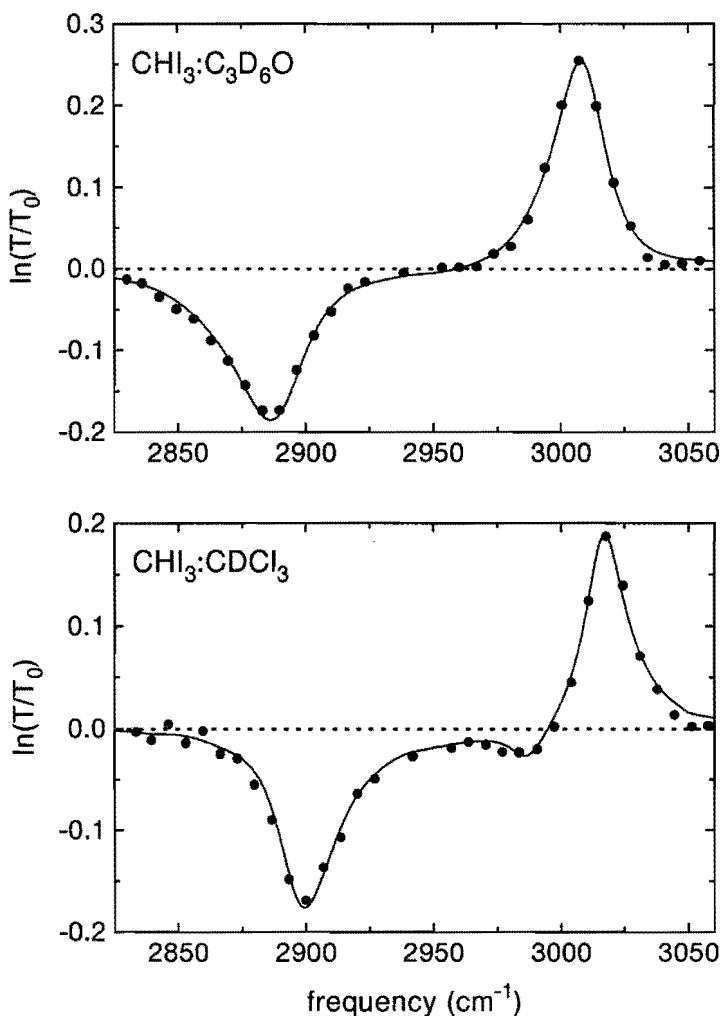


Figure 8.2: Transient spectra, transmission changes vs. wavenumber, recorded with a $1 \mu\text{J}$ probe pulse from the first branch, with the $150 \mu\text{J}$ pump tuned to the $(v=0) \rightarrow (v=1)$ transition of the C–H stretch vibration of iodoform in a) deuterated acetone ($\tilde{\nu}_{\text{pump}}=3007 \text{ cm}^{-1}$) (upper panel) and b) deuterated chloroform ($\tilde{\nu}_{\text{pump}}=3017 \text{ cm}^{-1}$) (lower panel). Transient spectra were recorded at a delay time between the pump and the probe of 35 ps, to avoid power broadening. The lines represent calculations described in the text.

For the pump-pump-probe experiments, the delay between the (1→2)-pump and the (0→1)-pump was fixed at 16 ps (the time at which the $v=1$ state population due to the (0→1)-pump is maximal). In these experiments, the delay of the probe pulse, of the same frequency as the (1→2)-pump, is varied. In Fig. 8.3 the transmission of the probe tuned to the 1→2 absorption with and without the second pump pulse are shown. Clearly, the (1→2)-pump excites a significant amount of oscillators to their second excited state. With the (0→1)-pump blocked, no signal was observed, confirming that the transmission changes due to the (1→2)-pump result from up-pumping of the C–H oscillators to their second vibrationally excited state. The large anharmonicity of the C–H stretch vibration (the $\sim 120\text{ cm}^{-1}$ difference between ground and excited state absorption) indicates the $v=2\rightarrow v=3$ transition is not involved in this measurement (assuming a Morse potential, the $v=2\rightarrow v=3$ transition frequency is readily calculated to be 2780 cm^{-1}). In the experiments, the polarizations of pump and probe pulses were parallel. This means that the observed signals can be affected

by the fast rotation of (excited) molecules: The pump-induced transmission increase will decay not only due to the decay of the excitation, but also due to the rotational motion of excited molecules, since rotation of excited molecules will lead to a decrease of the excitation component parallel to the polarization of the probe pulses. From the observation that the $0^*\rightarrow 1^*$ absorption rises with the same time-constants as the $v=1$ decays [72], it is apparent that reorientational motion (and the associated polarization diffusion) is either very fast or very slow compared to both the pulse duration and vibrational relaxation times, presumably very fast (see Ref. [159,160]). Hence, contributions to the signal arising from polarization diffusion play no role in the interpretation of the data.

There is a remarkable difference between the results of the pump-pump-probe experiment for the two solutions (Fig. 8.3): whereas for CHI_3 in CDCl_3 the transmission with the second pump remains larger than the transmission without the second pump at all delays, for CHI_3 in $\text{C}_3\text{D}_6\text{O}$ the two signal curves cross (see inset in Fig. 8.3a). The latter observation can be understood as follows: the probe pulse is monitoring the population difference between the $v=1$ and $v=2$ levels. If the oscillators in $v=2$ decay to $v=1$, then the long-time effect of the second pump pulse will be that there are more oscillators in $v=1$ than without the second pump pulse; the oscillators have been put 'on hold' in the $v=2$ state for a time $T_1^{2\rightarrow 1}$, so that the hot band (1→2 absorption) will effectively live somewhat longer with than without the second pump pulse. For CHI_3 in CDCl_3 , such a crossing is not observed. The effect is even more clearly observed in Fig. 8.4, where the transmission changes induced by the second pump pulse are plotted vs. delay.

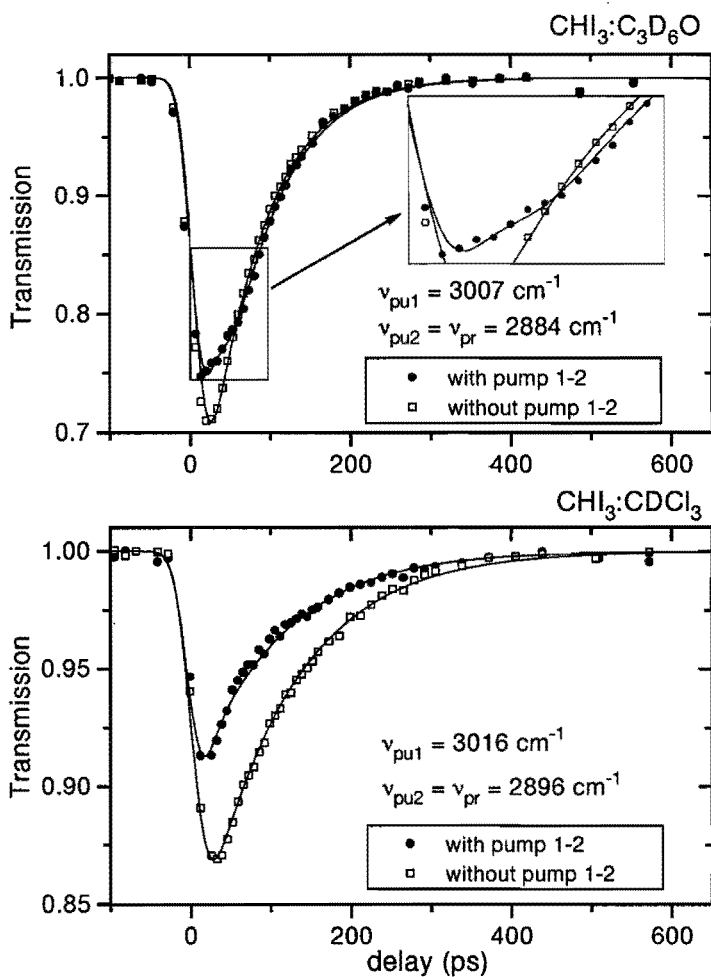


Figure 8.3: Transient transmission changes at the $1 \rightarrow 2$ frequency, after excitation with the $(0 \rightarrow 1)$ -pump, with and without the $(1 \rightarrow 2)$ -pump-pulse. The increased transmission with the second pump-pulse is due to excitation to the second excited state, whereafter absorption from $v=1$ to $v=2$ can no longer occur. Data are obtained in one experimental run: every other $(1 \rightarrow 2)$ -pump pulse is blocked. The lines are numerical solutions to the rate equations of the three-level system, assuming decay from $(2 \rightarrow 1)$ for a) acetone (upper panel) and direct decay to the ground state $(2 \rightarrow 0)$ for b) chloroform (lower panel).

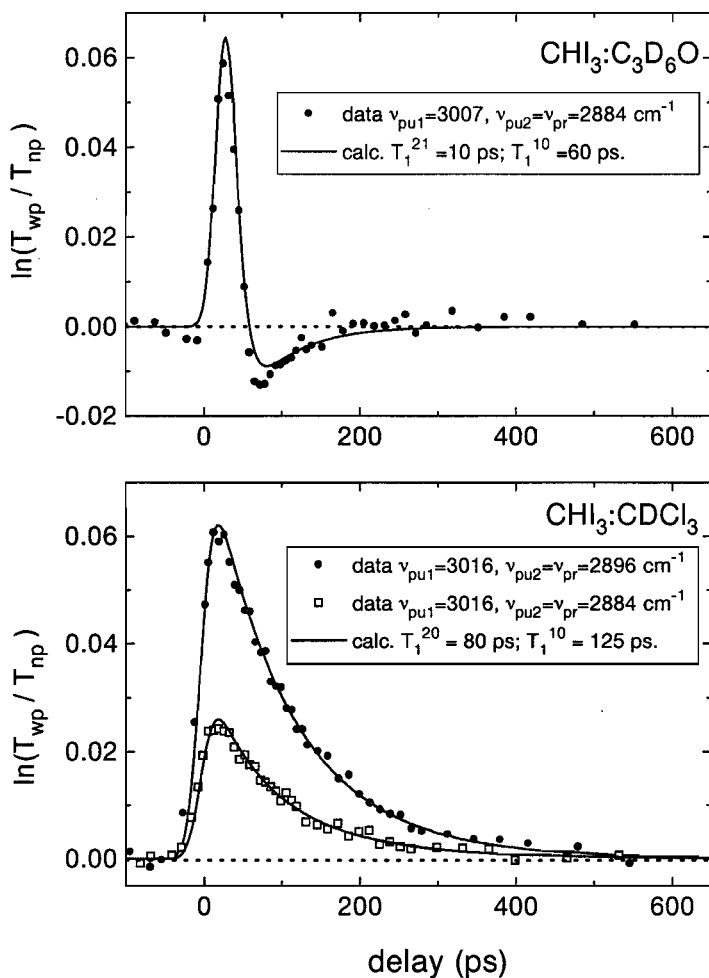


Figure 8.4: Transient ($1 \rightarrow 2$)-pump-pulse induced transmission changes at the $1 \rightarrow 2$ transition frequency: the logarithm of the transmission with both pump pulses (T_{wp}) normalized to the transmission without the second pump (T_{np}) for a) acetone and b) chloroform as solvent. Data with the second pump and the probe tuned to the peak of the hot band (\bullet) and with 12 cm^{-1} detuning to the red (\square). The line through the 2873 cm^{-1} -data (red side of hot band) for chloroform is the same the calculation for the 2885 cm^{-1} data, scaled to signal amplitude. Clearly, the $v=2$ does not relax to an anharmonically shifted $v=1^*$.

The data for CHI_3 in $\text{C}_3\text{D}_6\text{O}$ can be adequately described by numerically solving the rate equations for the three-level system, assuming a $2 \rightarrow 1 \rightarrow 0$ decay path (see lines in Figs. 8.3a and 8.4a). The energy decay time of the $1 \rightarrow 0$ transition was determined in a separate 2-colour ($0 \rightarrow 1$)-pump ($1 \rightarrow 2$)-probe experiment to be 60 ± 5 ps. From the width and the amplitude of the bleaching signal, the energy decay time $T_1^{2 \rightarrow 1}$ was found to be 10 ± 5 ps. In these calculations the rotational relaxation time was assumed to be zero. For CHI_3 in CDCl_3 , the data cannot be described by a $2 \rightarrow 1 \rightarrow 0$ decay path.

It could be that, for CHI_3 in CDCl_3 , the decay from $v=2$ occurs to a level $v=1^*$, where $v=1^*$ stands for $v_{\text{CH}}=1$ with other modes within the molecule excited, resulting in an anharmonic redshift as described above (Fig. 8.2b). If this anharmonic shift is sufficiently large, the $1^* \rightarrow 2^*$ absorption shifts out of the ($1 \rightarrow 2$)-probe laser bandwidth, after deexcitation from $2 \rightarrow 1^*$, and the transmission of the probe will remain larger than without $1 \rightarrow 2$ pump pulse at all delays. We checked for this effect by ($1 \rightarrow 2$)-pumping and -probing the red side of the hot band (open squares in Fig. 8.4b). In this experiment, decay to a $v=1^*$ state would result in a signal with a decreased transmission at delay times where IVR has, but IET has not yet occurred ($\gtrsim 35$ ps), as in Fig. 8.2b. It is clear however, from Fig. 8.4b that the data collected at the red side of the hot band show the same decay as the data at the peak of the hot band. Hence, we can exclude the $2 \rightarrow 1^*$ relaxation path for CHI_3 in CDCl_3 , and conclude that relaxation occurs directly from $2 \rightarrow 0^*$. Probing the $0 \rightarrow 1$ transition, no significant effect of the second pump pulse was observed. This supports the conclusion of direct relaxation from $2 \rightarrow 0^*$: It can be expected that the anharmonic shift of the $0^* \rightarrow 1^*$ after direct decay from $v=2$ will be larger than after decay from $v=1$, permitting the $v=0^*$ to $v=1^*$ transition to shift out of the laser bandwidth, resulting in a smaller signal probing the $0 \rightarrow 1$ transition.

Indeed, the data for CHI_3 in CDCl_3 can be described by calculations assuming direct decay of $v=2$ to $v=0$ (with $T_1^{1 \rightarrow 0}$ separately determined to be 125 ± 5 ps). The calculations for this system indicate two possible ranges of $T_1^{2 \rightarrow 0^*}$, smaller than 12 ps and between 60 and 100 ps. However, fast decay can be ruled out owing to the following considerations: (i) For the fast decay process, our numerical calculations predict a smaller effect of the second pump pulse than observed, when probing the $1 \rightarrow 2$ transition. In contrast, when slow decay is assumed the transmission change due to the second pulse is very well reproduced. (ii) Our calculations further show that, for fast decay from $v=2$ to $v=0$ the signal $\ln(T_{\text{wp}}/T_{\text{np}})$ probing the $0 \rightarrow 1$ transition would be equal to that probing the $1 \rightarrow 2$ transition. For fast decay from $v=2$ to $v=0^*$, the signal $\ln(T_{\text{wp}}/T_{\text{np}})$ probing the $0 \rightarrow 1$ transition would be half of that probing the $1 \rightarrow 2$ transition. For slow decay from $v=2$ to $v=0^*$ the $0 \rightarrow 1$ signal becomes even four times

smaller than the 1→2 signal. The data probing the 0→1 transition are not shown here, since no significant 1→2-pump induced transmission changes could be observed. This points to a signal much weaker than that probing the 1→2 transition, indicating that slow decay occurs from $v=2$. The results of calculations assuming slow decay ($T_1^{2 \rightarrow 0^*} = 80$ ps) from the second excited state are shown as lines in Figs. 8.3b and 8.4b.

8.3 The effect of solvent on the relaxation pathway

Recently, a theoretical model was developed which describes the effect of intermolecular (solute-solvent) interactions on the intramolecular energy transfer in small organic molecules.[72] This theory successfully describes the dependence of the $v_{\text{CH}}=1$ IVR relaxation rate on solvent. The theory predicts that the rate of IVR is determined by (i) the anharmonic coupling matrix element (describing the anharmonic coupling between the C–H stretching mode and the accepting modes, which are excited upon de-excitation of the C–H stretching mode), (ii) the energy difference between the C–H stretching mode and the combination of anharmonically coupled accepting modes (a measure of how good the energy match, or resonance, is) and (iii) the width of the absorption lines associated with vibrational transitions in the molecule (a measure of how important perfect resonance is). In the third lies the solvent-effect: the solvent influences the relaxation rate by influencing the transition energy distributions (i.e. the width of the absorption lines). Broader lines will imply larger possible overlap of the original mode with accepting mode combinations, resulting in faster decay.

Comparing the 2→1 to the 1→0 relaxation, the first and the last effects will increase the relaxation rate for both solvents, since (i) the $v=2$ wavefunction will be more spread out than the $v=1$, increasing the anharmonic coupling and (ii) as shown in Fig. 8.2, in both solvents the 1→2 absorption line is equally broadened compared to the 0→1 absorption line. However, the fact that in CDCl_3 relaxation from $v=2$ occurs directly to $v=0$ shows that in this case the 2→1 relaxation is very slow, and probably even slower than the 1→0 relaxation. Apparently, the energy mismatch is large for the 2→1 process compared to the 1→0. For the two solutions discussed in this Chapter one would expect similar intramolecular anharmonic couplings. Also, the energy mismatches are expected to be quite similar (although it must be noted that the solvent determines the *exact* position of the (0→1) and the (1→2) transitions, as can be seen in Fig. 8.1). Therefore, differences in relaxation paths and rates must be mainly due to differences in energy-mismatch compensation capacity of the solvent. In principle, the solvent effect on the energy-mismatch compensation is twofold: The solvent affects both the width of the C–H stretching mode and the width of low-frequency modes within the

molecule, which act as accepting modes in the relaxation process.

The hot band of CHI_3 in $\text{C}_3\text{D}_6\text{O}$ is very broad (Fig. 8.2a), indicative of the ability to compensate for large energy mismatches. This explains that in $\text{C}_3\text{D}_6\text{O}$ the $2 \rightarrow 1$ relaxation can occur, despite a large energy mismatch. Due to this large mismatch, the $2 \rightarrow 1$ relaxation for CHI_3 in CDCl_3 is very slow. As a consequence, the $2 \rightarrow 0$ relaxation becomes the dominant relaxation path, in spite of the fact that the anharmonic coupling can be expected to be much smaller for this transition. However, the direct $2 \rightarrow 0$ process can become relatively efficient, due to a small energy mismatch between the mode and the combination of accepting modes. It is unknown which specific low-frequency modes act as accepting modes, but when a larger amount of energy has to be disposed of, more low-frequency mode combinations are resonant with the energy: The low-frequency modes within the CHI_3 molecule [161] show that, with four accepting modes there is only one combination that lies within 100 cm^{-1} of the ($1 \rightarrow 0$) transition. For the ($2 \rightarrow 0$), with eight accepting modes, there are six possible relaxation channels within 100 cm^{-1} of this transition.

Obviously, the $2 \rightarrow 0$ process could also occur for CHI_3 in $\text{C}_3\text{D}_6\text{O}$, presumably with a rate similar to that of the $2 \rightarrow 0$ transition in CDCl_3 , since apparently for this transition there is no necessity for compensating large energy mismatches. However, the rate will be negligible compared to the $2 \rightarrow 1$ relaxation rate, and the $2 \rightarrow 0$ process is therefore not observed in the experiment.

Summarizing, the $2 \rightarrow 1$ process requires a large energy-mismatch compensation from the solvent, readily obtained from the acetone, but not from the chloroform. In chloroform, direct relaxation to the ground state becomes the principal relaxation pathway.

8.4 Conclusions

We have succeeded in resonantly climbing the vibrational ladder of the C-H stretch vibration in CHI_3 to the second excited state. The decay from this state depends crucially on the solvent. For a strongly polar solvent decay from $v=2$ first occurs to $v=1$, whereafter the first excited state decays to the ground state. For a less polar solvent, direct decay to the ground state is the dominant relaxation pathway. The difference is qualitatively explained in terms of energy-mismatch compensation by the solvent in the IVR process; apparently, for the $v=2$ to $v=1$ decay process, there is a large energy-mismatch between the energy associated with this transition and the combination of the anharmonically coupled accepting modes. In case of a strongly polar solvent (acetone), this energy mismatch is easily compensated for, resulting in

the $2 \rightarrow 1 \rightarrow 0$ relaxation route. In a less polar solvent (chloroform), energy-mismatch compensation is not so efficient and direct decay from $v=2$ to $v=0$ occurs.

Bibliography

- [1] G. HERZBERG, *Molecular spectra and molecular structure II. Infrared and Raman spectra of polyatomic molecules*, twelfth printing, D. van Nostrand, New York.
- [2] H. NIEMANTSVERDIET, *Spectroscopy in Catalysis*, (VCH publishers, New York, NY, 1993).
- [3] J.A. MOULIJN, P.W.N.M. VAN LEEUWEN, R.A. VAN SANTEN (Editors), *Catalysis: An Integrated Approach to Homogeneous, Heterogeneous and Industrial Catalysis*, Elsevier, Amsterdam, 1993.
- [4] M. CHERGUI (Editor), *Femtochemistry. Ultrafast Chemical and Physical Processes in Molecular Systems*, World Scientific, Singapore, 1996.
- [5] A. RAUKEMA AND A.W. KLEYN, *Phys. Rev. Lett.* **75**, 4333 (1995).
- [6] R.A. VAN SANTEN AND G.J. KRAMER, *Chem. Rev.* **95**, 637 (1995).
- [7] A. DYER, *An Introduction to Zeolite Molecular Sieves*, J. Wiley & Sons, Chichester, (1988).
- [8] M.W. MEIER, D.J. OLSON, AND CH. BAERLOCHER, *Atlas of zeolite structure types*, 4th rev. ed., Elsevier, London, 1996.
- [9] J.M. THOMAS, *Scient. Am.* **266**, (IV) 82 (1992).
- [10] A. ZECHINA AND C.O. AREAN, *Chem. Soc. Rev.* **25**, 187 (1996) *and refernces therein*.
- [11] P.W. ATKINS, *Physical Chemistry*, fourth edition, Oxford University Press, Oxford (1990).
- [12] P.F. BERNATH, *Spectra of Atoms and Molecules*, Oxford University Press, Oxford (1995).
- [13] S. BRATOS, *J. Chem. Phys.* **63**, 3499 (1975).
- [14] A. NITZAN AND J. JORTNER, *Mol. Phys.* **25**, 713 (1973).
- [15] A. NITZAN, S. MUKAMEL AND J. JORTNER, *J. Chem. Phys.* **60**, 3929 (1974).
- [16] J. JORTNER, *Mol. Phys.* **32**, 379 (1976).
- [17] D.W. OXTOBY, *Adv. Chem. Phys.* **40**, 1 (1979).
- [18] R. KUBO, M. TODA AND N. HASHITSUME, *Statistical Physics II: Nonequilibrium Statistical Mechanics*, (Springer-Verlag, Berlin, 1985).
- [19] R. KUBO, *Adv. Chem. Phys.* **15**, 101 (1969).
- [20] A.E. SIEGMAN, *Lasers*, University Science Books, Mill Valley (1986).
- [21] C.P. SLICHTER, *Principles of Magnetic Resonance*, third edition, Springer-Verlag, Berlin (1989).

- [22] M.J.P. BRUGMANS, H.J. BAKKER AND A. LAGENDIJK, *J. Chem. Phys.* **104**, 64 (1996).
- [23] Y.R. SHEN, *The Principles of Nonlinear Optics*, (J. Wiley & Sons, New York, 1984).
- [24] R. LOUDON, *The Quantum Theory of Light*, second edition, Oxford University Press, Oxford (1992).
- [25] R.W. BOYD, *Nonlinear Optics*, Academic Press (1992).
- [26] D. ZIMDARS, A. TOKMAKOFF, S. CHEN, S.R. GREENFIELD, M.D. FAYER, T.I. SMITH AND H.A. SCHWETTMAN, *Phys. Rev. Lett.* **70**, 2718 (1993).
- [27] S. WOUTERSEN, M. BONN, M.J.P. BRUGMANS, U. EMMERICHS AND H.J. BAKKER, *Opt. Lett.* **21**, 1579 (1996).
- [28] H. HAMAGUCHI AND T.L. GUSTAFSON, *Ann. Rev. Phys. Chem.* **45**, 593 (1994).
- [29] A. LAUBEREAU AND W. KAISER, *Rev. Mod. Phys.* **50**, 607 (1978).
- [30] H.J. BAKKER, *Time-resolved Vibrational Spectroscopy with Picosecond Infrared Pulses*, (PhD thesis, University of Amsterdam, 1991).
- [31] P.C.M. PLANKEN, *Generation and Application of Ultrashort Infrared Pulses*, (PhD thesis, University of Amsterdam, 1991).
- [32] M.J.P. BRUGMANS, *Relaxation Kinetics in Disordered Dense Phases*, (PhD thesis, University of Amsterdam, 1995).
- [33] A. CORMA, *Chem. Rev.* **95**, 559 (1995).
- [34] H. STACH, J. JÄNCHEN, H. JERSCHKEWITZ, U. LOHSE, B. PARLITZ, B. ZIBROWIUS AND M. HUNGER, *J. Phys. Chem.* **96**, 8473 (1992).
- [35] H. STACH, J. JÄNCHEN, H. JERSCHKEWITZ, U. LOHSE, B. PARLITZ, B. ZIBROWIUS AND M. HUNGER, *J. Phys. Chem.* **96**, 8480 (1992).
- [36] M. CROCKER, R.H.M. HEROLD, M.H.W. SONNEMANS, C. A. EMEIS, A. E. WILSON AND J.N. VAN DER MOOLEN, *J. Phys. Chem.* **97**, 432 (1993).
- [37] M. H. W. SONNEMANS, C. DEN HEIJER AND M. CROCKER, *J. Phys. Chem.* **97**, 440 (1993).
- [38] V.L. ZHOBLENKO, M.A. MAKAROVA AND J. DWYER, *J. Phys. Chem.* **97**, 5962 (1993).
- [39] I. BANKOÓS, J. VALYON, G.I. KAPUSTIN, D. KALLÓ, A.L. KLYACHKO AND T.R. BRUEVA, *Zeolites* **8**, 189 (1988).
- [40] M.P. CASASSA, E.J. HEILWEIL, J.C. STEPHENSON AND R.R. CAVANAGH, *J. Electron Spectrosc. Relat. Phenom.* **38**, 257 (1986).
- [41] R.R. CAVANAGH M.P. CASASSA, E.J. HEILWEIL, AND J.C. STEPHENSON, *J. Vac. Sci. Technol.* **A 5**, 469 (1987).
- [42] C. HIROSE, Y. GOTO, N. AKAMATSU, J. KONDO AND K. DOMEN, *Surf. Sc.* **283**, 244 (1993).
- [43] J. KUBOTA, M. FURUKI, Y. GOTO, J. KONDO, A. WADA, K. DOMEN AND C. HIROSE, *Chem. Phys. Lett.* **204**, 273 (1993).
- [44] M.J.P. BRUGMANS, A.W. KLEYN, A. LAGENDIJK, W.P.J.H. JACOBS AND R.A. VAN SANTEN, *Chem. Phys. Lett.* **217**, 117 (1994).
- [45] K. DOMEN, S.S. KANO, T. FUJINO, M. FURUKI, M. KASHITANI, J. KUBOTA, J. KONDO, A. WADA, M. ISHIDA, F. GOTO F. WAKABAYASHI AND C. HIROSE, *Surf. Sc.* **363**, 397 (1996).
- [46] T. FUJINO, M. FURUKI, M. KASHITANI, K. ONDA, J. KUBOTA, J. KONDO, A. WADA, K. DOMEN, C. HIROSE, F. WAKABAYASHI, M. ISHIDA, F. GOTO AND S.S. KANO, *J. Chem. Phys.* **105**, 279 (1996).
- [47] L.M. KUSTOV, V.Y. BOROVKOV AND V.B. KAZANSKY, *J. Catal.* **72**, 149 (1981).
- [48] W.H. PRESS ET AL., *Numerical Recipes*, second edition, Cambridge University Press, Cambridge (1992).

- [49] M. CZJZEK, H. JOBIC, A.N. FITCH AND T. VOGT, *J. Phys. Chem.* **96**, 1535 (1992).
- [50] A.J.M. DE MAN AND R.A. VAN SANTEN, *Zeolites* **12**, 269 (1992).
- [51] W.P.J.H. JACOBS, J.H.M.C. VAN WOLPUT AND R.A. VAN SANTEN, *Chem. Phys. Lett.* **210**, 32 (1993).
- [52] W.P.J.H. JACOBS, J.H.M.C. VAN WOLPUT H. JOBIC AND R.A. VAN SANTEN, *Zeolites* **14**, 117 (1994).
- [53] M.J.P. BRUGMANS, M. BONN, H.J. BAKKER AND A. LAGENDIJK, *Chem. Phys.* **201**, 215 (1995).
- [54] E.J. HEILWEIL, M.P. CASASSA, R.R. CAVANAGH, AND J.C. STEPHENSON *J. Chem. Phys.* **81**, 2856 (1984).
- [55] E.J. HEILWEIL, M.P. CASASSA, R.R. CAVANAGH, AND J.C. STEPHENSON *Chem. Phys. Lett.* **117**, 185 (1985).
- [56] J.R. ENGHOLM, U. HAPPEK, AND A.J. SIEVERS, *Chem. Phys. Lett.* **249**, 387 (1996).
- [57] E.J. HEILWEIL, *Chem. Phys. Lett.* **129**, 48 (1986).
- [58] U. HAPPEK, J.R. ENGHOLM, AND A.J. SIEVERS, *Chem. Phys. Lett.* **221**, 279 (1994).
- [59] H.J. BAKKER, P.C.M. PLANKEN, L. KUIPERS AND A. LAGENDIJK, *J. Chem. Phys.* **94**, 1730 (1991).
- [60] G.J. KRAMER AND R.A. VAN SANTEN, *J. Am. Chem. Soc.* **115**, 2882 (1993).
- [61] D.J. PARILLO, C. LEE AND R.J. GORTE, *Appl. Cat.* **110**, 67 (1994).
- [62] E.J. HEILWEIL, M.P. CASASSA, R.R. CAVANAGH AND J.C. STEPHENSON, *Ann. Rev. Phys. Chem.* **40**, 143 (1989).
- [63] M. FURUKI, K. KUBOTA, Y. GOTO, F. WAKABAYASHI, J. KONDO, A. WADA, K. DOMEN AND C. HIROSE, *J. Electron Spectrosc. Relat. Phenom.* **64-65**, 259 (1993).
- [64] D. HADŽI AND S. BRATOS, in: *The hydrogen bond*, Vol. 2, eds. P. Schuster, G. Zundel and C. Sandorfy (North-Holland, Amsterdam, 1976) p. 565.
- [65] P.A. JACOBS AND J.B. UYTTERHOEVEN, *J. Chem. Soc. Faraday Trans. I* **69**, 359 (1973).
- [66] H. GRAENER, T.Q. YE AND A. LAUBEREAU, *J. Chem. Phys.* **90**, 3413 (1989).
- [67] E.J. HEILWEIL, M.P. CASASSA, R.R. CAVANAGH AND J.C. STEPHENSON, *J. Chem. Phys.* **85**, 5004 (1986).
- [68] F. WAKABAYASHI, J. KONDO, W. AKIHIDE, K. DOMEN AND C. HIROSE, *J. Phys. Chem.* **97**, 10761 (1993).
- [69] M. BONN, M.J.P. BRUGMANS, A.W. KLEYN AND R.A. VAN SANTEN, *J. Chem. Phys.* **102**, 2181 (1995).
- [70] V.M. KENKRE, A. TOKMAKOFF AND M.D. FAYER, *J. Chem. Phys.* **101**, 10618 (1994).
- [71] P. MOORE, A. TOKMAKOFF, T. KEYES AND M.D. FAYER, *J. Chem. Phys.* **103**, 3325 (1995).
- [72] H.J. BAKKER, *J. Chem. Phys.* **98**, 8496 (1993).
- [73] J.T. YARDLEY, *Introduction to Molecular Energy Transfer*, Academic Press, New York (1980).
- [74] E.J. HEILWEIL, M.P. CASASSA, R.R. CAVANAGH AND J.C. STEPHENSON *J. Chem. Phys.* **82**, 5216 (1985).
- [75] E.J. HEILWEIL, R.R. CAVANAGH AND J.C. STEPHENSON, *J. Chem. Phys.* **89**, 230 (1988).
- [76] H. GRAENER, T.Q. YE AND A. LAUBEREAU, *J. Chem. Phys.* **91**, 1043 (1989).
- [77] H. GRAENER, *Chem. Phys. Lett.* **165**, 110 (1990).
- [78] A. TOKMAKOFF, B. SAUTER, AND M.D. FAYER, *J. Chem. Phys.* **100**, 9035 (1994).

- [79] S.M. ARRIVO, T.P. DOUGHERTY, W.T. GRUBBS AND E.J. HEILWEIL, *Chem. Phys. Lett.* **235**, 247 (1995).
- [80] A. NITZAN, S. MUKAMEL AND J. JORTNER, *J. Chem. Phys.* **63**, 200 (1975).
- [81] M.P. CASASSA, E.J. HEILWEIL, J.C. STEPHENSON AND R.R. CAVANAGH, *J. Chem. Phys.* **84**, 2361 (1986).
- [82] W.P.J.H. JACOBS, H. JOBIC, J.H.M.C. VAN WOLPUT AND R.A. VAN SANTEN, *Zeolites* **12**, 315 (1992).
- [83] H. JOBIC, *J. Catal.* **131**, 289 (1991).
- [84] A. NITZAN, S. MUKAMEL AND J. JORTNER, *J. Chem. Phys.* **63**, 200 (1975).
- [85] P. DUMAS, Y.J. CHABAL AND G.S. HIGASHI, *Phys. Rev. Lett.* **65**, 1124 (1990).
- [86] A. SEILMEIER, P.O.J. SCHERER AND W. KAISER, *Chem. Phys. Lett.* **105**, 140 (1984).
- [87] R. BONN, *Infrared Absorption Spectra of Molten Nitrates. A study of the structure of molten salt systems with the aid of moment analysis*, (PhD thesis, University of Amsterdam, 1969).
- [88] R. KUBO, *J. Phys. Soc. Jpn.* **9**, 935 (1954).
- [89] P.W. ANDERSON, *J. Phys. Soc. Jpn.* **9**, 316 (1954).
- [90] R.M. SHELBY, C.B. HARRIS AND P.A. CORNELIUS, *J. Chem. Phys.* **70**, 34 (1979).
- [91] S. MARKS, P.A. CORNELIUS AND C.B. HARRIS, *J. Chem. Phys.* **73**, 3069 (1980).
- [92] Y. MARECHAL AND A. WITKOWSKI, *J. Chem. Phys.* **48**, 3697 (1968).
- [93] J. YARWOOD AND G.N. ROBERTSON, *Nature* **257**, 41 (1975).
- [94] G.N. ROBERTSON AND J. YARWOOD, *Chem. Phys.* **32**, 267 (1978).
- [95] H. ABRAMCZYK, *Chem. Phys.* **144**, 319 (1990).
- [96] J.P. HAWRANEK AND M.A. BRODA, *Chem. Phys. Lett.* **98**, 373 (1983).
- [97] U.P. AGARWAL, R.S. GREEN AND J. YARWOOD, *Chem. Phys.* **74**, 35 (1983).
- [98] J. YARWOOD, R. ACKROYD AND G.N. ROBERTSON, *Chem. Phys. Lett.* **78**, 614 (1981).
- [99] M.I. CABAÇO, M. BESNARD AND J. YARWOOD, *Mol. Phys.* **75**, 139 (1992).
- [100] B. CZARNIK-MATUSEWICZ AND J.P. HAWRANEK, *Spectrochim. Acta*, **43A**, 791 (1987).
- [101] K. TOKHADZE, N. DUBOVNA, Z. MIELKE, M. WIERZEJWSKA-HNAT AND H. RATAJCZAK, *Chem. Phys. Lett.* **202**, 87 (1993).
- [102] J. YARWOOD, R. ACKROYD AND G.N. ROBERTSON, *Chem. Phys.* **32**, 283 (1978).
- [103] H. GRAENER, T. Q. YE AND A. LAUBEREAU, *Phys. Rev. B* **41**, 2597 (1990).
- [104] H. GRAENER, G. SEIFERT AND A. LAUBEREAU, *Phys. Rev. Lett.* **66**, 2092 (1991).
- [105] R. JANOSCHEK, E.G. WIEDEMANN AND G. ZUNDEL, *J. Chem. Soc. Faraday Trans. 2* **69**, 505 (1973).
- [106] D. BORGIS, G. TARJUS AND H. AZZOUZ, *J. Chem. Phys.* **97**, 1390 (1992).
- [107] S.J. KLIPPENSTEIN AND J.T. HYNES, *J. Phys. Chem.* **95**, 4651 (1991).
- [108] M. BONN, M.J.P. BRUGMANS, A.W. KLEYN AND R.A. VAN SANTEN, *Chem. Phys. Lett.* **233**, 309 (1995).
- [109] J. DWYER in: *Innovation in Zeolite Material Science*, eds. P.J. Grobet et al. (Elsevier, Amsterdam, 1988) p. 333.
- [110] C. SANDORFY, in: *Hydrogen bonds*, P. Schuster (Springer-Verlag, Berlin, 1984), p. 41.
- [111] N.D. BAKER, G.A. OZIN AND J. GODBER, *Catal. Rev. -Sci. Eng.* **27**, 591 (1985).
- [112] D.W. OXTOBY AND S.A. RYCE, *Chem. Phys. Lett.* **42**, 1 (1976).
- [113] M. BONN, M.J.P. BRUGMANS, H.J. BAKKER, *Chem. Phys. Lett.* **249**, 81 (1996).
- [114] B. BOULIL, O. HENRI-ROUSSEAU AND P. BLAISE, *Chem. Phys.* **126**, 263 (1988).
- [115] H. ABRAMCZYK, *Chem. Phys.* **144**, 305 (1990).
- [116] K.M. NEYMAN, P. STRODEL, S.P. RUZAKIN, N. SCHLENSOG, H. KNÖZINGER AND N. RÖSCH, *Cat. Lett.* **31**, 273 (1995).

- [117] P.A. MADDEN AND R.M. LYNDEN-BELL, *Chem. Phys. Lett.* **38**, 163 (1976).
- [118] M.R. BATTAGLIA AND P.A. MADDEN, *Mol. Phys.* **36**, 1601 (1978).
- [119] J.C. OWRUTSKY, D. RAFTERY AND R.M. HOCHSTRASSER, *Ann. Rev. Phys. Chem.* **45**, 519 (1994).
- [120] F. HUISKEN, A. KULCKE, C. LAUSH AND J.M. LISY, *J. Chem. Phys.* **95**, 3924 (1991).
- [121] S. COUSSAN, N. BAKKAS, A. LOUTELLIER, J.P. PERCHARD AND S. RACINE, *Chem. Phys. Lett.* **217**, 123 (1994).
- [122] A. KOGLBAUER AND J.A. LERCHER, *J. Chem. Soc. Faraday Trans.* **88**, 2283 (1992).
- [123] S.G. IZMAILOVA, I.V. KARETINA, S.S. KHVOSHCHIEV AND M.A. SHUBAEVA, *J. of Coll. and Interf. Sc.* **165**, 318 (1994).
- [124] S. WOUTERSEN, *private communication*.
- [125] PH. GRENIER, F. MEUNIER, P.G. GRAY, J. KÄRGER, Z. XU AND D.M. RUTHVEN, *Zeolites* **14**, 242 (1994).
- [126] A. STAIB AND J.T. HYNES, *Chem. Phys. Lett.* **204**, 197 (1993).
- [127] E.D. POTTER, J.L. HEREK, S. PEDERSEN, Q. LIU AND A.H. ZEWAIL, *Nature* **533**, 66 (1992).
- [128] J.C. POLANYI, A.H. ZEWAIL, *Acc. Chem. Res.* **28**, 119, (1995).
- [129] C.D. CHANG, *Hydrocarbons from methanol*, Marcel Dekker, New York, (1983).
- [130] A. ISON, AND R.J. GORTE, *J. Catal.* **89**, 150 (1984).
- [131] L. KUBELKOVÁ, J. NOVÁKOVÁ, K. JEDOMAVÁ, *J. Catal.* **124**, 441 (1990).
- [132] G. MIRTH AND J.A. LERCHER, *J. Phys. Chem.* **95**, 3736 (1991).
- [133] G. MIRTH, J.A. LERCHER, M.W. ANDERSON AND J. KLINOWSKI, *J. Chem. Soc. Faraday Trans.* **86**, 3039 (1990).
- [134] G. MIRTH, A. KOGLBAUER AND J.A. LERCHER, in: *Proc. 9th Int. Zeol. Conf. 1992, Montreal*, Eds. R. von Ballmoos et. al, 251 (1993).
- [135] H. JOBIC, A. RENOUPREZ, M. BEE AND C. POINSIGNON, *J. Phys. Chem.* **90**, 1059 (1986).
- [136] J.D. GALE, C.R.A. CATLOW, AND A.K. CHEETAM, *J. Chem. Soc. Chem. Commun.* **178** (1991).
- [137] F. HAASE AND J. SAUER, *J. Am. Chem. Soc.* **117**, 3780 (1995).
- [138] S.R. BLASZKOWSKI AND R.A. VAN SANTEN, *J. Phys. Chem.* **99**, 11728 (1995).
- [139] E. NUSTERER, P.E. BLÖCHL AND K. SCHWARZ, *Angew. Chem. Int. Ed. Engl.* **35**, 175 (1996).
- [140] R. SHAH, M.C. PAYNE AND J.D. GALE, *Science* **271**, 1395 (1996).
- [141] R. SHAH, M.C. PAYNE AND J.D. GALE, *J. Phys. Chem.* **100**, 11688 (1996).
- [142] S.P. GREATBANKS, I.H. HILLIER, N.A. BURTON AND P. SHERWOOD, *J. Phys. Chem.* **100**, 11688 (1996).
- [143] S.R. BLASZKOWSKI AND R.A. VAN SANTEN, *J. Am. Chem. Soc.* **118**, 5152 (1996).
- [144] J.D. GALE, *Topics in Catalysis* **3**, 169 (1996).
- [145] E. NUSTERER, P.E. BLÖCHL AND K. SCHWARZ, *Chem. Phys. Lett.* **253**, 448 (1996).
- [146] A.G. PELMENSHIKOV, J.H.M.C. VAN WOLPUT, J. JÄNCHEN AND R.A. VAN SANTEN, *J. Phys. Chem.* **99**, 3612 (1995).
- [147] J.A. LERCHER, *private communication*.
- [148] F. WAKABAYASHI, J.N. KONDO, K. DOMEN, AND C. HIROSE, *J. Phys. Chem.* **100**, 1442 (1996).
- [149] A. JENTYS, G. WARECKA, M. DEREWINSKI AND J.A. LERCHER, *J. Phys. Chem.* **93**, 4837, (1989) *and references therein*.

- [150] L. KUBELKOVÁ, J. NOVÁKOVÁ AND P. JÍRŮ, in: *Structure and reactivity of modified zeolites* P.A. Jacobs et al. (Eds.), Elsevier, Amsterdam (1984), p. 217.
- [151] M. BONN, H.J. BAKKER, A.W. KLEYN AND R.A. VAN SANTEN, *J. Phys. Chem.* **100**, 15301 (1996).
- [152] G. SEIFERT AND H. GRAENER, *J. Phys. Chem.* **98**, 11827 (1994).
- [153] W.T. GRUBBS, T.P. DOUGHERTY AND E.J. HEILWEIL, *J. Phys. Chem.* **99**, 10716 (1995).
- [154] H.J. BAKKER, P.C.M. PLANKEN AND A. LAGENDIJK, *Nature* **347**, 745 (1990).
- [155] D. RAFTERY, E. GOODING AND R.M. HOCHSTRASSER, In: *Ultrafast Phenomena IX*, eds. P. F. Barbara et al. Berlin: Springer (1994).
- [156] H. GRAENER AND A. LAUBEREAU, *Chem. Phys. Lett.* **102**, 100 (1983).
- [157] H. GRAENER, R. DOHLUS AND A. LAUBEREAU, *Chem. Phys. Lett.* **140**, 306 (1987).
- [158] P.W. ATKINS, *Molecular Quantum Mechanics*, Oxford University Press, Oxford (1992).
- [159] H. GRAENER, G. SEIFERT AND A. LAUBEREAU, *Chem. Phys. Lett.* **172**, 435 (1990).
- [160] G. SEIFERT AND H. GRAENER, *Opt. Commun.* **115**, 216 (1995).
- [161] T. SHIMANOCHI, *Table of Molecular Vibrational Frequencies, Consolidated Volume I*, NSRDS-NBS 39, Washington (1972).

Summary

Infrared spectroscopy is a widely applied tool in catalysis research, since vibrational spectra of catalysts, adsorbates (reactants) and probe molecules contain information on e.g. catalyst structure and microscopic adsorption configurations. In this thesis, time-resolved (picosecond) non-linear infrared spectroscopy is applied to study the vibrational dynamics of the catalytic sites in acidic zeolites, the interaction of these sites with adsorbates, and the vibrational dynamics of the adsorbates themselves. In the experiments, a specific vibration of the zeolite or the adsorbate is resonantly excited by means of an infrared laser pulse. The subsequent relaxation process can be monitored real-time by a second, non-perturbing, probe pulse.

From the vibrational relaxation rates of the O–D stretch vibration of deuterated zeolite hydroxyls, information about the local environment of these hydroxyls in different zeolites can be obtained: For hydroxyls in several zeolites the relaxation rate is found to vary within the absorption band of the O–D stretch vibration. This is caused by hydrogen bonding between the hydrogen atom of the hydroxyl and oxygen atoms in the zeolite lattice. Similarly, the presence of weakly bound (hydrogen-bonded) adsorbates greatly enhances the vibrational relaxation rate. The excess vibrational energy is not used to break this hydrogen bond, nor is any of the energy transferred to the adsorbate. The bulk of the energy is still transferred to the zeolite lattice. It is further demonstrated that upon relaxation, the excess energy is very rapidly delocalized over the whole zeolite lattice and converted into heat.

Non-linear spectroscopy is particularly enticing when different (time-resolved) results are obtained for systems with identical linear absorption spectra. In this thesis, two such cases are encountered. In the first case, two similar linear absorption lines of the zeolite O–D stretch vibration are caused by hydrogen bonding to two different hydrogen bond acceptors, namely oxygen atoms in the zeolite lattice and simple adsorbates. The non-linear technique reveals that the homogeneous linewidths hidden under the inhomogeneous absorption bands differ by over an order of magnitude: The

homogeneous dephasing mechanism (and its rate) is determined by the type of hydrogen bond. The dephasing mechanism can be elucidated by variation of the adsorbate. In the second case, of methanol clusters in zeolites and solution, the conventional absorption spectra are also very similar. The response to infrared excitation of an O–H stretch vibration of a hydroxyl group within a cluster is very different. Initially in both systems relaxation of the excitation leads to fragmentation of the cluster. This process occurs much faster in solution than inside the zeolite. Although the clusters in solution are found to be quite resilient (re-association of the fragments occurs very rapidly), in the zeolite the re-association process is over *two orders of magnitude* slower. These findings can be understood by noting the different microscopic environments of the methanol clusters.

Furthermore, the non-linear spectroscopic technique is employed to investigate the reactive system of methanol adsorbed to acid zeolites. Acid zeolites are widely applied industrially to catalyze the methanol-to-gasoline reaction. The equilibrium between two adsorption structures can be temporarily shifted towards the more reactive of the two complexes by excitation with picosecond infrared pulses. The dynamics of the conversion are dictated by the large anharmonicity of the hydrogen bond between the methanol and the reactive (Brønsted) site.

Finally, a novel experimental scheme is introduced that allows for the investigation of vibrational relaxation (rate and pathway) from the *second* excited state. These pump-pump-probe experiments demonstrate that for small organic molecules, interactions with the solvent play a crucial role in the relaxation process, dictating not only the relaxation rate, but even the relaxation pathway.

Nawoord

Ik heb de afgelopen jaren met veel plezier onderzoek gedaan. In eerste instantie wil ik daar mijn promotores Rutger van Santen en Aart Kleyn voor bedanken vanwege alle mogelijkheden die ze me gaven en de grote vrijheid die ik kreeg. Jullie beider enthousiasme werkte keer op keer aanstekelijk.

Marco Brugmans heeft me ingewijd in de geheimen van de tijdsopgeloste infrarood spectroscopie en onze opstelling PUPIL. Zonder Marco was het lang niet zo snel en goed gegaan. Mijn dank hiervoor.

Huib Bakker kwam halverwege mijn promotie terug op het AMOLF. Als ik superlatieven wil vermijden, moet ik volstaan te zeggen dat onze samenwerking inspirerend en leerzaam voor me was. Met Huib kwamen Uli *'non-linear optics'* Emmerichs en Sander Woutersen (*"Je weet het niet; je weet het nooit. Ik neem nog 'n Brownie."*). Ook zij hebben –ieder op geheel onnavolgbare wijze– veel bijgedragen aan dit proefschrift. Ik zal de groep vibratie-dynamica missen.

De technische ondersteuning van Erik Kossen was onmisbaar. Richard Schaafsma, Frans Giskes, Rob Kemper en de mannen van de werkplaats stonden ook altijd klaar.

Er zijn nog een heleboel anderen die me hebben geholpen en het zo leuk hebben gemaakt; op het AMOLF waren dit o.a. Jan v/d Elsen, Meint, Diederik W., Bas, Eloy, David, Malcolm, Diederik M., Rutger, Oscar, en natuurlijk –elke morgen– Els (wat jammer dat je er zo laat achterkwam!), in Nieuwegein Paul en Nils, en in Eindhoven: Solange, Jos, Annemieke, en alle anderen die ik hier vergeet.

Mijn vriendjes willen dat ik hier schrijf dat ik het zonder hen nooit had kunnen klaarspelen. Waar ze het precies over hebben, weet ik niet, maar goed: Bij deze.

Rob en Tineke, mijn ouders, hebben me voortdurend ondersteund en schaamteloos verwend. Rob wil ik bijzonder bedanken voor het corrigeren van de eerste versie van dit proefschrift. Daniel dank ik voor vriend- en broederschap. En de champagne.

Hester, mijn liefste, je hebt me laten zien dat het zó veel vriendschappelijker is met z'n tweetjes. En dat is het zeker.

Curriculum Vitae

Schrijver dezes werd op 25 januari 1971 geboren te Nijmegen. Na het behalen van het VWO diploma, begon hij in 1988 met de studie Scheikunde aan de Universiteit van Amsterdam. Na zijn propaedeuse studeerde hij een jaar filosofie, om vervolgens terug te keren naar de Faculteit Scheikunde. Aldaar heeft hij zich in het laatste jaar van zijn studie beziggehouden met dynamische lichtverstrooiing aan colloïdale suspensies in de groep Macroscopische Fysische Chemie van prof.dr. J. van der Elsken. Het doctoraal examen werd in mei 1993 (cum laude) behaald. In juli 1993 begon hij met het onderzoek uitgevoerd op het FOM-instituut voor Atoom- en Molecuulfysica (AMOLF), dat in dit proefschrift beschreven staat, onder leiding van prof.dr. R.A. van Santen (TUE), prof.dr. A.W. Kleyn (AMOLF), en dr. H.J. Bakker (AMOLF).

STELLINGEN

bij het proefschrift

Picosecond nonlinear infrared spectroscopy in zeolites and solution

1. De bewering van M. Broquier *et al.* dat het niet mogelijk zou zijn om uit hun ver-infrarood pomp-probe metingen de levensduur T_1 te bepalen, is onjuist. Een bepaling van T_1 was wel mogelijk geweest als de auteurs hadden onderkend dat de gemeten signalen sterk worden beïnvloed door coherente koppelings- en vibron-polariton propagatie effecten.
M. Broquier et al., Optics Commun. 118, 255 (1995).
2. Yarwood *et al.* concluderen ten onrechte dat uit het lineaire infrarood absorptie-spectrum van de hoogfrequente X-H strek mode van een waterstof-gebrugd X-H...Y systeem, de frequentie van de laagfrequente waterstofbrug mode vastgesteld kan worden.
J. Yarwood et al., Nature 257, 41 (1975).
3. Het defaseren van de hoogfrequente X-H strek mode van een waterstof-gebrugd (X-H...Y) systeem door interactie met de waterstof brug, hangt sterk af van het *type* waterstofbrug.
4. De dispersierelatie van geluidsmodes in colloïdale suspensies kan eenvoudig begrepen worden in de limieten $k \rightarrow 0$ en $k \rightarrow \infty$. De indirecte theoretische beschrijving van Jing *et al.* geeft wel informatie over de toestandsdichtheid voor alle k , maar geen fysische inzichten in de aard van de modes, ook niet in de limietgevallen.
X. Jing et al., Phys. Rev. Lett. 66, 1240 (1991).
5. De amplitude van het electromagnetische veld van parametrisch gegeneerd incoherent infrarood licht kan niet worden beschreven als een gaussisch stochastisch proces.

6. Het afval van Algemene Vuilverbrandings Installaties (AVI-vliegias) is volgens de samenstellingsgegevens altijd gevaarlijk chemisch afval. Dat AVI-vliegias al jaren via speciale ontheffingen hergebruikt mag worden –bedongen door sterke en bekwame lobbies– houdt risico's in voor toekomstige generaties.
7. Niet-lineaire optica is niet alleen niet-lineair in het electro-magnetische veld.
8. 'Supposing a tree fell down, Pooh, when we were underneath it'
'Supposing it didn't' said Pooh after careful thought.
A.A. Milne, 'The House at Pooh Corner'
9. Een gat is Niets, omgeven door Iets. Het Niets bestaat dan ook alleen maar bij gratie van het Iets, en andersom. Als er alleen Niets zou zijn, zou er niets meer zijn. Zelfs geen gaten. En zeker geen filosofie.
vrij naar: K. Tucholsky

Mischa Bonn
Amsterdam, 13 november 1996